

UNIVERSITAT POLITÈCNICA DE VALÈNCIA

**INSTITUTO INTERUNIVERSITARIO DE INVESTIGACIÓN DE
RECONOCIMIENTO MOLECULAR Y DESARROLLO TECNOLÓGICO**



**Design and development of new bio-gated
nanodevices for targeted controlled drug release**

PhD. THESIS

Submitted by
Amelia Ultimo

PhD. Supervisors:
Prof. María Dolores Marcos Martínez
Dr. Félix Sancenón Galarza

Valencia, September 2019

María Dolores Marcos Martínez, PhD in Chemistry and Professor at the *Universitat Politècnica de València*, and Félix Sancenón Galarza, PhD in Chemistry and Lecturer at the *Universitat Politècnica de València*.

CERTIFY:

That the work "*Design and development of new bio-gated nanodevices for targeted controlled drug release*" has been developed by Amelia Ultimo under their supervision at the Instituto Interuniversitario de Investigación de Reconocimiento Molecular y Desarrollo Tecnológico (IDM) of the *Universitat Politècnica de València*, as a Thesis Project in order to obtain the degree of PhD in Biotechnology at the *Universitat Politècnica de València*.

Valencia, September 2019.

Prof. María Dolores Marcos Martínez

Dr. Félix Sancenón Galarza

Abstract

The present PhD thesis, entitled “Design and development of new biogated nanodevices for targeted controlled drug release” is focused on the design, synthesis, characterization and *in vitro* evaluation of new hybrid organic-inorganic nanosystems as innovative strategies for the targeted and controlled delivery of therapeutic molecules.

The first chapter of this work is a general introduction that defines the context in which the projects carried out during this thesis are placed. In particular, the concept of nanomedicine is described, as well as the main strategies for the development of efficient nanopharmaceutical devices and the related challenges. Furthermore, a brief presentation of mesoporous silica materials is given.

Next, the general objectives that are addressed in the following experimental chapters are introduced.

The third chapter is focused on the development of a targeting delivery system directed to Toll-like receptor 3 (TLR3) and based on mesoporous silica nanoparticles capped with the synthetic double stranded RNA (dsRNA) polyinosinic-polycytidylic acid (poly(I:C)). Poly(I:C) has shown cytotoxic effects in different types of cancer, and the results obtained in this work demonstrate its ability to trigger apoptotic pathways in breast cancer cells, thanks to its interaction with TLR3. Furthermore, loading the mesopores with the anthracycline antibiotic doxorubicin, a commonly used chemotherapeutic agent, allowed to achieve an enhanced therapeutic effect. In fact, a higher decrease of the cellular viability in SK-BR-3 cell line was observed.

Chapter four shows the design of a nanoparticles cooperation strategy. The aim of this work is to improve the efficacy of the previously developed therapeutic approach for breast cancer through the combination of two gated mesoporous silica nanoparticles sets able to cooperate to achieve a medical goal. The first type, in fact, induces changes that enhance the interaction of the second one with the target cancer cell. In order to do that, nanoparticles loaded with 9-cis-retinoic acid

Abstract

and capped with interferon- γ , and nanoparticles loaded with sulforhodamine B dye and gated with poly(I:C) were synthesized. Taking advantage of the ability of both interferon- γ and 9-cis-retinoic to increase TLR3 expression, we intended to improve the interaction of poly(I:C) functionalized nanoparticles with target cells. The obtained results show that the proposed combination strategy actually increased the uptake levels of poly(I:C) gated nanodevices in the cellular model selected.

In the fifth chapter a system based on dendrimer-like mesoporous silica nanoparticles is presented. The higher pore volume of such materials makes them suitable for the achievement of the main aim of this project: the topical administration and controlled delivery of anti-vascular endothelial growth factor (VEGF) small interfering-RNA (siRNA) molecules to retinal pigmented epithelial cells. The nanodevices were synthesized, loaded with siRNA and finally functionalized with polyethylenimine chains, that act as molecular gate for the controlled release of the siRNA molecules and endosomal escape agent for cytosolic delivery. The obtained results in VEGF silencing in ARPE-19 cells highlight the noteworthy potential of the designed system as siRNA carrier.

General conclusions regarding the works collected in this thesis are summarized in chapter six.

Resumen

La presente tesis doctoral, titulada “Diseño y desarrollo de nuevos nanodispositivos con puertas biomoleculares para la liberación dirigida y controlada de fármacos”, está centrada en el diseño, síntesis, caracterización y evaluación *in vitro* de nuevos nanosistemas híbridos orgánicos-inorgánicos como estrategias innovadoras para la administración dirigida y controlada de moléculas terapéuticas.

El primer capítulo de este trabajo es una introducción general que define el contexto en el que se sitúan los proyectos llevados a cabo a lo largo de esta tesis. En particular, se describe el concepto de nanomedicina, así como las principales estrategias para el desarrollo de dispositivos nanofarmacéuticos eficientes y los desafíos que esto conlleva. Además, se presentan brevemente los materiales mesoporosos de sílice.

Sucesivamente, se presentan los objetivos generales que se abordan en los siguientes capítulos experimentales.

El tercer capítulo se centra en el desarrollo de un sistema de administración dirigida al Toll-like receptor 3 (TLR3), basado en nanopartículas mesoporosas de sílice funcionalizadas con el RNA sintético de doble cadena ácido polinosínico-policitidílico (poly(I:C)). El poly(I:C) ha mostrado efectos citotóxicos en diferentes tipos de cáncer, y los resultados obtenidos en este trabajo demuestran su capacidad de desencadenar respuestas apoptóticas en células de cáncer de mama, gracias a su interacción con TLR3. Asimismo, la carga del antibiótico antraciclínico doxorubicina en los mesoporos, ha permitido conseguir un efecto terapéutico aún más intenso. De hecho, se ha observado una mayor disminución de la viabilidad en la línea celular SK-BR3.

El capítulo cuatro muestra el diseño de una estrategia de cooperación entre nanopartículas. El objetivo de este trabajo es el de mejorar la eficacia de la aproximación terapéutica para cáncer de mama desarrollada precedentemente, a través de la combinación de dos tipos de nanopartículas mesoporosas de sílice con

puertas moleculares capaces de cooperar con el fin de conseguir un objetivo terapéutico. El primer tipo, de hecho, induce cambios que incrementan la interacción del segundo con la célula tumoral diana. Para ello, se han sintetizado nanopartículas cargadas con ácido 9-cis retinoico y funcionalizadas en su superficie con interferón- γ , y nanopartículas cargadas con el colorante sulforodamina B y con poly(I:C) anclado en superficie. Aprovechando la habilidad del interferón- γ del ácido 9-cis retinoico de aumentar la expresión del TLR3, nuestra intención era la de mejorar la interacción de las nanopartículas funcionalizadas con poly(I:C) con las células diana. Los resultados obtenidos demuestran que la estrategia de combinación propuesta realmente ha producido un aumento de los niveles de internalización de los nanodispositivos funcionalizados con poly(I:C) en el modelo celular seleccionado.

En el quinto capítulo se presenta un sistema basado en nanopartículas mesoporosas de sílice dendriméricas. El volumen de poro más amplio de este tipo de materiales hace de ellos unos dispositivos adecuados para lograr el objetivo principal de este proyecto: la administración local y la liberación controlada de moléculas de RNA pequeño de interferencia (siRNA) anti-factor de crecimiento vascular endotelial (VEGF) en células del epitelio pigmentado retinal. Los nanodispositivos se han sintetizado, cargado con siRNA y finalmente funcionalizado con cadenas de polietilenimina, que actúan de puerta molecular para la liberación controlada de las moléculas de siRNA y como agentes de escape endosomal para su liberación en el citosol. Los resultados obtenidos en el silenciamiento de VEGF en las células ARPE-19 resaltan el considerable potencial del sistema diseñado como transportador de siRNA.

Las conclusiones generales en relación con los trabajos recopilados en esta tesis se resumen en el capítulo seis.

Resum

La present tesi doctoral, titulada “Disseny i desenvolupament de nous nanodispositius amb portes biomoleculares per a l’alliberament dirigit i controlat de fàrmacs”, està centrada en el disseny, síntesi, caracterització i avaluació *in vitro* de nous nanosistemes híbrids orgànics-inorgànics com a estratègies innovadores per a l’administració dirigida i controlada de molècules terapèutiques.

El primer capítol d'aquest treball és una introducció general que defineix el context en el qual es situen els projectes duts a terme al llarg d'aquesta tesi. En particular, es descriu el concepte de nanomedicina, així com les principals estratègies per al desenvolupament de dispositius nanofarmacèutics eficients i els desafiaments que això comporta. A més, es presenten breument els materials mesoporosos de sílice.

Successivament, es presenten els objectius generals que s’aborden en els següents capítols experimentals.

El tercer capítol es centra en el desenvolupament d'un sistema d'administració dirigida al Toll-like receptor 3 (TLR3), basat en nanopartícules mesoporoses de sílice funcionalitzades amb l'RNA sintètic de doble cadena àcid polinosínic-policitidílic (poly(I:C)). El poly(I:C) ha mostrat efectes citotòxics en diferents tipus de càncer, i els resultats obtinguts en aquest treball demostren la seua capacitat de desencadenar respostes apoptòtiques en cèl·lules de càncer de mama, gràcies a la seua interacció amb TLR3. Així mateix, la càrrega de l'antibiòtic antraciclínic doxorubicina en els mesopors, ha permès aconseguir un efecte terapèutic encara més intens. De fet, s'ha observat una major disminució de la viabilitat en la línia cel·lular SK-BR3.

El capítol quatre mostra el disseny d'una estratègia de cooperació entre nanopartícules. L'objectiu d'aquest treball és el de millorar l'eficàcia de l'aproximació terapèutica per a càncer de mama desenvolupada precedentment, mitjançant la combinació de dos tipus de nanopartícules mesoporoses de sílice amb portes moleculars capaces de cooperar amb la fi d'aconseguir un objectiu

terapèutic. El primer tipus, de fet, indueix canvis que incrementen la interacció del segon amb la cèl·lula tumoral diana. Per a això, s'han sintetitzat nanopartícules carregades amb àcid 9-cis retinoic i funcionalitzades en la seua superfície amb interferó- γ , i nanopartícules carregades amb el colorant sulforodamina B i amb poly(I:C) ancorat en superfície. Aprofitant l'habilitat de l'interferó- γ de l'àcid 9-cis retinoic d'augmentar l'expressió del TLR3, la nostra intenció era la de millorar la interacció de les nanopartícules funcionalitzades amb poly(I:C) amb les cèl·lules diana. Els resultats obtinguts demostren que l'estratègia de combinació proposada realment ha produït un augment dels nivells d'internalització dels nanodispositius funcionalitzats amb poly(I:C) en el model cel·lular seleccionat.

El cinquè capítol presenta un sistema basat en nanopartícules mesoporoses de sílice dendrímèriques. El volum de porus més ampli d'aquest tipus de materials fa d'ells uns dispositius adequats per a aconseguir l'objectiu principal d'aquest projecte: l'administració local i l'alliberament controlat de molècules d'RNA xicotet d'interferència (siRNA) anti-factor de creixement vascular endotelial (VEGF) en cèl·lules de l'epiteli pigmentat retinal. Els nanodispositius s'han sintetitzat, carregats amb siRNA i finalment funcionalitzats amb cadenes de polietilenimina, que actuen de porta molecular per a l'alliberament controlat de les molècules de siRNA i com a agents d'escap endosomal per al seu alliberament en el citosol. Els resultats obtinguts en el silenciament de VEGF en les cèl·lules ARPE-19 ressalten el considerable potencial del sistema dissenyat com a transportador de siRNA.

Les conclusions generals en relació amb els treballs recopilats en aquesta tesi es resumeixen en el capítol sis.

Abbreviations and Acronyms

ADME	adsorption, distribution, metabolism and excretion
AMD	age-related macular degeneration
APTES	3-aminopropyltriethoxysilane
BET	Brunauer-Emmet-Teller
BJH	Barrett-Joyner-Halenda
bPEI 10,000	branched polyethylenimine with MW 10,000
CAF	cell-associated fluorescence
CNV	choroidal neovascularization
cRGDY	cyclic(arginine-glycine-aspartic acid-tyrosine)
CTAB	cetyltrimethylammonium bromide
CTATos	cetyltrimethylammonium p-toluenesulfonate
DAPI	4',6-diamidino-2-phenylindole
DLS	dynamic light scattering
DMEM	Dulbecco's Modified Eagle Medium
DMEM/F12	Dulbecco's Modified Eagle Medium: Nutrient Mixture F-12
DNA	deoxyribonucleic acid
Dox	doxorubicin
ds-RNA	double stranded ribonucleic acid
EA	elemental analysis
EDC	1-Ethyl-3-(3-dimethylaminopropyl)carbodiimide
EDTA	ethylenediaminetetraacetic acid
EGFR	epidermal growth factor receptor
ELISA	enzyme-linked immunosorbent assay

Abbreviations and Acronyms

EMA	European medicines agency
EPR	enhanced permeability and retention
FBS	fetal bovine serum
FDA	Food and Drug Administration
HER2	human epidermal growth factor receptor 2
IC₅₀	inhibitory concentration 50
IFN	interferon- γ
LP-MSNs	large pores mesoporous silica nanoparticles
MCM-41	Mobile crystalline material 41 (hexagonal arrangement of the pores)
MCM-48	Mobile crystalline material 41 (cubic arrangement of the pores)
MCM-50	Mobile crystalline material 41 (lamellar arrangement of the pores)
miRNA	micro ribonucleic acid
MSNs	mesoporous silica nanoparticles
PEG	polyethylene glycol
PAMAM	polyamidoamine
PBS	phosphate-buffered saline
PhC	phase contrast
PLGA	poly(lactic-co-glycolic acid)
PEI	polyethyleneimine
PIC	polyinosinic-polycytidylic acid
Poly(I:C)	polyinosinic-polycytidylic acid
PMSF	phenylmethysulfonyl fluoride
PXRD	powder X-ray diffraction
RA	9-cis-retinoic acid
RGD	arginine-glycine-aspartatic acid

RGDY	arginine-glycine-aspartic acid-tyrosine
RhB	rhodamine B
RhB-ITC	rhodamine B isothiocyanate
RNA	ribonucleic acid
RPE	retinal pigment epithelium
SD	standard deviation
SDA	structure-directing agent
SEM	scanning electron microscopy
siRNA	small interfering ribonucleic acid
sulf	sulforhodamine B
TEA	triethanolamine
TEM	transmission electron microscopy
TEOS	tetraethyl orthosilicate
TLCT	true liquid-crystal templating
TLR	Toll-like receptor
TMOS	tetramethyl orthosilicate
UV	ultraviolet-visible
VEGF	vascular endothelial growth factor
XRD	X-ray diffraction
WGA	wheat germ agglutinin
WST-1	water-soluble tetrazolium salt 1
λ_{em}	emission wavelength
λ_{ex}	excitation wavelength

Table of Contents

Chapter 1. General introduction	1
1.1 Nanomedicine	3
1.2 Targeted drug delivery	10
1.2.1 The protein corona.....	14
1.3 Endosomal escape	17
1.4 Stimuli-responsive release of cargo	22
1.5 Mesoporous silica materials.....	26
1.5.1 Ordered mesoporous silica materials	27
1.5.2 Dendrimer-like mesoporous silica materials.....	31
1.5.3 Gated mesoporous silica nanomaterials.....	34
Chapter 2. Objectives	39
Chapter 3. Targeting Innate Immunity with dsRNA-Conjugated Mesoporous Silica Nanoparticles Promotes Anti-Tumor Effects on Breast Cancer Cells	43
3.1 Abstract	47
3.2 Introduction.....	47
3.3 Results and discussion.....	50
3.4 Conclusions.....	58
3.5 References.....	59
3.6 Supporting Information.....	61
Chapter 4. Nanoparticle-cell-nanoparticle communication by stigmergy to enhance poly(I:C) induced apoptosis in cancer cells	69
4.1 Abstract	73
4.2 Introduction.....	73
4.3 Results and discussion.....	77
4.4 Conclusions.....	82
4.5 References.....	82
4.6 Supporting Information.....	84

Table of contents

Chapter 5. High capacity mesoporous silica nanocarriers for retinal delivery of siRNA.....	93
5.1 Abstract	97
5.2 Introduction.....	97
5.3 Results and discussion.....	100
5.4 Conclusions.....	109
5.5 Experimental section.....	110
5.6 References.....	115
Chapter 6. Conclusions and Perspectives	121

Chapter 1: General introduction

1.1 Nanomedicine

Several descriptions of what nanomedicine denotes can be found in literature. According to the international review Nature, that possibly gives the most exhaustive definition, “nanomedicine is a branch of medicine that applies the knowledge and tools of nanotechnology to the prevention and treatment of disease. Nanomedicine involves the use of nanoscale materials, such as biocompatible nanoparticles and nanorobots, for diagnosis, delivery, sensing or actuation purposes in a living organism.”¹ On the other hand, the European Science Foundation provides a more detailed explanation of nanomedicine main purposes as “the comprehensive monitoring, control, construction, repair, defence and improvement of all human biological systems, working from the molecular level using engineered devices and nanostructures, ultimately to achieve medical benefit.”² Nanoscale, generally intended as the range from one to hundreds of nanometres, is indeed the dimension in which molecular interactions take place in the cellular environment (Figure 1).^{2,3} One nanometre (nm) is one billionth or 10^{-9} of a metre. Thus, nanotechnology applied to living organisms is aimed to operate at cellular or sub-cellular level, combining several areas of knowledge as medicine, cellular and molecular biology, engineering, physics and chemistry in order to do that.

¹ Nanomedicine - Latest research and news | Nature. (n.d.). Retrieved from <https://www.nature.com/subjects/nanomedicine>.

² Nanomedicine. An ESF-European Medical Research Councils (EMRC) Forward Look Report | Nanowerk. (n.d.). Retrieved from <https://www.nanowerk.com/nanotechnology-report.php?reportid=53>.

³ M. Saha, *Oman Medical Journal*, **2009**, 24, 242.

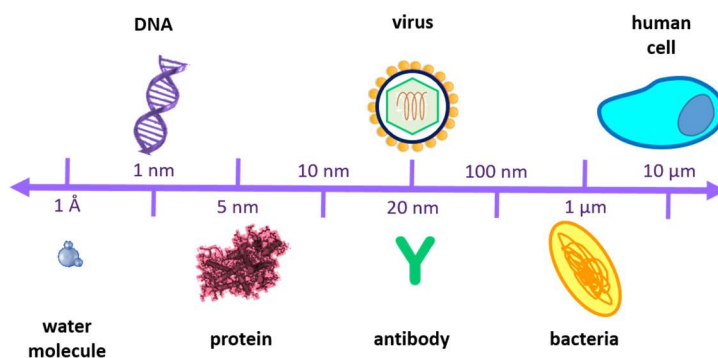


Figure 1. Biological elements on a scale from 1 Å to 10 μm. *Adapted from J. Pers. Med.* 2017, 7, 12.

Even if the first nanobio scientific conference “Biological Approaches and Novel Applications for Molecular Nanotechnology” was held in 1996,⁴ the interest of the scientific community in nanomedicine has spread considerably in the last fifteen years, considering the amount of related articles published in this time span.⁵ This is probably due to an urgent need to overcome some common and limiting issues in the development of new therapies, as the inadequate pharmacokinetics and biopharmaceutical properties of most of small molecules and biologicals, that hinder their delivery to the target site of action.^{6,7} Drug delivery systems, hence, could represent an excellent solution to reach an improved delivery of therapeutic agents, increasing their medical efficacy and safety, and overall patients’ quality of life, while reducing side effects and drug doses needed. In this context, the design and development of nanomaterials with a precise drug transport and delivery purpose takes on considerable significance. Nanomedicines, in fact, are not only nanodevices carrying encapsulated, dispersed, adsorbed or conjugated drugs and/or imaging agents,⁶ but provide the added value of dimension-dependent phenomena: nanomaterials show unique abilities to cross and interact with biological entities that are missing in the same materials at larger

⁴ J. R. Baker, J. B. B. Ward, T. P. Thomas, *Clinical and Translational Science*, **2009**, 123.

⁵ A. Duschl, *Immune Rebalancing*, **2016**, 251.


⁶ O. M. Koo, I. Rubinstein, H. Onyuksel, *Nanomedicine Nanotechnology, Biol. Med.*, **2005**, 1, 193.

⁷ P. M. Glassman, V. R. Muzykantov, *J. Pharmacol. Exp. Ther.*, **2019**, p. jpet.119.257113.

sizes, so that they employ the nano-range size specific features to reach objectives unattainable for free drugs or voluminous materials.^{4,6,8} General features, common to different kinds of nanotransporters, are high surface areas and surface-to-volume ratio, biocompatibility, control of size and surface characteristics, stealth properties, capacity for loading both lipophilic or hydrophilic molecules, versatility and possibility to be engineered for targeting and controlled release.^{4,9} Such characteristics allow prolonged circulation times and reduced volumes of distribution, meaning extended drug half-life, reduced unspecific delivery and optimal concentrations of drug at sites of interest over a desired period and, consequently, an increased therapeutic efficacy. Furthermore, nanocarriers have great potential for the development of combination therapies based in the simultaneous administration of more than one kind of active molecule, leading to likely synergetic effects and possibly reducing drug resistance.⁹ Table 1 resumes the main characteristics associated with the administration of free or nanoformulated drugs.

Table 1. Free versus nanoformulated drugs' administration features.

FREE DRUGS	NANO-FORMULATED DRUGS
<ul style="list-style-type: none"> - Low solubility - Limited stability - Short plasma half life - Biological barriers - Drug resistance - Systemic toxicity 	<ul style="list-style-type: none"> - Increased half life - Selective targeting - Sustained release - Higher safety - Less side effects - Reduced doses - Reduced administration frequency - Possibility of combination therapy - Decreased drug resistance - Increased therapeutic efficacy



⁸ "Considering Whether an FDA-Regulated Product Involves the Application of Nanotechnology | FDA.". Available: <https://www.fda.gov/regulatory-information/search-fda-guidance-documents/considering-whether-fda-regulated-product-involves-application-nanotechnology>.

⁹ F. Dilnawaz, S. Acharya, S. K. Sahoo, *Int. J. Pharm.*, **2018**, 538, 263.

A large variety of nanomaterials has been developed and studied as medical functional devices, combining supramolecular chemistry, colloid and polymer science, physics and engineering knowledge. Nanodrug formulations include liposomes, polymers, micelles, nanocrystals, metals/metal oxides and other inorganic materials and carbon nanotubes (Figure 2).^{10,11} Among the most commonly used kinds of nanocarriers, liposomes, phospholipid vesicles that normally present chemically modified surfaces, are doubtlessly the most extensively studied and the base for the design of the first approved nanopharmaceutical products and of most of the new ones under clinical trials. This is due to their ability to carry both hydrophilic and hydrophobic molecules, their low immunogenicity and toxicity and quick degradation.^{12,13,14} Dendrimers, branched and globular molecules with radial and well defined three dimensional structure, the most common of which are polyamidoamine (PAMAM), poly(propylene imine) (PPI) and poly(L-lysine) (PLL), and several kinds of polymers, as poly(lactic-co-glycolic acid) (PLGA), polyethylene glycol (PEG), chitosan and hyaluronic acid, are often used to obtain dispersion/solubilisation matrices for improving drug pharmacokinetics and pharmacodynamics features.^{15,16,17} In the field of theranostics, instead, both carbon nanotubes and magnetic nanoparticles are considered suitable options thanks to their physical properties that make them very attractive for targeted delivery, high-resolution imaging and medical

¹⁰ C. L. Ventola, *PT*, **2017**, *42*, 742.

¹¹ G. G. Genchi, A. Marino, C. Tapeinos, G. Ciofani, *Front. Bioeng. Biotechnol.*, **2017**, *5*, 80.

¹² C. Fornaguera, M. J. García-Celma, *J. Pers. Med.*, **2017**, *7*, 12.

¹³ U. Kauscher, M. N. Holme, M. Björnmalm, M. M. Stevens, *Adv. Drug Deliv. Rev.*, **2019**, *138*, 259.

¹⁴ A. J. Urquhart, A. Z. Eriksen, *Drug Discov. Today*, **2019**, doi: 10.1016/j.drudis.2019.04.004.

¹⁵ A. Akbarzadeh, R. Khalilov, E. Mostafavi, N. Annabi, T. Kafshdooz, R. Herizchi, T. Kavetsky, S. Saghfi, A. Nasibova, S. Davaran, *Exp. Oncol.*, **2018**, *40*, 178.

¹⁶ D. Huang, D. Wu, *Mater. Sci. Eng. C*, **2018**, *90*, 713.

¹⁷ J. Siepmann, A. Fahamb, S.-D. Clasc, B. J. Boydd, V. Jannine, A. Bernkop-Schnürch, H. Zhao, S. Lecommandoux, J. C. Evansh, C. Allenh, O. M. Merkele, G. Costabilei, M. R. Alexanderj, R. D. Wildmank, C. J. Robertsj, J.-C. Lerouxl, *Int. J. Pharm.*, **2019**, *558*, 128.

hyperthermia.^{18,19,20} Quantum dots, on the other hand, thanks to their small size and optical and electronic properties, are also relevant for imaging techniques, especially multimodal imaging that allows to obtain deep and precise results.^{18,21} Mesoporous silica nanoparticles (MSNs) also represent versatile drug delivery systems, and will be described more in depth later on. Thus, the array of available nanomaterials is rich with options, and even combination of different materials can be assembled for the development of the next generation of nanopharmaceuticals.

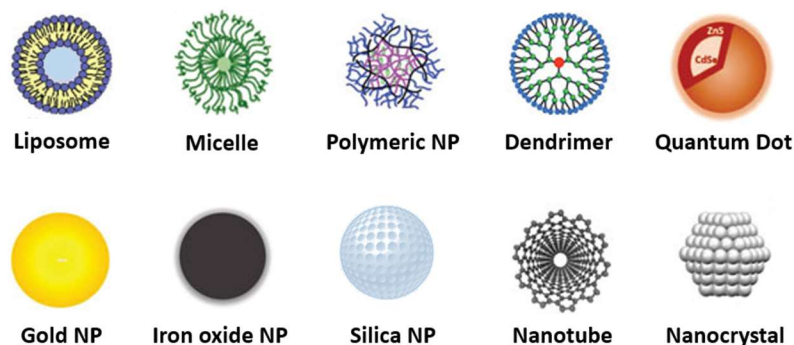


Figure 2. Schematic depiction of different types of nanomaterials used for nanomedicine applications. Adapted from *Adv. Funct. Mater.* 2017, 27, 1700489. Copyright © 2017 Wiley-VCH.

AmBisome (liposomal amphotericin B for fungal infections) has been the first product approved by the European Medicines Agency (EMA) in 1990, while in US the first nanomedicine approved by the Food and Drug Administration (FDA) and commercialized has been Doxil (PEGylated liposomal doxorubicin for several types of cancers) in 1995.^{12,22} In the last two decades, nanomedicines for the treatment of several kind of solid tumours and leukaemia or other pathologies like

¹⁸ S. Marchesan, M. Prato, *ACS Med. Chem. Lett.*, **2013**, 4, 147.

¹⁹ S. Sánchez-Cabezas, R. Montes-Robles, J. Gallo, F. Sancenón, R. Martínez-Máñez, *Dalt. Trans.*, **2019**, 48, 3883.

²⁰ M. I. Sajid, U. Jamshaid, T. Jamshaid, N. Zafar, H. Fessi, A. Elaissari, *Int. J. Pharm.*, **2016**, 501, 278.

²¹ C. Matea, T. Mocan, F. Tabaran, T. Pop, O. Mosteanu, C. Puia, C. Iancu, L. Mocan, *Int. J. Nanomedicine*, **2017**, 12, 5421.

²² Y. H. Choi, H.-K. Han, *J. Pharm. Investig.*, **2018**, 48, 43.

allergies, infections, autoimmune, metabolic or degenerative diseases have also been approved.⁹ Nevertheless, although the huge amount of basic investigations in nanomedicine and related publications, the number of commercialized nanotherapies available for the clinical practice is poor, merely 51 by the year 2016.^{10,12,22,23} A reason for that is the low level of knowledge about pharmacokinetics of drug nanocarriers. While the transported molecules are often already approved drugs, with well described adsorption, distribution, metabolism and excretion (ADME) processes, the same information for the whole nanoformulation is frequently lacking, due to an increased complexity, assays limitations and a reduced amount of studies about the transporters compared to the ones on the active molecules.⁷ It is well known that nanocarriers shape, size and surface charge are the fundamental parameters that determine their behaviour and interaction with biological systems once administered, affecting distribution, stability, circulation time, recognition, cellular uptake, intracellular transport, accumulation and elimination.^{10,24} Deep characterization of the systems developed in research laboratories is still an issue, as it results extremely complicated to analyse so many parameters (beyond those already mentioned above, composition, stability and surface coverage with ligands) separately and then establishing relationships between them. Therefore, a detailed understanding of the physico-chemical properties of nanomaterials is essential for the evaluation of their toxicological impact within acceptable pharmaceutical levels. Better designed characterization methods and more exhaustive pharmacokinetics studies are necessary for a more accurate prediction of the pharmacologic effects of nanomaterials.

Another controversial issue is the weakness of the specific regulation: even if in last years the regulatory agencies have tried to fill the gap between small drugs and nanoformulations, it is evident that the legislative sphere goes slower than nanopharmaceutical evolution.²³ Recently, the European Union has stated that more rigorous control strategies are needed for nanotechnology-based medicines

²³ J.-B. Coty, C. Vauthier, *J. Control. Release*, **2018**, 275, 254.

²⁴ C. Azevedo, M. H. Macedo, B. Sarmiento, *Drug Discov. Today*, **2018**, 23, 944.

due to their unique properties, highlighting the importance of establishing a bottom-up quality assessment, meaning that nanomedicines quality has to be verified in each step of their development and not only in the final product.²⁵ At the same time, the EMA has indicated a series of parameters that should be carefully analysed, due to their relevance in drug nanocarriers: size, size distribution and polydispersity index, shape and morphology, surface charge, surface composition, encapsulation efficiency, non-encapsulated active pharmaceutical ingredients, release, polymers molecular weight and biodegradability, interactions with biological medium, conjugation chemistry, functionality of targeting moieties, aggregation, polymorphism and in-use stability.²⁵ Although a large amount of data has been collected until now about the most common types of materials employed in approved applications (Figure 3), further steps must be taken in order to guarantee the quality, safety, efficacy and risk-benefit ratio of innovative nanomaterials-based products developed for unmet medical needs.

Finally, last bottleneck for the clinical translation of drug nanocarriers is the scale up their production and the establishment of robust quality controls to avoid batch to batch variations.²³ Nevertheless, even if nanomedicines development has to face many challenges, the triennium 2013-2015 registered the highest number of clinical trials involving nanoformulated drugs, while the estimated market value of the new ones expected to be developed in 2019 is of around \$ 178 billion.¹⁰

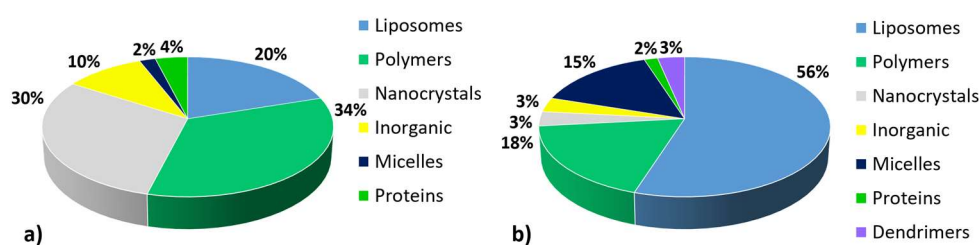


Figure 3. a) Types of nanomaterials in FDA approved drugs available in the market for clinical use. b) Types of nanomaterials in FDA approved drugs for clinical trials. *Adapted from P&T 2017, 42(12), 742.*

²⁵ R. Pita, F. Ehmman, R. Thürmer, *Biomed. Appl. Funct. Nanomater.*, **2018**, 653.

1.2 Targeted drug delivery

Considering the facts mentioned above, and bearing in mind the concept of precision medicine as an interdisciplinary field whose aims are very sensitive and targeted theranostics approaches, where the targets are specific cell types, proteins or disease markers, nanomedicine products can be undoubtedly labelled as precision devices based on a nanotransporter, a bioactive molecule and a targeting moiety.^{12,26} Nanomedicines, hence, can be designed for pursuing personalized medicine, developing therapeutic strategies directed to individuals or groups of individuals with common characteristics, what is of particular interest in the treatment of cancers. Neoplastic diseases, indeed, are the result of multiple intrinsic and extrinsic factors, that produce as a consequence a great heterogeneity in patients' response to chemotherapeutics. Thus, personalization of cancer treatment, understood as the administration of the adequate drug with the adequate dose to a given patient, is an essential challenge.²⁶ In this context, the possibility of designing customizable nanotransporters is especially valuable.

The main strategy for nanocarriers customization is the development of targeted systems able to discriminate between healthy and diseased tissues, and to direct the drug or signalling molecule to the site of interest. Even if targeted approaches are already available in standard pharmaceutical, as for example the employment of monoclonal antibodies, until now any targeted nanomedicine can be found among the already approved ones.²⁷ Nevertheless, TargomiRs, miRNAs loaded minicells targeted to the epidermal growth factor receptor (EGFR) for the treatment of malignant pleural mesothelioma, already passed a phase 1 clinical trial,²⁸ while doxorubicin loaded liposomes targeted to human epidermal growth

²⁶ I. K. Herrmann, M. Rösslein, *Nanomedicine*, **2016**, *11*, 1.

²⁷ M. B. Deci, M. Liu, Q. T. Dinh, J. Nguyen, *Wiley Interdiscip. Rev. Nanomedicine Nanobiotechnology*, **2018**, *10*, 1.

²⁸ N. van Zandwijk, N. Pavlakis, S. C. Kao, A. Linton, M. J. Boyer, S. Clarke, Y. Huynh, A. Chrzanowska, M. J. Fulham, D. L. Bailey, W. A. Cooper, L. Kritharides, L. Ridley, S. T. Pattison, J. MacDiarmid, H. Brahmbhatt, G. Reid, *Lancet Oncol.*, **2017**, *18*, 1386.

factor receptor 2 (HER2)²⁹ and fluorophores labelled silica nanoparticles functionalized with RGDY targeting peptide for real time imaging²⁷ are in phase 1 and phase 2 clinical trials, respectively.

Targeting of site of interest can be achieved through two different approaches, passive or active targeting (Figure 4). Passive targeting relies on the pathophysiological features of tumour blood vessels. Due to its rapid growth, cancer vessels exhibit loose junctions and hyperpermeability that facilitate nanoparticles extravasation and accumulation at the tumour site, generating the so-called enhanced permeability and retention (EPR) effect, also thanks to a low presence of functional lymphatic vessels.^{30,31} Nevertheless, passive targeting does not guarantee the absence of off-target drug delivery, while the EPR effect seems not to be so clearly exhibited in all types of cancer and presents great heterogeneity even in the same tumour.³¹ The heterogeneity in the rate of fenestrations in the tumour endothelium, in the blood flow through the different tumour areas, in the pericytes coverage, in the basement membrane and in the density of the extracellular matrix makes it impossible to refer to the tumour microenvironment as a whole; the central hypoxic areas, for example, show less accumulation of nanoparticles and nanomaterials.^{31,32} Figure 5 is a schematic representation of the complexity of tumour microenvironment.

²⁹ E. Geretti, S. C. Leonard, N. Dumont, H. Lee, J. Zheng, R. De Souza, D. F. Gaddy, C. W. Espelin, D. A. Jaffray, V. Moyo, U. B. Nielsen, T. J. Wickham, B. S. Hendriks, *Mol. Cancer Ther.*, **2015**, *14*, 2060.

³⁰ T. D. Clemons, R. Singh, A. Sorolla, N. Chaudhari, A. Hubbard, K. S. Iyer, *Langmuir*, **2018**, *34*, 15343.

³¹ J. Fang, H. Nakamura, H. Maeda, *Adv. Drug Deliv. Rev.*, **2011**, *63*, 136.

³² F. Danhier, *J. Control. Release*, **2016**, *244*, 108.

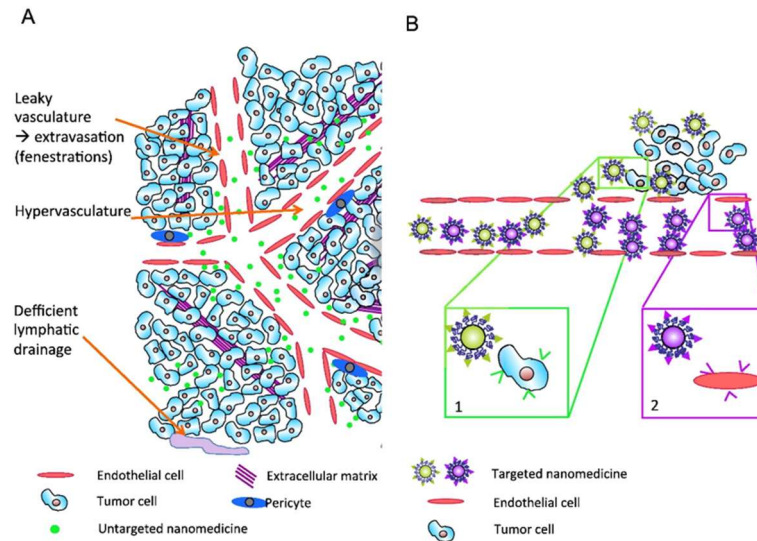


Figure 4. a) Schematic representation of the EPR effect and the consequent accumulation of nanomedicines. b) Schematic representation of the active targeting approach using nanomedicines targeted to specific receptors of cancer or endothelial cells. *Reprinted with permission from J. Control. Release 2016, 244, 108. Copyright © 2016 Elsevier B.V.*

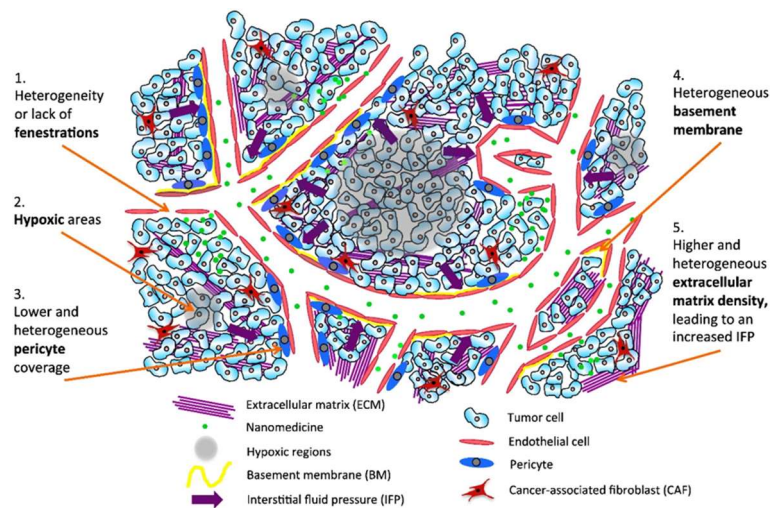


Figure 5. The heterogeneity of the human tumour microenvironment and the consequent heterogeneous passive retention of untargeted nanomedicines. *Reprinted with permission from J. Control. Release 2016, 244, 108. Copyright © 2016 Elsevier B.V.*

Finally, it should be considered that, to take advantage of the particular anatomical characteristics of tumour vessels, it would be necessary a prolonged circulation of the nanocarriers in the blood stream avoiding any interaction with opsonins and the mononuclear phagocytic system, what can be achieved coating nanomaterials surface with stealth polymers, as for example PEG.⁹ PEGylation of nanomaterials make them hydrophilic, so that the captured water molecules constitute a barrier that prevents protein adsorption. Otherwise, the development of biomimetic surfaces represents an alternative strategy, in which natural membrane coating enables to avoid clearance and to increase the biocompatibility of the material.²⁴

Targeted approaches, on the other hand, involve surface physical or chemical integration of nanomaterials with affinity ligands of overexpressed receptor or other biological targets, using a wide catalogue of biomolecules such as peptides and proteins,³³ sugars,³⁴ aptamers,³⁵ small molecules³⁶ and monoclonal antibodies³⁷ among others, with the aim to induce a recognition and a specific uptake via receptor-mediated endocytosis.^{38,39} Coupling of ligands to nanotransporters surface can be achieved by covalent and non-covalent binding: disulfide bonds formation, primary amines cross-linking, carboxylic acid and

³³ B. Albertini, V. Mathieu, N. Iraci, M. Van Woensel, A. Schoubben, A. Donnadio, S. M. L. Greco, M. Ricci, A. Temperini, P. Blasi, N. Wauthoz, *Mol. Pharm.*, **2019**, doi: 10.1021/acs.molpharmaceut.9b00047.

³⁴ D. Muñoz-Espín, M. Rovira, I. Galiana, C. Giménez, B. Lozano-Torres, M. Paez-Ribes, S. Llanos, S. Chaib, M. Muñoz-Martín, A. C. Ucerro, G. Garaulet, F. Mulero, S. G. Dann, T. VanArsdale, D. J. Shields, A. Bernardos, J. R. Murguía, R. Martínez-Máñez, M. Serrano, *EMBO Mol. Med.*, **2018**, *10*, e9355.

³⁵ L. Pascual, C. Cerqueira-Coutinho, A. García-Fernández, B. de Luis, E. Bernardes, M. S. Albernaz, S. Missailidis, R. Martínez-Máñez, R. Santos-Oliveira, M. Orzaez, F. Sancenón, *Nanomedicine Nanotechnology, Biol. Med.*, **2017**, *13*, 249.

³⁶ Y. Y. Luo, X. Y. Xiong, F. Cheng, Y. C. Gong, Z. L. Li, Y. P. Li, *Int. J. Biol. Macromol.*, **2017**, *105*, 711.

³⁷ J.-M. Montenegro, V. Grazu, A. Sukhanova, S. Agarwal, J. M. de la Fuente, I. Nabiev, A. Greiner, W. J. Parak, *Adv. Drug Deliv. Rev.*, **2013**, *65*, 5, 677.

³⁸ J. Kydd, R. Jadia, P. Velpurisiva, A. Gad, S. Paliwal, P. Rai, *Pharmaceutics*, **2017**, *9*, 46.

³⁹ L. Y. Rizzo, B. Theek, G. Storm, F. Kiessling, T. Lammers, *Curr. Opin. Biotechnol.*, **2013**, *24*, 1159.

primary amine, maleimide and thiol, hydrazide and aldehyde or primary amine and free aldehyde reactions are mostly used for covalent binding of ligands, while non-covalent attachment through electrostatic interactions is also commonly adopted, even if do not enable ligands orientation.⁶

The selection of adequate targeting ligands is of essential importance. At the same time, a more in-depth knowledge about target tissue receptors clustering and their spatiotemporal variations on the surface of the target cells can affect the efficacy of the targeting strategy, having influence on nanomaterials binding and uptake.²⁷ Furthermore, it should be pointed out that in many cases, even if overexpressed in diseased tissues, the target receptor can be anyway expressed in healthy tissues, so that the relative rates of expression are a critical parameter to consider when designing a targeted nanocarrier.⁷ Finally, it should be taken into account that the amount of receptor available on cell surface could decrease due to continuous administration of the nanomedicine and the consequent internalization of the receptor-ligand complex, as already occurring with monoclonal antibodies.⁴⁰ Thus, with the aim of obtaining nanocarriers able to respond to spatiotemporal variations of receptors expression on the cellular membrane and to precisely bind them, a full characterization of receptors behaviour would allow a more weighed and precise design of the ligand grafting onto nanocarriers surface for an improved ligand-receptor interaction. Nevertheless, more sensitive methods to characterize ligands conformation, density and homogeneity on the final nanosystem should also be developed to foresee the efficacy of the targeting strategy and possible improvements.²³

1.2.1 The protein corona

An important consideration deserves to be made regarding the adsorption of proteins and biomolecules present in the physiological fluids to which

⁴⁰ R. T. Meijer, R. P. Koopmans, I. J. M. ten Berge, P. T. A. Schellekens, *J. Pharmacol. Exp. Ther.*, **2002**, *300*, 346.

nanomedicines are exposed after their administration. This phenomenon, the formation of a so-called protein corona, has been observed and partially studied in the last decade, and is due to the high free energy of nanomaterials surfaces.⁴¹ The protein corona can affect several physicochemical properties of nanoparticles, including size, surface charge, surface composition and functionality, constituting an essential element of biological identity of the administered nanodevices and determining this way their behaviour in the biological context (circulation time, bioavailability, biodistribution, cellular uptake, toxicity, therapeutic or diagnostic functionality).⁴² It has been shown how the presence of a protein corona can significantly alter nanoparticles interaction with cells, in particular lowering the uptake levels but at the same time decreasing nanomaterials toxicity related to the bare surface potentially prejudicial features and reducing recognition by the immune system.^{43,44} Based on the results of different studies, it seems that the reduced toxicity of nanomaterials in presence of a protein corona is given by four main occurrences: decreased reactive oxygen species, diminished agglomeration (even if in some cases nanoparticles aggregation can be induced by the formation of protein bridges),⁴² mitigated effect of surfactants used for particles suspension and protection from metal ions toxicity during biodegradation.⁴⁵ The targeting abilities of ligand-functionalized nanocarriers can be likely annulled due to the biomolecular shield, although recent results demonstrate how non-covalent grafting of targeting molecules on nanoparticles surface could reduce their loss of functionality compared to covalent binding.⁴⁶

⁴¹ M. P. Monopoli, C. Åberg, A. Salvati, K. A. Dawson, *Nat. Nanotechnol.*, **2012**, *7*, 779.

⁴² V. H. Nguyen, B.-J. Lee, *Int. J. Nanomedicine*, **2017**, *12*, 3137.

⁴³ A. Lesniak, F. Fenaroli, M. P. Monopoli, C. Åberg, K. A. Dawson, A. Salvati, *ACS Nano*, **2012**, *6*, 5845.

⁴⁴ F. Wang, L. Yu, M. P. Monopoli, P. Sandin, E. Mahon, A. Salvati, K. A. Dawson, *Nanomedicine Nanotechnology, Biol. Med.*, **2013**, *9*, 1159.

⁴⁵ R. Cai, C. Chen, *Adv. Mater.*, **2018**, e1805740.

⁴⁶ M. Tonigold, J. Simon, D. Estupiñán, M. Kokkinopoulou, J. Reinholz, U. Kintzel, A. Kaltbeitzel, P. Renz, M. P. Domogalla, K. Steinbrink, I. Lieberwirth, D. Crespy, K. Landfester, V. Mailänder, *Nat. Nanotechnol.*, **2018**, *13*, 862.

The presence of a protein corona comprising a wide range of proteins (>300) and with a short time of generation, less than 30 seconds, has been observed on a large variety of nanoparticles.⁴⁷ Generally, albumin is the most recurrent component of the corona, being the most abundant protein in serum; however, despite their lower concentrations in serum, other proteins like immunoglobulins, apolipoproteins and fibrinogen can be found in higher amounts in the corona.⁴⁸ The relative amounts of components of the protein corona, indeed, not always correspond with their concentrations in the exposure fluid, as the adsorption is determined by both protein-nanoparticles interactions and protein-protein interaction.⁴²

A bilayer structure has been identified in most cases, with a first monolayer of tightly bound biomolecules, the hard corona, and, on the top, a second layer of not so strongly adsorbed biomolecules that change continuously, the soft corona.^{42,49} As it is composed by proteins and molecules with high affinity for the nanomaterials surface, it is evident that protein corona configuration depends on its physicochemical features as size, shape, charge, presence of functional groups, as well as on the origin of the biological fluid that determines the biomolecules population composition.^{42,44,45} The analysis of the corona, indeed, can also give information on the places the nanoparticles have moved through, as part of the hard corona that has not been modified with time comes from the first sites of passage.⁴¹ It seems, instead, that part of the original corona is kept on the nanoparticles surface even during the cellular uptake and once inside the cells.⁴⁴ Of course, only that molecules and proteins that are able to bind the surface over the period of time necessary for the nanoparticles displacement and crossing of plasma membrane will be transported inside the cell, and the results obtained until now show that the exchanging times varies from seconds in case of the soft corona to

⁴⁷ S. Tenzer, D. Docter, J. Kuharev, A. Musyanovych, V. Fetz, R. Hecht, F. Schlenk, D. Fischer, K. Kiouptsi, C. Reinhardt, K. Landfester, H. Schild, M. Maskos, S. K. Knauer, R. H. Staube, *Nat. Nanotechnol.*, **2013**, *8*, 772.

⁴⁸ C. C. Fleischer, C. K. Payne, *Acc. Chem. Res.*, **2014**, *47*, 2651.

⁴⁹ S. Palchetti, L. Digiacomio, D. Pozzi, G. Peruzzi, E. Micarelli, M. Mahmoudi, G. Caracciolo, *Nanoscale*, **2016**, *8*, 12755.

several hours in the hard one.⁴¹ Figure 6 shows how biomolecules can be replaced on nanoparticles surface or how their presence determine the adsorption of other kinds of molecules.

Nevertheless, due to the complexity of the protein corona and of the numerous factors that influence its composition and exchange rates and times, it is essential to elaborate reliable methods to predict the nature of the corona and the consequent possible effects on the fate of the designed nanomedicines. Furthermore, this natural process of bioactive molecules coating of nanomedicines surface should be exploited to achieve improved materials, for example, selecting plasma proteins with intrinsic targeting abilities,⁴⁵ with reduced associated risks.

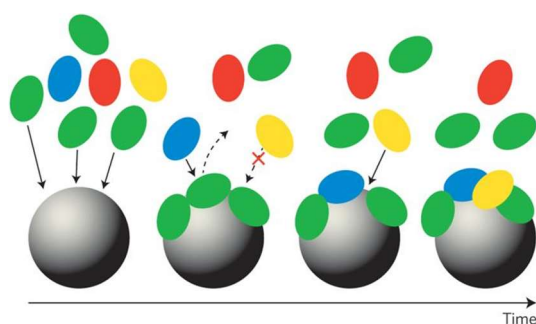


Figure 6. Variation of protein corona composition on the surface of a nanoparticle over the time. Green circles represent abundant but low affinity biomolecules, while blue circles are biomolecules with high affinity to the nanomaterial surface, able to displace the first ones. Yellow circles are molecules whose affinity, low at the beginning, increases due to the presence of the already adsorbed biomolecules. Red circles represent molecules with no affinity for the nanoparticle surface. *Reprinted with permission from Nat. Nanotechnol. 2012, 7, 779. Copyright © 2012 Macmillan Publishers Limited.*

1.3 Endosomal escape

Once nanomedicines reach the cells of interest, whether by passive or active targeting, endocytosis is generally the main mechanism of cellular uptake, although direct translocation or fusion of lipid nanoparticles with cellular membranes are also possible options. Endocytosis can occur through different

pathways: clathrin-dependent, caveolae-dependent, unspecific clathrin/caveolae-independent mechanisms and micropinocytosis.⁵⁰ The way of entering cells can influence the subsequent intracellular trafficking, but this correlation can vary for each nanoparticle/cell type pair, also depending on the protein corona bound to the surface of the nanoparticle. The lack of specific markers and inhibitors for endocytosis pathways (the commonly used ones often exhibit off-target effects) make the comprehension of these phenomena still unclear.⁵¹ Nevertheless, it seems that independently of the endocytic way of entering, in most cell lines the endocytic vesicles fuse with early endosomes within few minutes from the uptake.⁵⁰ Then, endosomes can be recycled back to the cell surface, possibly bringing with them part of the materials that undergo this way a quick exocytosis,⁵² or can join late endosomes and finally lysosomes. Here, nanotransporters are generally degraded, together with their cargo if it is not able to cross lysosomal membranes. A schematic representation of the possible internalization processes is shown in Figure 7. Even if it seems that all the possible endocytic pathways lead to endosomal entrapment, it has been shown that the mechanism of entry has a considerable influence on the final fate of the nanoparticles and on their ability to release their content in the cytoplasm, but it is supposed that the key relies on the different interactions that take place in each case inside the endosomal vesicles.⁵⁰

⁵⁰ L. I. Selby, C. M. Cortez-Jugo, G. K. Such, A. P. R. Johnston, *Wiley Interdiscip. Rev. Nanomedicine Nanobiotechnology*, **2017**, *9*, e1452.

⁵¹ T.-G. Iversen, T. Skotland, K. Sandvig, *Nano Today*, **2011**, *6*, 176.

⁵² D. Rosenblum, N. Joshi, W. Tao, J. M. Karp, D. Peer, *Nat. Commun.*, **2018**, *9*, 1410.

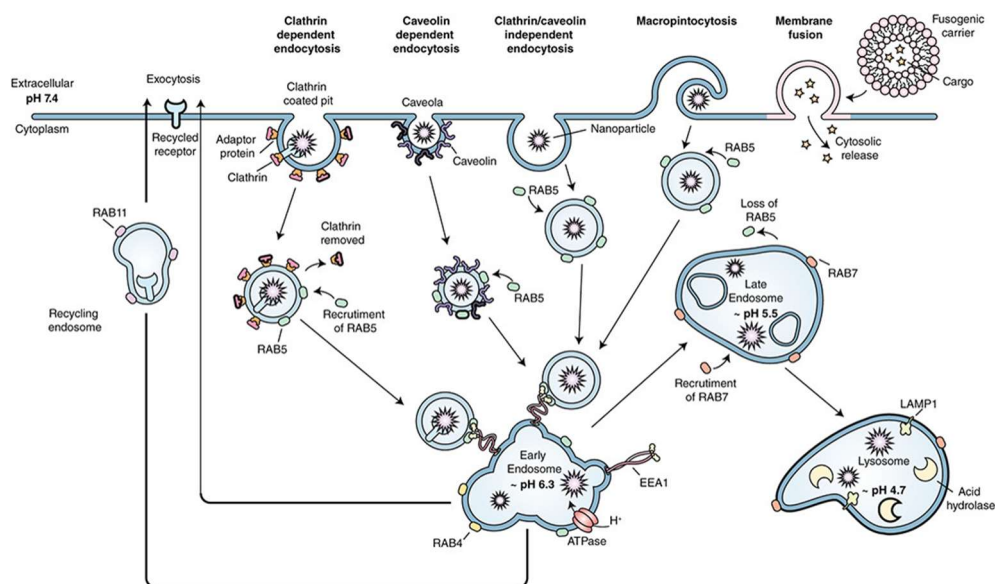


Figure 7. Nanoparticles can be endocytosed into vesicles coated with clathrin, caveolin or by a clathrin/caveolin-independent manner. Macropinocytosis also involves the formation of vesicles. RAB5 is a signalling protein recruited by the vesicles that guides them to early endosomes interacting with the early endosome antigen 1 (EEA1). While the early endosome is recycled back to the cell membrane, its content is trafficked first to late endosomes and finally to lysosomes. Direct translocation of nanocarriers or membran fusion can also occur, leading to cytosolic release. *Reprinted with permission from WIREs Nanomed. Nanobiotechnol.* 2017, 9:e1452. Copyright © 2017 Wiley Periodicals, Inc.

The main interest in nanomedicine is the delivery of active molecules that exert their effect in either the cytosol or the nucleus, especially biomolecules that are too big to spontaneously cross endosomal membranes. Special interest in the recent years has been demonstrated towards nucleic acids delivery. In this context, it has to be taken into account that both siRNAs and miRNAs, directed to the RNA-induced silencing complex (RISC), and mRNAs, directed to the translational machinery, have to be delivered in the cytoplasm, while DNA requires to be further transported to the nucleus.⁵³ Thus, to reach their intracellular targets, nanocarriers have to escape during the first moments after the cellular uptake, before lysosomal

⁵³ H. Yin, R. L. Kanasty, A. A. Eltoukhy, A. J. Vegas, J. R. Dorkin, D. G. Anderson, *Nat. Rev. Genet.*, **2014**, 15, 541.

entrapment. This time span has been quantified in 5-15 minutes for lipid nanoparticles.⁵⁴

Until now, four main strategies have been identified for endosomal escape induction (Figure 8).^{50,52} The most common one is the exploitation of the proton sponge effect, based on the protonation of the amines of cationic polymers in the acid environment of the endosomes; such protonation determines the influx of counter ions and, subsequently, of water, what destabilizes the endosomal membranes due to a high osmotic pressure.⁵⁵ Polyethylenimine (PEI) and PAMAM dendrimers are often associated to this mechanisms, but this topic is deeply debated. Recent studies, although confirming the existence of the proton sponge effect, argue that probably it is not the dominant mechanism in polycationic materials release.⁵⁶ An alternative hypothesis has been proposed: the polymer protonation induces the disassembly of the particle into many subunits, causing this way an osmotic shock that damages endosomal membranes.⁵⁷ The second process inducing endosomal escape regards lipid or amphiphilic materials, whose membranes can fuse with the endosomal membrane releasing the loaded molecules to the cytoplasm. The third strategy is the use of peptides able to interact with endosomal membranes producing small pores, while the fourth one is similar, but based on the use of polymers that originate bigger holes. PEI seems also to be involved in this last mechanism.⁵⁰ Nevertheless, cationic polymers tolerance *in vivo* has yet to be examined more in-depth.

⁵⁴ A. Wittrup, J. Lieberman, *Nat. Rev. Genet.*, **2015**, *16*, 543.

⁵⁵ M. S. Shim, Y. J. Kwon, *Adv. Drug Deliv. Rev.*, **2012**, *64*, 1046.

⁵⁶ R. V Benjaminsen, M. A. Matthebjerg, J. R. Henriksen, S. M. Moghimi, T. L. Andresen, *Mol. Ther.*, **2013**, *21*, 149.

⁵⁷ H. Lomas, M. Massignani, K. A. Abdullah, I. Canton, C. Lo Presti, S. MacNeil, J. Du, A. Blanz, J. Madsen, S. P. Armes, A. L. Lewis, G. Battaglia, *Faraday Discuss.*, **2008**, *139*, 143.

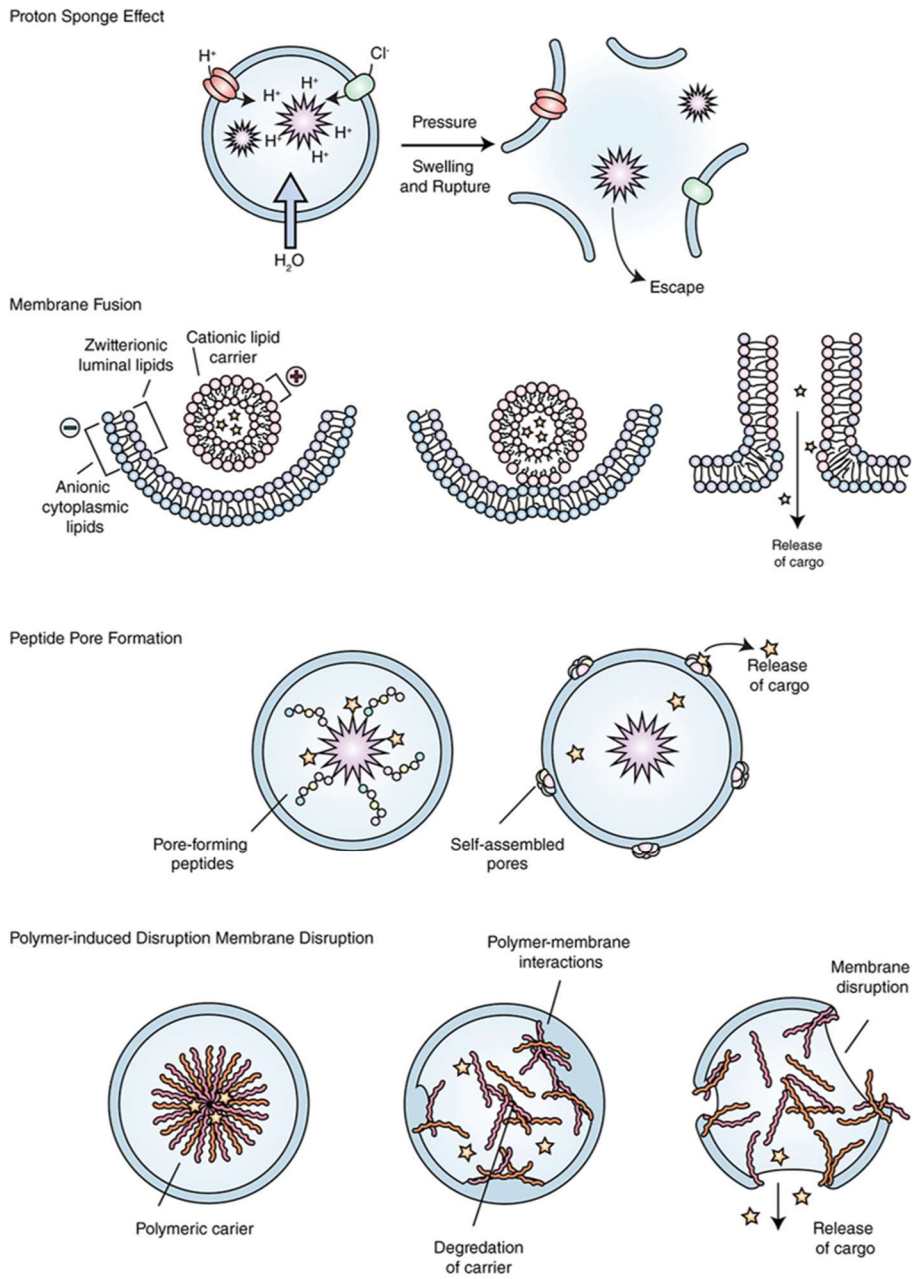


Figure 8. The four mainly described mechanisms of endosomal escape. *Reprinted with permission from WIREs Nanomed. Nanobiotechnol. 2017, 9:e1452. Copyright © 2017 Wiley Periodicals, Inc.*

It is evident the need of a more exhaustive understanding of both the internalization and the endosomal escape mechanisms, maybe possible through a combination of several precise techniques. Especially relevant would be quantifying in a more precise manner the escape efficiency. Nowadays it is studied by fluorescent labelling of the materials or of the cargos and the following analysis of their intracellular distribution, with considerable background and interference issues, by *in vitro* or *ex vivo* membranes leakage assays or by indirect determination through transfection assays, that can potentially confirm the nanoparticles escape without giving any clue about the process.⁵⁰

1.4 Stimuli-responsive release of cargos

Another way to minimize the risk of systemic exposure of non-target tissues to drugs, thus avoiding undesired side effects and drug-plasma interactions, and to increase the site-specific concentration of a drug or of a signalling molecule, is the development of stimuli-responsive nanocarriers for the controlled release of an encapsulated cargo. One of the key points for nanomaterials success in biomedical research is surely the possibility of synthesizing systems able to modify their physicochemical properties in response to external stimuli or environmental conditions, producing a variation in their structure or functions.¹¹ This ability is a perfect illustration of the concept of nanostructures, defined by the EMA as systems with specific properties not obtainable with their isolated individual components, properties that, furthermore, are expected to provide clinical advantages.²⁵

There are several methods to initiate the release of the active molecules entrapped into the carriers, that are generally classified into endogenous and exogenous. Among the first group, the most commonly used are pH, redox potential, osmotic pressure, viscosity, enzymatic activity or presence of specific sequences of nucleic acids, the latter being probably the most adequate ones due

to their high affinity for their substrates.^{9,58} In the second group, instead, temperature, light, electromagnetism and ultrasound can be enumerated; the application of such stimuli, providing a spatiotemporal control over the activation of the nanomaterials, can only be directed to the target tissues allowing to reduce the adverse effects.^{9,58} Nevertheless, the employment of both kinds of stimuli presents some drawback: in case of internal stimuli, it is common that nanomaterials react also to other similar stimuli at undesired sites, while the external ones normally require more costly protocols and present problems related to their depth of penetration in body tissues and to the difficulty to discriminate between healthy and diseased tissues.⁵⁸ A solution to overcome the mentioned issues could be the design of more complex nanosystems responsive to more than one stimulus, likely an endogenous and an exogenous one.

The design of stimuli-responsive delivery strategies can be applied to different kinds of nanotransporters. Polymeric nanocarriers,⁵⁹ self-assembled-DNA nanomaterials,⁶⁰ liposomes⁶¹ and porous inorganic nanodevices⁶² can be tuned in order to obtain structures able to respond to given stimuli. Regarding polymeric nanoparticles, controlled release is generally obtained through four main mechanisms: (I) drug diffusion through water-filled pores, when water is absorbed by the particles and produces enlargement of the pores facilitating drug release, (II) simple diffusion through the polymer matrix, (III) osmotic pumping and (IV) erosion, that exhibits reproducible and controllable kinetics.⁶³ Nevertheless, depending on the polymeric nanocarriers composition, other approaches can be planned through the application of the above-mentioned stimuli. Self-assembled-DNA nanomaterials rely on the predictable nature of DNA base-pairing principle, that

⁵⁸ A. P. Blum, J. K. Kammeyer, A. M. Rush, C. E. Callmann, M. E. Hahn, N. C. Gianneschi, *J. Am. Chem. Soc.*, **2015**, *137*, 2140.

⁵⁹ N. Kamaly, B. Yameen, J. Wu, O. C. Farokhzad, *Chem. Rev.*, **2016**, *116*, 2602.

⁶⁰ Z. Dai, H. M. Leung, P. K. Lo, *Small*, **2017**, *13*, 1602881.

⁶¹ Y. Lee, D. H. Thompson, *Wiley Interdiscip. Rev. Nanomed. Nanobiotechnol.*, **2017**, *9*, e1450.

⁶² E. Aznar, M. Oroval, L. Pascual, J. R. Murguía, R. Martínez-Mañez, F. Sancenón, *Chem. Rev.*, **2016**, *116*, 561.

⁶³ S. Fredenberg, M. Wahlgren, M. Reslow, A. Axelsson, *Int. J. Pharm.*, **2011**, *415*, 34.

permits a highly precise design and modulation of nanostructures.⁶⁴ Rational design of DNA-based nanocarriers is, thus, quite easy and allow to develop pH-sensitive or metal ions-sensitive materials (depending on the abundance of one kind of nitrogenous base or another) or, in case of introducing extra organic or inorganic molecules into the structure, systems able to respond to stimuli related with such extra molecules properties.⁶⁰ Liposomes, as already stated before, are the most studied and used nanomaterials in nanomedicine, so that a wide literature is available about controlled release depending on a broad range of endogenous and exogenous stimuli, for liposomes alone or combined with other nanoparticles, as for example gold nanoparticles.^{61,65} Hybrid mesoporous gated nanomaterials, finally, are generally composed by a porous inorganic support and molecular or supramolecular entities that, once anchored on the external surface, are responsible for the control of the transport of the cargo loaded into the mesopores from inside to outside the pores.⁶² A huge number of possibilities are conceivable, depending on the combination of supports, molecular gates and opening mechanisms of different classes. A schematic representation of controlled release from a mesoporous nanoparticle is depicted in Figure 9.

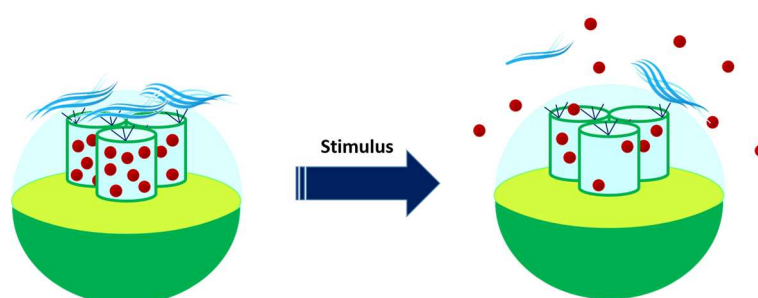


Figure 9. Schematic representation of a stimuli-responsive mesoporous material.

⁶⁴ Z. Li, J. Wang, Y. Li, X. Liu, Q. Yuan, *Mater. Chem. Front.*, **2018**, 2, 423.

⁶⁵ G. Wu, A. Mikhailovsky, H. A. Khant, J. A. Zasadzinski, *Methods in enzymology*, **2009**, 464, 279.

There are several mechanisms through which the response of the nanomaterials to a stimulus can be given. Blum and colleagues, in a detailed review about stimuli-responsive nanomaterials for biomedical applications, described seven main mechanisms:⁵⁸

- direct release: for example, the direct enzymatic cleavage of a molecule or the response to a given pH;⁶⁶ these strategies are easier to design but can result not specific enough;
- expansion: when the particles are able to expand or contract in response to a stimulus, making the release of the entrapped molecules possible; this mechanism is especially interesting for polymeric nanomaterials using pH as triggering stimulus,⁶⁷
- gatekeeping: uses organic or inorganic molecules as molecular gates grafted onto the surface of the nanocarriers; this strategy is commonly used with MSNs with a great variety of gates and stimuli, and presents the same issues than direct release;^{68,69,70}
- disassembly and degradation: can occur following different patterns, as a single- or multiple-event. In the first case, the presence of a stimulus starts the degradation of the material in a one-to-one⁷¹ or cascade⁷² model, being the latter useful for signal amplification; in case of multiple-event triggered degradation, two independent stimuli are needed for the cargo release, increasing the specificity of the system;⁷³

⁶⁶ J.-Z. Du, X.-J. Du, C.-Q. Mao, J. Wang, *J. Am. Chem. Soc.*, **2011**, *133*, 17560.

⁶⁷ A. H. Colby, Y. L. Colson, M. W. Grinstaff, *Nanoscale*, **2013**, *5*, 3496.

⁶⁸ C. de la Torre, L. Mondragón, C. Coll, F. Sancenón, M. D. Marcos, R. Martínez-Mañez, P. Amorós, E. Pérez-Payá, M. Orzáez., *Chem. - Eur. J.*, **2014**, *20*, 15309.

⁶⁹ A. Bernardos, E. Aznar, C. Coll, R. Martínez-Mañez, J. M. Barat, M. D. Marcos, F. Sancenón, A. Benito, J. Soto, *J. Control. Release*, **2008**, *131*, 181.

⁷⁰ A. Ultimo, C. Giménez, P. Bartovsky, E. Aznar, F. Sancenón, M. D. Marcos, P. Amorós, A. R. Bernardo, R. Martínez-Mañez, A. M. Jiménez-Lara, J. R. Murguía, *Chem. - Eur. J.*, **2016**, *22*, 1582.

⁷¹ A. Kumari, S. K. Yadav, S. C. Yadav, *Colloids Surfaces B Biointerfaces*, **2010**, *75*, 1.

⁷² C. Kojima, S. Tsumura, A. Harada, K. Kono, *J. Am. Chem. Soc.*, **2009**, *131*, 6052.

⁷³ S. Samarajeewa, R. Shrestha, M. Elsabahy, A. Karwa, A. Li, R. P. Zentay, J. G. Kostelc, R. B. Dorshow, K. L. Wooley, *Mol. Pharm.*, **2013**, *10*, 1092.

- assembly and aggregation: the assembly of different units into a new structure with additional properties is commonly based on a two-step targeting mechanism, based on the separated administration of two units and the accumulation of the first one due to targeting strategies, and of the second one due to its interaction with the first.⁷⁴ Generally provides a high selectivity;
- morphology switches: as explained before, nanomaterials morphology affects their pharmacokinetics, therefore modifying materials shape in an intentional way can lead to desired consequences in drug delivery;⁷⁵
- autonomous motion: maybe the most challenging mechanism nowadays, it is based on the development of nanomaterials able to move themselves and sensitive to the abundant presence of a given molecule that acts as a fuel. Acoustic waves⁷⁶ and magnetisms⁷⁷ are proper stimuli for these systems.

1.5 Mesoporous silica materials

Silica has been “Generally Recognized As Safe” by FDA, which means that presents satisfactory biocompatibility.⁷⁸ A system developed for cRGDY-peptide-targeted molecular imaging of integrin-expressing cancers, and based on core-shell silica nanoparticles termed Cornell dots, already received FDA Investigational New Drug (IND) approval, and demonstrated adequate safety levels in a pilot clinical trial.⁷⁹ In addition, as previously mentioned, another similar system directed to

⁷⁴ S. D. Perrault, W. C. W. Chan, *Proc. Natl. Acad. Sci. U. S. A.*, **2010**, *107*, 11194.

⁷⁵ J.-Z. Du, H. Y. Long, Y. Y. Yuan, M. M. Song, L. Chen, H. Bi, J. Wang, *Chem. Commun.*, **2012**, *48*, 1257.

⁷⁶ W. Wang, S. Li, L. Mair, S. Ahmed, T. J. Huang, T. E. Mallouk, *Angew. Chem. Int. Ed.*, **2014**, *53*, 3201.

⁷⁷ V. Garcia-Gradilla, J. Orozco, S. Sattayasamitsathit, F. Soto, F. Kuralay, A. Pourazary, A. Katzenberg, W. Gao, Y. Shen, J. Wang, *ACS Nano*, **2013**, *7*, 9232.

⁷⁸ D. Ni, D. Jiang, E. B. Ehlerting, P. Huang, W. Cai, *Acc. Chem. Res.*, **2018**, *51*, 778.

⁷⁹ E. Phillips, O. Penate-Medina, P. B. Zanzonico, R. D. Carvajal, P. Mohan, Y. Ye, J. Humm, M. Gönen, H. Kalaigian, H. Schöder, H. W. Strauss, S. M. Larson, U. Wiesner, M. S. Bradbury,

HER2 receptor is in a phase 2 clinical trial.²⁷ These examples show how silica nanoparticles constitute a promising platform for biomedical applications.

In particular, mesoporous silica nanoparticles (MSNs) represent a valid choice as carriers in nanomedicine due to their unique characteristics such as high internal surface area and pore volume, with a consequent high loading capacity, colloidal stability, tuneable pore size and the possibility to functionalize them with a great variety of organic or inorganic molecules both inside the pores and on the external surface.⁸⁰ Their synthesis, indeed, allows the easy incorporation of functional groups of interest for the loading or grafting of active molecules.¹⁸

According to the definition of the International Union of Pure and Applied Chemistry (IUPAC), mesoporous materials exhibit a pore size range between 2-50 nm, while lower and higher sizes are typical of microporous and macroporous materials, respectively.⁸¹

1.5.1 Ordered mesoporous silica nanomaterials

The development of a family of periodic mesoporous silica with a well-defined pore size distribution between 2-10 nm was carried on in 1992 by researchers from Mobil Oil Company. This class of materials, identified as M41S phases, mainly comprises three kinds of structures: Mobile Crystalline Material (MCM)-41, MCM-48 and MCM-50 with hexagonal, cubic and lamellar arrangement of the mesopores, respectively (Figure 10).⁸² The main characteristics of such materials, in addition to the specific range of pore size, are high specific surface (500-1000 m² g⁻¹), high pore volume (1 cm³ g⁻¹), chemical inertness and thermal stability.

Sci. Transl. Med., **2014**, *6*, 260ra149.

⁸⁰ C. Argyo, V. Weiss, C. Bräuchle, T. Bein, *Chem. Mater.*, **2014**, *26*, 435.

⁸¹ D. H. Everett, *Pure Appl. Chem.*, **1972**, *31*, 577.

⁸² C. T. Kresge, M. E. Leonowicz, W. J. Roth, J. C. Vartuli, J. S. Beck, **1992**, *Nature*, *359*, 710.

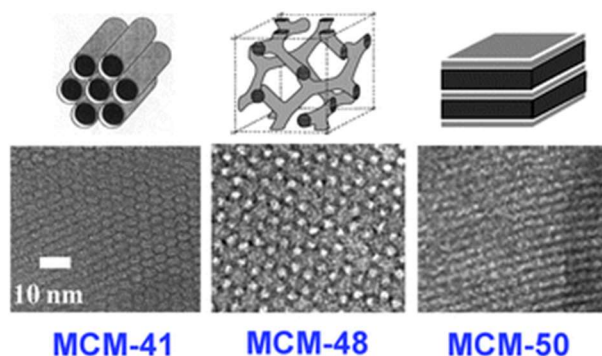


Figure 10. The ordered mesoporous structures of M41S materials family. A representation of the three-dimensional structures (top) and the corresponding transmission electron microscopy (TEM) images of the pores arrangement (bottom) are shown for each kind of material. *Reprinted with permission from Chem. Soc. Rev. 2013, 42, 3663. Copyright © 2013 The Royal Society of Chemistry.*

More than two decades after M41S materials development, ordered mesoporous materials are generally still synthesized by methods that involve liquid templating mechanisms and silica precursors.⁸³ Two possible mechanisms can be followed: the first one is the true liquid-crystal templating (TLCT), in which the high concentration of the surfactant employed as structure-directing agent (SDA) promotes the formation of a lyotropic liquid-crystalline phase that do not require the presence of the silica precursor. On the other hand, the second process is the cooperative liquid-crystal templating mechanism, that allows the generation of the lyotropic liquid-crystalline phase even at lower concentration of surfactant if there is a cooperative self-assembly of the SDA with the already added inorganic precursor.⁸⁴

The TLCT is the method employed in this PhD thesis for the synthesis of ordered mesoporous nanomaterials. When the ionic surfactant reaches its critical micelle concentration, cylindrical micelles are formed. Supramolecular aggregates of surfactant micelles are used as a template for the silica precursor deposition. Polymeric silica precursors are obtained from different sources of silica like sodium

⁸³ Z. ALOthman, ALOthman, Z. A., *Materials (Basel)*, **2012**, *5*, 2874.

⁸⁴ F. Hoffmann, M. Cornelius, J. Morell, M. Fröba, *Angew. Chemie Int. Ed.*, **2006**, *45*, 3216.

silicate, tetraethyl orthosilicate (TEOS) or tetramethyl orthosilicate (TMOS). Different tailored mesostructured morphologies and sizes can be obtained controlling the synthesis parameters (especially surfactant chemical nature and concentration) as the surfactant can assemble acquiring several mesophases and morphologies.⁸⁵ Following the increase of surfactant concentration, the micelles form hexagonal, cubic or laminar phases. In a second step of the reaction, the polymeric precursor is added and hydrolysed, so that the oligomeric silicates and the surfactant micelles spontaneously assemble providing a rigid material with a determined porous geometry. The last step to obtain a final ordered mesoporous material is the removal of the surfactant from inside of the mesopores, that can be achieved by extraction with adequate solvents or by aerobic high temperature calcination. Additional reaction parameters that can influence the final result are pH, temperature, water content and ionic strength of the reaction mixture, as well as time and the kind of silica source, thus giving materials with different diameter, volume and wall thickness of the pores. It is important to emphasize that at larger pore volumes correspond thinner silica walls, that are related with better biodegradation.⁸⁵

The most studied and commonly used ordered mesoporous material from M41S family is the hexagonal mesostructured MCM-41, generally obtained at basic pH values (whereby the silica species are present as anions) from TEOS polymerization around supramolecular aggregates of the cationic surfactant cetyltrimethylammonium bromide (CTAB) micelles. The synthetic process for obtaining MCM-41-like silica mesoporous materials through TLCT method is resumed in Figure 11.

⁸⁵ S.-H. Wu, C.-Y. Mou, H.-P. Lin, *Chem. Soc. Rev.*, **2013**, *42*, 3862.

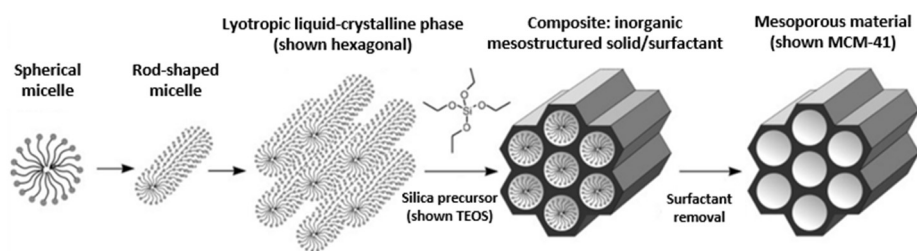


Figure 11. Formation of mesoporous materials using structure-directing agents and following a true liquid-crystal template mechanism. Adapted from *Angew. Chem. Int. Ed.* 2006, 45, 3216. Copyright © 2006 Wiley-VCH.

The inorganic structures obtained through the described method have a huge value for the development of hybrid organic-inorganic materials, especially appealing for combining both the stability and robustness of the inorganic support and the wide functional possibilities of the organic chemistry. There are three possible ways to incorporate organic functional groups into silica mesoporous structures: the grafting procedure, that implicates a subsequent modification of the pore surface of a pure inorganic silica material; the co-condensation method, that involves the simultaneous addition of the silica precursor and organosilanes and leads to materials with organic moieties covalently attached to the pore walls; finally, the incorporation of organic groups as bridging components directly into the pore walls allowing an homogeneous distribution in the material and the production of periodic mesoporous organosilicas (PMOs).⁸⁴

The ordered mesoporous nanomaterials developed in this thesis were functionalized by grafting organic groups onto the silica surface. The surface of the synthesized silica nanomaterials is rich in free silanol groups (Si-OH) that react with organosilanes of different kinds, being the most commonly used the type (R'O)₃SiR trialkoxysilane derivative, that give a nucleophilic substitution (Figure 12).⁸⁴ Diversification of the organic residue R' allows to achieve a large variety of functionalized hybrid materials that keep the starting mesostructural features but present improved surface properties, as for example a given surface reactivity or the protection of the surface against chemical attacks.

A further step in the development of ordered mesoporous nanostructures is represented by the so-called SBA-15 material, with hexagonal pores arrangement, obtained at acidic pH values using triblock polyoxyalkylene copolymers as templates.⁸⁶ This method allows to achieve a pore size range of 5-30 nm.

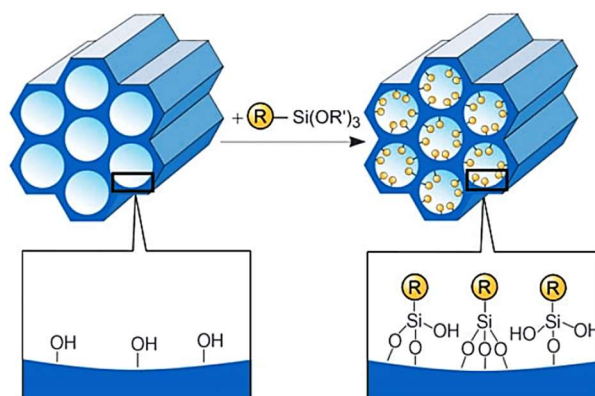


Figure 12. Post-synthetic functionalization of a pure silica mesoporous scaffold by grafting procedure with type $(R'O)_3SiR$ trialkoxysilane derivative. R: organic functional group. Adapted from *Angew. Chem. Int. Ed.* 2006, 45, 3216. Copyright © 2006 Wiley-VCH.

1.5.2 Dendrimer-like mesoporous silica nanomaterials

Following the inception of template-directed synthesis of mesoporous silica materials, countless studies have been carried out on generating a large variety of products with different morphologies. Nevertheless, a further step in the evolution of mesoporous silica materials is the development of dendrimer-like particles with three-dimensional centre-radial channels and hierarchical pores, with gradually augmented pore sizes from the interior of the particle to the surface (Figure 13). These materials exhibit unique structural properties that improve conventional mesoporous materials. In dendrimer-like mesoporous silica there are no ordered

⁸⁶ D. Zhao, J. Feng, Q. Huo, N. Melosh, G. H. Fredrickson, B. F. Chmelka, G. D. Stucky, *Science*, **1998**, 279, 548.

structures as for M41S family materials. Non-uniform pores with different length scales from micro- to mesopores, and even macropores in some cases, constitute hierarchical architectures that provide several advantages. In fact, larger pore sizes and volumes, enhanced surface areas and highly accessible inner spaces facilitate the interactions with other species and harmonize the diffusion process of cargo molecules with different sizes while allowing their simultaneous loading.⁸⁷ Such features are of special interest in applications that necessitate significant mass transport, as can be the field of drug or active molecules delivery, as they permit an easy loading of large amounts of cargo or even of other kinds of nanoparticles with theranostic functionalities.

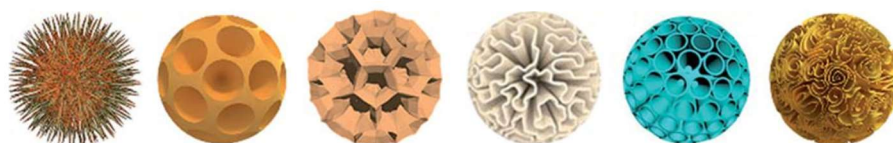


Figure 13. General morphological models for spherical dendrimer-like mesoporous silica nanoparticles. Adapted from *J. Mater. Chem. A* 2019, 7, 5111. Copyright © 2019 The Royal Society of Chemistry.

The first reported synthesis of dendritic-like mesoporous silica particles dates back to 2010, when the KCC-1 high-surface area silica nanospheres with fibrous morphology were developed. The synthesis of KCC-1 nanospheres uses cetylpyridinium bromide or CTAB as template and TEOS as silica precursor, hydrolyzed by urea.⁸⁸ Monodispersed colloidal spheres of sizes between 250-450 nm and fibres growing uniformly from the centre of the sphere along the free radial directions were obtained this way. Figure 14 shows representative images of KCC-1 material; the scanning electron microscopy (SEM) image displays irregular-shaped pores between the nanowrinkles appearing on the surface of the nanosphere. Their diameters vary between 11-35 nm.

⁸⁷ Y. Wang, X. Du, Z. Liu, S. Shi, H. Lv, *J. Mater. Chem. A*, **2019**, 7, 5111.

⁸⁸ V. Polshettiwar, D. Cha, X. Zhang, and J. M. Basset, *Angew. Chem. Int. Ed.*, **2010**, 49, 9652.

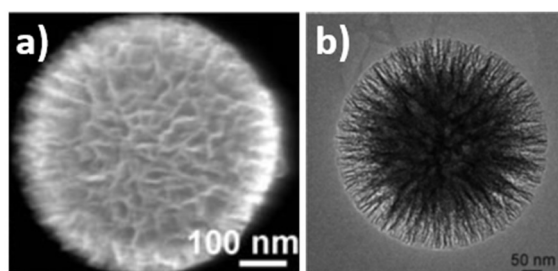


Figure 14. a) Scanning electron microscopy (SEM) image of KCC-1 nanospheres. b) High-resolution transmission electron microscopy image of KCC-1 nanospheres. *Adapted from Angew. Chem. Int. Ed. 2010, 49, 9652. Copyright © 2010 Wiley-VCH.*

Nevertheless, generally dendrimer-like mesoporous silica materials present too large sizes, of more than 200 nm, for a safe and non-toxic application in a biological context. In 2013, the large-scale synthesis of monodispersed dendrimer-like silica nanoparticles with size less than 130 nm was achieved. Three morphologically different kinds of materials were developed using three different types of small organic amines, triethyleneamine, triethanolamine or 2-amino-2-(hydroxymethyl)propane-1,3-diol.⁸⁹ Cetyltrimethylammonium *p*-toluenesulfonate (CTATos) was employed as templating surfactant and triethyleneamine acted as mineralizing agent for the synthesis of stellate particles (Figure 15), while CTAB and triethanolamine or 2-amino-2-(hydroxymethyl)propane-1,3-diol were used for the synthesis of raspberry or worm-like materials, respectively, also modifying the pH of the reaction and the amines concentrations.⁸⁹ TEOS was used in all cases as silica precursor. As the synthesis is carried on with a surfactant concentration lower than its critical micelle concentration, a cooperative templating mechanism is proposed for the nanoparticle generation, with self-assembly of partially silicated micelles. Furthermore, a block-by-block aggregation process is suggested due to the imperfect-centred stellate morphology.⁸⁹

⁸⁹ K. Zhang, L.-L. Xu, J.-G. Jiang, N. Calin, K.-F. Lam, S.-J. Zhang, H.-H. Wu, G.-D. Wu, B. Albelá, L. Bonneviot, P. Wu, *J. Am. Chem. Soc.*, **2013**, *135*, 2427.

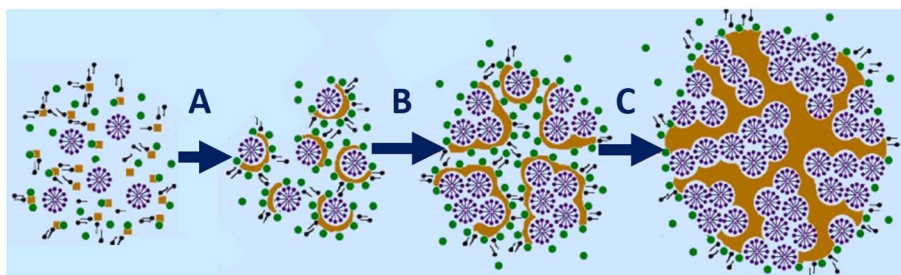


Figure 15. Stellate mesoporous nanoparticles formation employing CTATos and triethylamine. A) Partly silicated micelles. B) Block formation. C) Block aggregation into a stellate morphology. *Adapted from J. Am. Chem. Soc. 2013, 135, 2427. Copyright © 2013 American Chemical Society.*

The dendrimer-like mesoporous silica nanoparticles developed for this thesis have been synthesized following a reported method based on the illustrated synthesis of stellated materials and employed for the generation of nanoparticles with a size of 90-120 nm and centre-radial large pores with a diameter range of 8-40 nm, used for successful in vitro gene delivery.⁹⁰

Dendrimer-like mesoporous silica materials are gaining attention due to their improved features. They can be chemically modified with functional groups of interest in the same way than the silica ordered materials, thanks to the presence of silanols on their surface and by similar grafting or co-condensation procedures. Although several applications for this kind of materials are possible, the most valuable one in the nanomedicine field is maybe the transport and delivery of encapsulated nucleic acids, as MCM-41-like nanoparticles has relatively small pore size to accommodate such biomacromolecules inside.

1.5.3 Gated mesoporous silica nanomaterials

Considering the possibility of finely manipulating mesopores size, morphology and interconnection and of combining precisely designed mesoporous silica nanomaterials with molecular or supramolecular functionalities, it is easy to

⁹⁰ X. Du, L. Xiong, S. Dai, F. Kleitz, S. Zhang Qiao, *Adv. Funct. Mater.*, **2014**, *24*, 7627.

understand how such hybrid materials have attracted high interest as scaffolds for selective sensing and delivery applications. The gatekeeping mechanism is undoubtedly the most commonly used to develop stimuli-responsive system based on MSNs or LP-MSNs. In this scheme, switchable entities attached on the external surface of mesoporous supports not only avoid the early release of the cargo, but allow its specific spatio-temporal delivery upon the application of an external stimulus or in response to given changes in the biological environment in which they are administered.

As for the other types of nanomaterials applied in nanomedicine, several kinds of stimuli can be used and transduced into predefined responses in controlled release strategies that employ mesoporous nanosilica. On one hand, the endogenous specific conditions of pH, redox processes, molecules concentration and enzymatic activity can determine gates opening, while, on the other hand, exogenous stimuli carried out via an external physical treatment as light, temperature, alternating magnetic field and ultrasound, can be applied.^{62,91,92} Generally, the gating responses depend on a combination of charge, local interactions and steric effects of the distinct components that occupy the pore.⁹¹

Specifically, in the works reported in this PhD thesis two of the available endogenous mechanisms have been exploited: the lysosomal enzymatic activity and the endosomal-lysosomal pH.

Enzymatic activity represents an appealing triggering stimulus for the design of gated mesoporous nanoparticles, as provides a great variety of possibilities for the selection of the organic derivative/enzyme pair allowing high selectivity in cargo delivery. Oxidoreductases, transferases, hydrolases, lipases, nucleases, phosphatases, glycosidases, lyases, isomerases and ligases are the most common enzymes involved in the development of stimuli-responsive systems.⁹³

⁹¹ S. Alberti, G. J. A. A. Soler-Illia, O. Azzaroni, *Chem. Commun.*, **2015**, 51, 6050.

⁹² Y. Song, Y. Li, Q. Xu, Z. Liu, *Int. J. Nanomedicine*, **2016**, 2017, 87.

⁹³ A. Llopis-Lorente, B. Lozano-Torres, A. Bernardos, R. Martínez-Mañez, F. Sancenón, *J. Mater. Chem. B*, **2017**, 5, 3069.

Bearing in mind that most of the nanocarriers enter cells via receptor-mediated endocytosis, it should be noted that lysosomes contain a wide pattern of degradative enzymes specific to a wide range of substrates, including lipids, proteins, nucleic acids, carbohydrates and biological polymers.⁹⁴ An example of MSNs opened by a lysosomal enzyme is a system designed for doxorubicin delivery capped with a peptide for site-specific cleavage by cathepsin-B (Figure 16).⁶⁸ The external surface of MSNs was functionalized with 3-(azidopropyl) triethoxysilane and an alkynyl-derivatised peptide (alkynyl-GIV RAK EAE GIV RAK-OH) was attached through a click reaction with the azidopropyl groups. The release of the loaded cargo was achieved only in cell lines expressing the required enzyme, and not in presence of specific enzyme inhibitors.

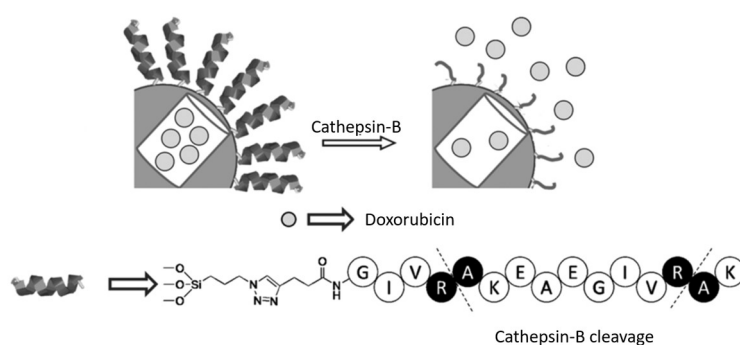


Figure 16. Schematic representation of aMSN functionalized with 3-(azidopropyl)triethoxy-silane and capped with a peptide for the cargo controlled delivery based on the selective cleavage of the peptide by cathepsin-B. Adapted from *Chem. Eur. J.* 2014, 20, 15309. Copyright © 2014 Wiley-VCH.

Variation of pH in different biological compartments (extracellular space/endosomal-lysosomal vesicles, or normal tissues/tumour or inflammatory tissues) is the most usual stimulus applied to gated materials in nanomedicine. Mesopores opening in pH-driven systems can be produced by changes in size or shape, or by attraction/repulsion interactions with charged species due to proton

⁹⁴ B. Rathore, K. Sunwoo, P. Jangili, J. Kim, J. H. Kim, M. Huang, J. Xiong, A. Sharma, Z. Yang, J. Qu, J. S. Kim, *Biomaterials*, **2019**, 211, 25.

addition or abstraction.⁶² Multilayered polyelectrolytes are commonly used as blocking materials in pH-responsive mesoporous structures for cargo delivery, due to the effect of pH on the interactions between the different polyelectrolyte layers.⁹¹ One of the first examples of pH-driven release platform based on mesoporous silica rods took advantage of the oppositely charged ionic interaction between carboxylic acid modified SBA-15 rods and poly(dimethyldiallylammonium chloride), a cationic polyelectrolyte.⁹⁵ The designed nanodevice allowed to achieve a controlled release of vancomycin at acidic pH values, as once the ionized carboxylate groups (COO^-) were protonated (COOH), the interaction with the polycation was weakened producing its removal from the rods surface (Figure 17).

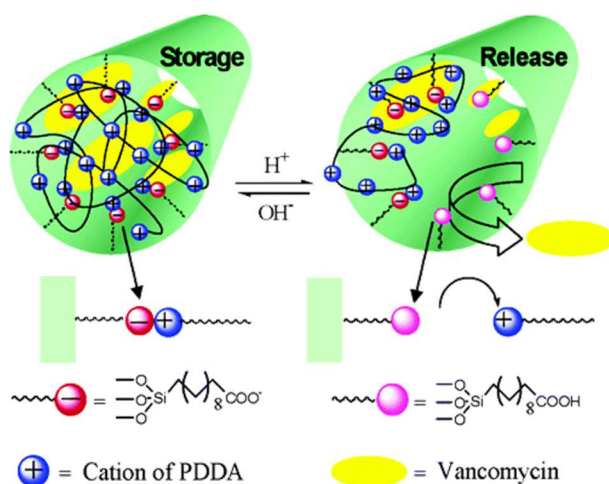


Figure 17. Schematic representation of a pH-responsive drug delivery system based on the interaction between negative carboxylic acid modified SBA-15 silica rods with poly(dimethyldiallylammonium chloride) (PDDA). Reprinted with permission from *Chem. Mater.* 2005, 17, 5999. Copyright © 2005 American Chemical Society.

PEI can be used itself as delivery vehicle, but can also be employed as molecular gate if attached to mesoporous nanoparticles through covalent or electrostatic interactions. An example of that is the external functionalization with 3-trihydroxysilylpropyl methylphosphonate, and in a second step with PEI, of MSNs

⁹⁵ Q. Yang, S. Wang, P. Fan, L. Wang, Y. Di, K. Lin, F.-S. Xiao, *Chem. Mater.*, **2005**, 17, 5999.

designed to transport plasmids, siRNA and paclitaxel presented by Zink and co-workers.⁹⁶ While plasmids and siRNA were adsorbed into the polymeric coating, paclitaxel was loaded into the mesopores. PEI protonation in the endosomes allowed the cytosolic delivery of the external plasmids and siRNA, but at the same time the release of paclitaxel from inside the pores, confirming its ability to act as responsive entity for on-command release.

In conclusion, using lysosomal enzymes or pH as release triggering stimuli provides the opportunity to develop autonomous controlled delivery systems, even though it can result in unintentional opening of the gated nanocarriers in non-target cells. Nevertheless, the powerful combinations of stimuli potentially available for the design of gated MSNs are expected to offer remarkable applications in nanomedicine.

⁹⁶ T. Xia¹, M. Kovochich, M. Liong, H. Meng, S. Kabehie, J. I. Zink, A. E. Nel, *ACS Nano*, **2009**, *3*, 3273.

Chapter 2: Objectives

The field of nanomedicine has gained great attention in the last two decades, due to the appropriateness of nanomaterials as active molecules carriers and their high potential impact in the development of novel approaches for unmet medical needs.

In this context, this PhD thesis has been focused on the design, synthesis, characterization and *in vitro* evaluation of new hybrid organic-inorganic nanosystems as innovative strategies for the targeted and controlled delivery of therapeutic molecules.

The specific objectives that have been addressed are:

- To develop a doxorubicin delivery system, targeted to TLR3 receptor thanks to its external functionalization with poly(I:C) moieties, applied to the treatment of breast cancer.
- To design of a stigmergic cooperation approach based on two different sets of nanodevices, with the aim to obtain an enhanced therapeutic effect in breast cancer.
- To develop a high capacity nanodevice based on dendrimer-like mesoporous silica nanoparticles for the topical and controlled administration of siRNA molecules to the retinal pigmented epithelial cells.

***Chapter 3: Targeting Innate Immunity with
dsRNA-Conjugated Mesoporous Silica
Nanoparticles Promotes Anti-Tumor Effects
on Breast Cancer Cells***

Targeting Innate Immunity with dsRNA-Conjugated Mesoporous Silica Nanoparticles Promotes Anti-Tumor Effects on Breast Cancer Cells

Amelia Ultimo,^{+[a,b]} Cristina Giménez,^{+[a,b]} Pavel Bartovsky,^[a,b] Elena Aznar,^[a,b] Félix Sancenón,^[a,b] M. Dolores Marcos,^[a,b] Pedro Amorós,^[c] Ana R. Bernardo,^[d] Ramón Martínez-Mañez,^{*[a,b]} Ana M. Jiménez-Lara^{*[d]} and José R. Murguía^[a,b]

[a] A. Ultimo, Dr. C. Giménez, Dr. P. Bartovsky, Dr. E. Aznar, Dr. F. Sancenón, Dr. M.D. Marcos, Prof. R. Martínez-Mañez, Dr. J.R. Murguía
Centro de Reconocimiento Molecular y Desarrollo Tecnológico (IDM). Unidad Mixta Universitat Politècnica de València-Universitat de València. Camino de Vera s/n 46022, Valencia, Spain

[b] A. Ultimo, Dr. C. Giménez, Dr. P. Bartovsky, Dr. E. Aznar, Dr. F. Sancenón, Dr. M.D. Marcos, Prof. R. Martínez-Mañez, Dr. J.R. Murguía
CIBER de Bioingeniería, Biomateriales y Nanomedicina (CIBERBBN)
E-mail: rmaez@qim.upv.es

[c] Dr. P. Amorós
Instituto de Ciencia de los Materiales (ICMUV), Universidad de Valencia, Valencia, Spain

[d] Dr. A.R. Bernardo, Dr. A.M. Jiménez-Lara
Instituto de Investigaciones Biomédicas A. Sols CSIC-UAM. Arturo Duperier, 4, 28029 Madrid, Spain
E-mail: amjimenez@iib.uam.es

Published online: January 7, 2016

(Reprinted with permission from *Chem. Eur. J.* 2016, 22, 1582-1586.

Copyright © 2016, WILEY-VCH Verlag GmbH & Co. KGaA, Weinheim)

3.1 Abstract

We describe herein a Toll-like receptor 3 (TLR3) targeting delivery system based on mesoporous silica nanoparticles capped with the synthetic double stranded RNA polyinosinic-polycytidylic acid (poly(I:C)) for controlled cargo delivery in SK-BR-3 breast carcinoma cells. Our results show that poly(I:C)-conjugated nanoparticles efficiently targeted breast cancer cells due to dsRNA-TLR3 interaction. Such interaction also triggered apoptotic pathways in SK-BR-3, significantly decreasing cells viability. Poly(I:C) cytotoxic effect in breast carcinoma cells was enhanced by loading nanoparticles' mesopores with the anthracyclinic antibiotic doxorubicin, a commonly used chemotherapeutic agent.

3.2 Introduction

Breast cancer is the most commonly diagnosed malignancy and the deadliest among women worldwide, accounting for 25% of all cancer cases and 15% of all cancer deaths.^[1] Breast cancer incidence is especially high in developed countries, where it seems to be destined to augment due to the expected increase of the elderly population; more than 40% of breast cancer patients, in fact, are women aged over 65.^[2] Therefore, improving existing breast cancer treatment strategies, that still present significant adverse effects or limited efficacy in some molecular subtypes of the disease and in metastatic patients, is a medicinal challenge.

An interesting field in cancer-fighting research is immunotherapy, not directed to eliminate cancer cells but to activate and enhance the innate immune system performance against tumours.^[3] In recent years different kinds of immunotherapeutic approaches have been developed following two main paths: immune checkpoints blockade, to avoid immunosuppressive mechanisms often

enhanced in tumours, and the use of ligands for Toll-like receptors (TLRs) to potentiate immune stimulatory pathways. In the present work, we focused on this second option, taking into account the fact that the innate immunity receptors TLRs are functionally expressed in different types of tumour cells, where they may influence cancer growth and host immune responses.^[4]

Currently, only few TLRs ligands have US Food and Drug Administration approval: Imiquimod, a TLR7 agonist used for the treatment of non-invasive transitional cell carcinoma of the bladder, and two TLR2/TLR4 agonists, the bacillus Calmette-Guérin (BCG), applied to superficial basal cell carcinoma, and the monophosphoryl lipid A (MPL), approved as a component of the human papillomavirus (HPV)-16/18 vaccine.^[5] However, another interesting compound that has shown cytotoxic effects in different types of cancer is polyinosinic-polycytidylic acid (poly(I:C)), a synthetic dsRNA agonist of TLR3. dsRNA efficacy in oncologic treatments was tested in different studies carried out between the 1970s and 1990s. In the last decade, Salaun and co-workers not only found that poly(I:C) can directly kill cancer cells of different breast cancer cell lines, inducing apoptosis through a complex pathway that determines the production of type I interferons and the consequent activation of the apoptotic effector caspase 3, the death ligand TRAIL and the tumour suppressor protein p53, but also demonstrated that breast carcinoma patients overexpressing TLR3 respond adequately to dsRNA adjuvant treatments.^[6]

From another point of view the design of gated silica mesoporous materials for mass transport and controlled release has recently attracted a great attention. Since the first example reported by Fujiwara and co-workers in 2003,^[7] several mesoporous gated materials displaying controlled release triggered by target chemical,^[8] physical^[9] and biochemical^[10] stimuli have been described. Furthermore, the possibility of retaining the cargo and releasing it on command and spatiotemporally is a relevant feature that makes this technology suitable for the development of new efficient and safe drug-delivery nanodevices. In this context, mesoporous silica nanoparticle (MSN) supports are widely used in nanomedicine applications thanks to their unique characteristics, such as high homogeneous

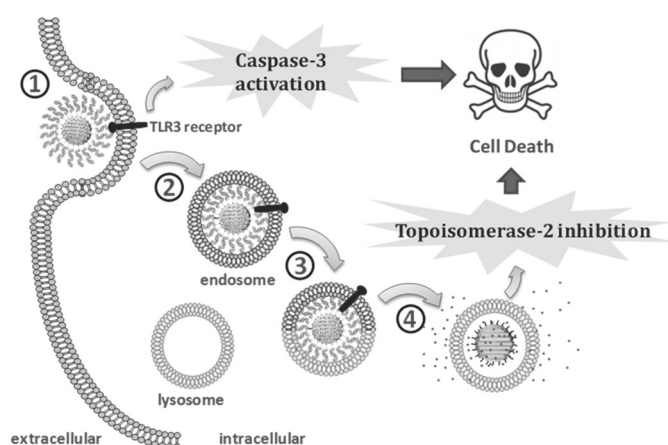
porosity, inertness, robustness, thermal stability and high loading capacity.^[11] Owing to their properties, these supports have been reported to be able to act as multifunctional delivery platforms for the controlled release of therapeutic agents for the treatment of a wide variety of disease models, including cancer models, at cellular and *in vivo* levels.^[12] MSNs are able to enclose and protect hydrophobic and hydrophilic drugs during their transport, overcoming common issues such as poor solubility and stability or the existence of undesired side effects.^[13] In addition, surface functionalization with specific targeting moieties allows these nanodevices to gain selectivity towards specific cells types.^[14] In order to achieve this, specific biomolecules the receptors for which are overexpressed in target cells can be anchored to the surface of the nanoparticles. To date, several specific ligands of overexpressed cancer cell receptors have been studied^[15] as a step forward to an active and specific tumour-targeting strategy. However, this is still an incipient area of research using MSNs and there is a need for further studies.

In this context, and bearing in mind the interest in the design of new delivery systems, we were interested in attempting the design of targeted delivery nanoparticles to breast cancer cells. In this scenario, despite the use of ligands for TLR3 (such as poly(I:C)) in certain clinical studies, their combination with nanoparticles has not been reported yet. Here, we describe a targeting delivery system based in MSNs decorated with synthetic dsRNA (poly(I:C)), as a novel vehicle for drug delivery in breast cancer cells. We took advantage of a breast cancer cell system (SK-BR-3) which expresses TLR3^[16] to characterize the effect of dsRNA-conjugated nanoparticles in tumour-cell viability. Our delivery system is depicted in Scheme 1. It is based on the use of MSNs as carrier support, loaded with a suitable reporter (i.e., sulforhodamine B, **S1** material) or with a cytotoxic drug (i.e., doxorubicin, **S2** material) and externally functionalized with the synthetic double-stranded RNA poly(I:C) that would block the pores thus inhibiting cargo release. Since TLR3 is located in the plasma membrane and in the endosomal compartment, we speculated that poly(I:C) would interact with TLR3, resulting in caspase-3 activation and receptor-mediated endocytosis of the nanoparticles in breast cancer cells. Once endocytosed, lysosomal enzymes would degrade the poly(I:C) chains,

induce the uncapping of the pores and release the entrapped guest. In the case of the **S2** nanoparticle, loaded with doxorubicin, a synergistic effect was expected due to the action of poly(I:C) and the cytotoxicity of doxorubicin through topoisomerase-2 inhibition.^[17]

3.3 Results and discussion

In order to prepare the gated nanodevices, silica mesoporous (MCM-41-type) nanoparticles were selected as inorganic scaffolds. Calcined MCM-41 nanoparticles were loaded with a suitable dye (sulforhodamine B) and the external surface was functionalized with 3-aminopropyltriethoxysilane. Then, the reaction of the anchored amino groups with the previously activated phosphate groups of poly(I:C) chains resulted in a poly(I:C)-functionalized solid (**S1**; see the Supporting Information for details).



Scheme 1. Expected performance of **S2** material in SK-BR-3 breast cancer cells. 1) Poly(I :C) decorated MSNs recognition by TLR3 and receptor-mediated endocytosis; TLR3 activation triggers the apoptotic cascade; 2) MSNs entrapment in the endosome; 3) Intracellular transport and endosome fusion with the lysosome; 4) MSNs degradation by lysosomal digestive enzymes and doxorubicin release. Doxorubicin intercalation into DNA causes topoisomerase II inhibition by stabilization of the DNA-topoisomerase-2 complex, leading to cell death.

The structure of the starting MSNs and of the final **S1** material was confirmed by X-ray diffraction and TEM studies (Figure 1). The X-ray diffraction pattern of **S1** showed the characteristic diffraction peak (100) indicating that the structure of the mesoporous scaffold was not modified by the dye-loading process and functionalization to obtain the capped material. N₂ adsorption-desorption isotherm of **S1** (see the Supporting Information) was typical of capped mesoporous systems, and a significant decrease in the N₂ volume adsorbed and surface area (116.5 m² g⁻¹) was observed when compared with the starting MCM-41-based MSNs (1045.7 m² g⁻¹). Moreover, the content of 15.6 mg g⁻¹ SiO₂ of dye and 191.8 mg g⁻¹ SiO₂ of poly(I:C) on solid **S1** were determined by elemental analysis and thermogravimetric studies.

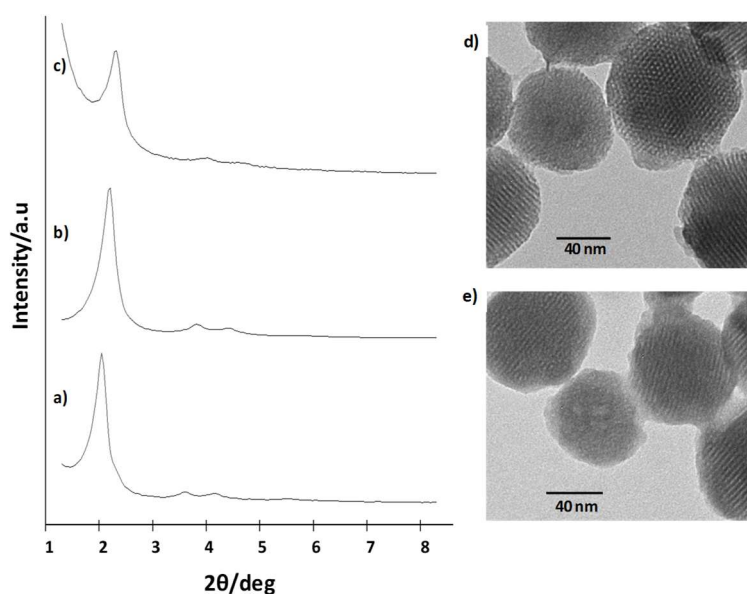


Figure 1. Powder X-ray diffraction pattern of: a) as made MCM-41, b) calcined MCM-41, and c) solid **S1** showing the typical reflections of MCM-41 hexagonal array. TEM representative images of: d) calcined MCM-41, and e) solid **S1** showing typical porosity of MCM-41 mesoporous matrix.

To test the gating properties of the solid, *in vitro* studies of sulforhodamine B delivery from MSNs **S1** were performed.

In a typical experiment, 1 mg of **S1** was suspended in 500 mL of deionized water. The suspension was divided into two aliquots of 250 mL and 1 mL of 10 mM PBS or 1 mL of purified lysosomal extract was added. The purified lysosomal extract was obtained using the lysosome isolation kit (LYSISO1). The suspensions were stirred and aliquots were taken at scheduled times. The amount of dye released from **S1** was determined by monitoring sulforhodamine B emission in the solution as a function of time ($\lambda_{\text{ex}}=554 \text{ nm}$, $\lambda_{\text{em}}=575 \text{ nm}$). In PBS medium, a poor delivery was found (Figure 2) indicating that most of the dye remained in the nanoparticles. In contrast, in the lysosomal extract media a large release of sulforhodamine B was observed. This was attributed to the enzymatic degradation of poly(I:C) chains which resulted in cargo delivery. The obtained results confirmed the triggering event hypothesis, that is, whereas solid **S1** displayed a very low release, the presence of lysosomal enzymes induced the delivery of the entrapped guest.

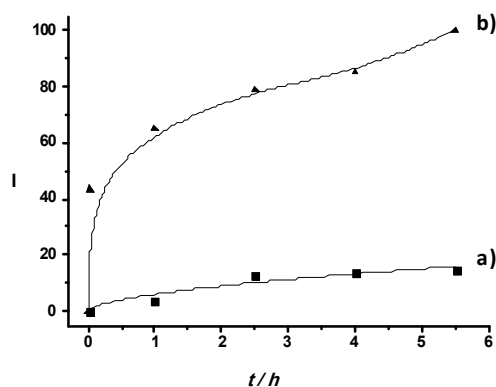


Figure 2. Sulforhodamine B release profile from solid **S1**: a) in 10 mM PBS medium, and b) in the presence of purified lysosomal extract.

Controlling cell targeting and penetrability of drugs is an important issue in modern medicine. Therefore, after demonstrating the effective capping and delivery in lysosomal extract of **S1**, we evaluated **S1**-induced TLR3 internalization in breast cancer SK-BR-3 cells, which express high levels of the membrane receptor TLR3.

As stated above, interaction of the TLR3 receptor with poly(I:C) has been described to induce its rapid internalization and to trigger caspase-3 activation and cell death. In order to demonstrate the interaction of nanoparticles **S1** with TLR3, followed by internalization, cargo delivery and cell death, we evaluated the effect of the nanoparticles on SK-BR-3 cells. In a typical experiment SK-BR-3 cells were incubated for 48 h with **S1**, and sulforhodamine B release was monitored by confocal microscopy. Remarkably, **S1**-treated SK-BR-3 cells clearly exhibited sulforhodamine B release from nanoparticles (Figure 3).

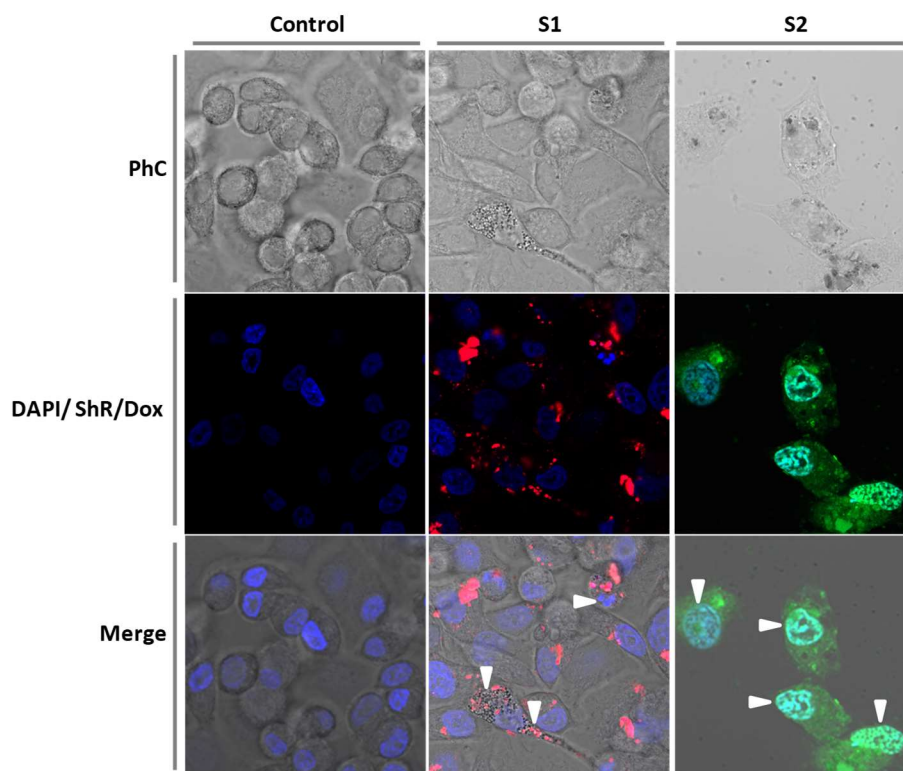


Figure 3. Internalization and release of sulforhodamine B or doxorubicin by **S1** and **S2** nanoparticles, respectively, in SK-BR-3 cells. Cells were treated with $50 \mu\text{g mL}^{-1}$ of equivalent poly(I:C) in **S1** or **S2** nanoparticles for 48 h. DAPI nuclei staining was carried out before confocal microscope observation. Representative phase contrast (PhC), DAPI, sulforhodamine B (ShR), doxorubicin (Dox) and combined (Merge) images are shown. White symbols indicate apoptotic cell degradation (nuclear fragmentation, cytoplasmic degeneration). In **S2**-treated cells DAPI and doxorubicin co-localize in the nuclei.

In another step, we evaluated the effect of **S1** on the viability of SK-BR-3 cells. Figure 5a shows dose-response experiments after 48h when using **S1** as a function of the amount of poly(I:C) in the nanoparticles. As seen, treatment with **S1** nanoparticles produced a decrease in SK-BR-3 cell viability with IC_{50} values of about $10^2 \mu\text{g mL}^{-1}$. As stated above it has been reported that poly(I:C) can directly kill cancer cells inducing apoptosis and therefore cell viability of free poly(I:C) on SK-BR-3 cells was also evaluated using a similar experimental procedure to that followed for **S1**. However, in this case the amount of poly(I:C) of about $10^3 \mu\text{g mL}^{-1}$ was only able to reduce cell viability to approximately 80%. These experiments allowed us to conclude that poly(I:C) is much more effective in killing SK-BR-3 cells when incorporated in **S1**, compared with free poly(I:C), most likely due to an “enhanced concentration effect” due to the presence of a large amount of poly(I:C) on the surface of **S1**.

Moreover, in order to corroborate the specific targeting of **S1** in SK-BR-3 cells, we also performed competition assays with the TLR3-dsRNA complex inhibitor from Calbiochem. In these experiments, the viability of SK-BR-3 cells significantly decreased (to ca. 50%) after treatment with **S1**, while previous cell exposure to the inhibitor and further treatment with **S1** resulted in a cell viability of about 100% (Figure 5b). This evidence clearly suggests the direct interaction between the gating and targeting synthetic dsRNA poly(I:C) in **S1** and the TLR3 receptor. Moreover, it was also observed that cell exposure to the inhibitor or to bare nanoparticles (data not shown) had no effect on cell viability (Figure 5b). Additionally, to prove that the viability decrease observed when SK-BR-3 cells are exposed to **S1** is due to the interaction of poly(I:C) with the TLR3 receptor and the activation of the apoptotic pathway (Scheme 1), we confirmed the activation of caspase-3 by Western blot assays after treatment of SK-BR-3 cells with **S1**. All these data indicated that **S1** triggers cell death in breast cancer SK-BR-3 cells by induction of apoptosis, which is accomplished through TLR3-induced internalization.

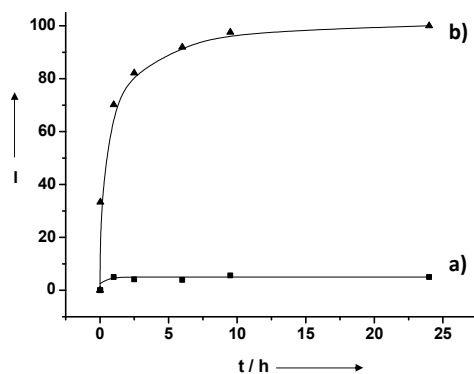


Figure 4. Doxorubicin release profile from solid **S2**: a) in 10 mM PBS medium, and b) in the presence of purified lysosomal extract.

One advantage when using gated MSNs is the possibility to design polyfunctional carriers with enhanced functionalities. As we have seen above, the design of **S1** makes full use of the great affinity of the synthetic dsRNA poly(I:C) to TLR3 receptor overexpressed in breast cancer SK-BR-3 cells and the activation of the apoptotic cascade. In addition, we envisioned that the toxicity of the nanoparticles could be enhanced by the preparation of a new carrier also capped with poly(I:C) but loaded in this case with the cytotoxic doxorubicin (nanoparticles **S2**). Solid **S2** was prepared using a similar procedure to that followed for **S1** and was fully characterized (see the Supporting Information for details).

The X-ray diffraction pattern of **S2** shows the typical characteristic diffraction peak (100). Moreover, the N₂ adsorption-desorption isotherm of **S2** was typical of capped mesoporous materials, with a surface area of 180.46 m² g⁻¹. Finally, the contents of 204.5 mg g⁻¹ SiO₂ of doxorubicin and 79.9 mg g⁻¹ SiO₂ of poly(I:C) on solid **S2** were determined.

The possibility to retain cargo inside a carrier until its target is reached is an important and highly desirable feature in drug-delivery systems to reduce side effects. In this context, *in vitro* release studies of doxorubicin from **S2** were performed in water (10 mM PBS) and in the presence of lysosomal extract (Figure 4) following a similar procedure to that used for **S1** (*vide ante*). In PBS a remarkable

baseline was observed, which indicated that doxorubicin remained in the nanoparticles without release. For instance, cargo delivery was lower than 10% at 24 h. In contrast, cargo release in the presence of lysosomal extract was clearly found as an increase of the doxorubicin fluorescence versus time.

Cell viability studies of **S2** in SK-BR-3 cells with dose-response experiments were carried out and the results are shown in Figure 5a. Treatment of SK-BR-3 cells with **S2** resulted in a remarkable decrease in cell viability when compared with free poly(I:C) and with **S1**. For instance, for **S2** IC_{50} values of about $10 \mu\text{g mL}^{-1}$ were found, which indicated that **S2** shows a similar toxicity to **S1** when **S2** was used in concentrations 10-times lower. Cell death was also evaluated by confocal microscopy (Figure 3). Cells showing apoptotic degradation (nuclear fragmentation, cytoplasmic degeneration) and co-localization in the nuclei of doxorubicin and DAPI dye were observed. The performed cellular studies suggested that **S2** induced cell death in SK-BR-3 cells through both: 1) interaction between capping molecules of poly(I:C) and the TLR3 receptor which induced caspase-3 activation, and 2) doxorubicin delivery. As stated above, the specific targeting of TLR3 by poly(I:C) has previously been described in breast cancer cells, however this is the first time that poly(I:C) has been combined with MSNs, additionally containing doxorubicin. Remarkably the nanoparticles capped with poly(I:C) and loaded with doxorubicin (i.e., **S2**) are much more toxic than those only functionalized with poly(I:C) [i.e., **S1**], suggesting a synergistic effect in killing cancer cells. Moreover, targeting of doxorubicin to TLR3-expressing cells did not only enhance its antitumor effect but would diminish toxicity in normal cells.

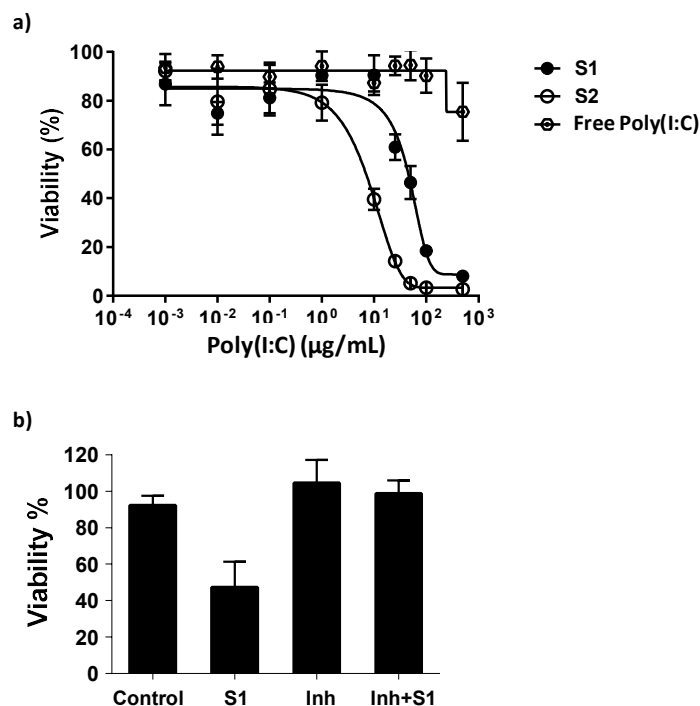


Figure 5. a) Cells were treated with varying concentrations (from 0.001 to 500 $\mu\text{g mL}^{-1}$) of free poly(I:C) or of equivalent poly(I:C) in **S1** or **S2** nanoparticles during 48 h and viability was determined with the cell proliferation reagent WST-1 (water soluble tetrazolium salt-1) assay. Nanoformulation improves poly(I:C) cytotoxicity on SK-BR-3 cells and **S2** toxicity is higher than **S1**, due to the combined poly(I:C)-doxorubicin effect. All values are shown as the mean \pm SD (n=3). b) SK-BR-3 cells were either pre-treated or not for 4 h with 10 $\mu\text{g mL}^{-1}$ of TLR3-dsRNA complex inhibitor, and then treated with 50 $\mu\text{g mL}^{-1}$ of equivalent poly(I:C) in **S1** for 48 h. Control cells did not undergo any treatment, and a control of just inhibitor treatment was included to confirm the lower toxicity. **S1** nanoparticle cytotoxicity was not observed while pre-treating with the inhibitor.

TLR3 neutralization by different molecules has been previously reported to show a strong cytotoxic activity. In this context killing TLR3-expressing breast cancer cells by using a specifically designed nanocarrier such as **S2**, showing enhanced cytotoxicity, can be an effective approach to induce antitumoral activity in breast cancer cells. From a therapeutic perspective, it is noteworthy that breast cancer cells retain the ability to sense and respond to mimetics of viral dsRNA in our nanoformulation. Currently, several ligands for TLR3 are being developed, such as Hiltonol (Oncovir Inc.), Ampligen (Hemixpherx) or IPH3102 (Innate Pharma), and

their antineoplastic effect is being evaluated in different clinical trials.^[18] Moreover, as the TLR3 receptor is also overexpressed in other cancer cells (e.g., melanoma,^[6] prostate^[19]), the specific targeting of chemotherapeutic agents to TLR3 receptor in nanosystems such as **S2** could be an effective strategy to treat different malignancies in which TLR3 overexpression has been described.

3.4 Conclusions

In conclusion, we have shown that synthetic dsRNA-conjugated nanoparticles effectively target TLR3-expressing breast cancer cells, and produce a TLR3-mediated internalization of the nanoparticles, which correlates with a caspase-dependent apoptosis induction. Importantly, the nanoformulation improved cytotoxic effects when compared to naked poly(I:C) on breast cancer cells. We have also shown that dsRNA-conjugated nanoparticles can act as nanocarriers for the chemotherapeutic drug doxorubicin, improving the cytotoxicity of dsRNA-conjugated nanoparticles. It is worth noting that TLR3 levels can be modulated by retinoic acid (RA) and other antitumor drugs.^[16] Hence, by upregulating TLR3 levels with such treatments, it would be possible to further enhance the cytotoxicity of dsRNA-conjugated nanoparticles in breast tumours thus opening up new opportunities to be exploited. In particular, targeting innate immunity sensors with dsRNA-conjugated nanodevices may provide an effective strategy for increasing the efficacy of current anticancer therapies in breast tumours.

Acknowledgements

We thank the Spanish Government (projects SAF2010-21195 and MAT2012-38429-C04-01) and the Generalitat Valenciana (project PROMETEOII/2014/047) for support. A.U. and C.G. are grateful to the Ministry of Education, Culture and Sport for their doctoral fellowships. We thank J. M. Cosgaya and M. J. Latasa for helpful discussions.

3.5 References

- [1] L.A. Torre, F. Bray, R.L. Siegel, J. Ferlay, J. Lortet-Tieulent, A. Jemal, *CA Cancer J. Clin.*, **2015**, *65*, 87-108.
- [2] A. McGuire A., J.A.L. Brown, C. Malone, R. McLaughlin, M.J. Kerin, *Cancers*, **2015**, *7*, 908-929.
- [3] S. Stier, C. Maletzki, U. Klier, M. Linnebacher, *Clin. Dev. Immunol.*, **2013**, *2013*, 271246.
- [4] B. Huang, J. Zhao, H. Li, K. L. He, Y. Chen, S. H. Chen, L. Mayer, J. C. Unkeless, H. Xiong, *Cancer Res*, **2005**, *65*, 5009-5014.
- [5] Vacchelli E., A. Eggermont, C. Sautés-Fridman, J. Galon, L. Zitvogel, G. Kroemer, L.Galluzzi, *Oncoimmunology*, **2013**, *2*, 8.
- [6] a) B. Salaun, I. Coste, M.C. Rissoan, S.J. Lebecque, T. Renno, *J. Immunol.*, **2006**, *176(8)*, 4894-901; b) B. Salaun, L. Zitvogel, C. Asselin-Paturel, Y. Morel, K. Chemin, C. Dubois, C. Massacrier, R. Conforti, M. P. Chenard, J.-C. Sabourin, A. Goubar, S.J. Lebecque, M. Pierres, D. Rimoldi, P. Romero, F. Andre, *Cancer Res.*, **2011**, *71*, 1607-1614.
- [7] N. K. Mal, M. Fujiwara, Y. Tanaka, *Nature*, **2003**, *421*, 350-353.
- [8] a) R. Casasús, E. Climent, M. D. Marcos, R. Martínez-Máñez, F. Sancenón, J. Soto, P. Amorós, J. Cano, E. Ruiz, *J. Am. Chem. Soc.*, **2008**, *130*, 1903-1917; b) E. Climent, R. Martinez-Manez, F. Sancenon, M. D. Marcos, J. Soto, A. Maquieira, P. Amoros, *Angew Chem Int Ed*, **2010**, *49*, 7281-7283; c) C.-Y. Lai, B. G. Trewyn, D. M. Jeftinija, K. Jeftinija, S. Xu, S. Jeftinija, V. S. Y. Lin, *J. Am. Chem. Soc.*, **2003**, *125*, 4451-4459; d) R. Liu, P. Liao, J. Liu, P. Feng, *Langmuir*, **2011**, *27*, 3095-3099; e) C. Park, K. Oh, S. C. Lee, C. Kim, *Angew. Chem. Int. Ed.*, **2007**, *46*, 1455-1457.
- [9] a) E. Aznar, L. Mondragón, J. V. Ros-Lis, F. Sancenón, M. D. Marcos, R. Martínez-Máñez, J. Soto, E. Pérez-Payá, P. Amorós, *Angew. Chem.Int. Ed.*, **2011**, *50*, 11172-11175; b) E. Bringas, O. Koyuren, D. V. Quach, M. Mahmoudi, E. Aznar, J. D. Roehling, M. D. Marcos, R. Martinez-Manez, P. Stroeve, *Chem. Commun.*, **2012**, *48*, 5647-5649; c) Q. Fu, G. V. R. Rao, L. K. Ista, Y. Wu, B. P. Andrzejewski, L. A. Sklar, T. L. Ward, G. P. López, *Adv. Mater.*, **2003**, *15*, 1262-1266.
- [10] a) A. Bernardos, L. Mondragón, E. Aznar, M. D. Marcos, R. Martínez-Máñez, F. Sancenón, J. Soto, J. M. Barat, E. Pérez-Payá, C. Guillem, P. Amorós, *ACS Nano*, **2010**, *4*, 6353-6368; b) E. Climent, A. Bernardos, R. Martínez-Máñez, A. Maquieira, M. D. Marcos, N. Pastor-Navarro, R. Puchades, F. Sancenón, J. Soto, P. Amorós, *J. Am. Chem. Soc.*, **2009**, *131*, 14075-14080; c) C. Park, H. Kim, S. Kim, C. Kim, *J. Am. Chem. Soc.*, **2009**, *131*, 16614-16615; d) K. Patel, S. Angelos, W. R. Dichtel, A. Coskun, Y.-W. Yang, J. I. Zink, J. F. Stoddart, *J. Am. Chem. Soc.*, **2008**, *130*, 2382-2383; e) A. Schlossbauer, J. Kecht, T. Bein, *Angew. Chem.Int. Ed.*, **2009**, *48*, 3092-3095; f) A. Schlossbauer, S. Warncke, P. M. E. Gramlich, J. Kecht, A. Manetto, T. Carell, T. Bein, *Angew. Chem.Int. Ed.*, **2010**, *49*, 4734-4737; g) A. Agostini, L. Mondragón, L. Pascual, E. Aznar, C. Coll, R. Martínez-Máñez, F. Sancenón, J. Soto, M. D. Marcos, P. Amorós, A. M. Costero, M. Parra, S. Gil, *Langmuir*, **2012**, *28*, 14766-14776.
- [11] C. T. Kresge, M. E. Leonowicz, W. J. Roth, J. C. Vartuli, J. S. Beck, *Nature*, **1992**, *359*, 710-712.
- [12] N. Z. Knezevic, J.-O. Durand, *Chem. Plus Chem.*, **2015**, *80*, 26-36.
- [13] a) C. Argyo, V. Weiss, C. Bräuchle, T. Bein, *Chem. Mat.*, **2013**, *26*, 435-451; b) D. Peer, J. M. Karp, S. Hong, O. C. Farokhzad, R. Margalit, R. Langer, *Nature Nano*, **2007**, *2*, 751-760; c) R. A. Petros, J. M. DeSimone, *Nature Rev Drug Discov*, **2010**, *9*, 615-627; d) V. Wagner, A. Dullaart, A.-K. Bock, A. Zweck, *Nature Biotech*, **2006**, *24*, 1211-1217.

- [14] A. Agostini, L. Mondragón, A. Bernardos, R. Martínez-Máñez, M. D. Marcos, F. Sancenón, J. Soto, A. Costero, C. Manguan-García, R. Perona, M. Moreno-Torres, R. Aparicio-Sanchis, J. R. Murguía, *Angew. Chem. Int. Ed.*, **2012**, *51*, 10556-10560.
- [15] a) M. Xie, H. Shi, Z. Li, H. Shen, K. Ma, B. Li, S. Shen, Y. Jin, *Colloids and Surfaces B: Biointerfaces*, **2013**, *110*, 138-147; b) Y. Wang, W. Shi, W. Song, L. Wang, X. Liu, J. Chen, R. Huang, *J. Mater. Chem.*, **2012**, *22*, 14608-14616; c) D. P. Ferris, J. Lu, C. Gothard, R. Yanes, C. R. Thomas, J.-C. Olsen, J. F. Stoddart, F. Tamanoi, J. I. Zink, *Small*, **2011**, *7*, 1816-1826; d) B. Xu, Y. Ju, G. Song, Y. Cui, *Journal of Nanoparticle Research*, **2015**, *15*, 1-12; e) C.-P. Tsai, C.-Y. Chen, Y. Hung, F.-H. Chang, C.-Y. Mou, *J. Mater. Chem.*, **2009**, *19*, 5737-5743.
- [16] A. R. Bernardo, J. M. Cosgaya, A. Aranda, A. M. Jimenez-Lara, *SO - Cell Death Dis.*, **2013**, Jan 31;4:e479. doi: 10.1038/cddis.2013.5.
- [17] a) S. Patel, A. U. Sprung, B. A. Keller, V. J. Heaton, L. M. Fisher, *Molecular Pharmacology*, **1997**, *52-4*, 658-666; b) Y. L. Lyu, J. E. Kerrigan, C. P. Lin, A. M. Azarova, Y. C. Tsai, Y. Ban, L.F. Liu, *Cancer Res*, **2007**, *67*, 8839-8846.
- [18] L. Galluzzi, E. Vacchelli, A. Eggermont, W. H. Fridman, J. Galon, C. Sautes-Fridman, E. Tartour, L. Zitvogel, G. Kroemer, *Oncoimmunology*, **2012**, *1*, 699-716.
- [19] A. Paone, D. Starace, R. Galli, F. Padula, P. De Cesaris, A. Filippini, E. Ziparo, A. Riccioli, *Carcinogenesis*, **2008**, *29*(7), 1334-42.

3.6 Supporting information

Chemicals

The chemicals tetraethylorthosilicate (TEOS), *n*-cetyltrimethylammonium bromide (CTAB), sodium hydroxide (NaOH), Sulforhodamine B, 3-aminopropyltriethoxysilane (APTES), 1-Ethyl-3-(3-dimethylaminopropyl)carbodiimide (EDC), D6046 DMEM medium, monoclonal anti- α -tubulin antibody, Anti-mouse IgG (whole molecule)-Peroxidase antibody and the Lysosome Isolation Kit (LYSISO1) were provided by Aldrich. Cell Proliferation Reagent (WST-1) was provided by Roche, while polyinosinic:polycytidylic acid (Poly (I:C)) was provided by American Custom Chemical Corporation and doxorubicin hydrochloride from Sequoia Research Products. Caspase-3 antibody was provided by Cell Signalling, Western Blotting Detection Reagents and Analysis System Kit and Anti-rabbit IgG Horseradish Peroxidase linked antibody were purchased from GE Healthcare Life Sciences, the TLR3/dsRNA Complex Inhibitor from Calbiochem and SK-BR-3 human breast carcinoma cells from American Type Culture Collection. All reactives were used as received.

General Techniques

Powder XRD, TG analysis, elemental analysis, TEM, SEM and N₂ adsorption-desorption techniques were employed to characterize the prepared materials. Powder X-ray measurements were performed on a Seifert 3000TT diffractometer using CuK α radiation. Thermo-gravimetric analysis (TGA) were carried out on a TGA/SDTA 851e Mettler Toledo equipment, using an oxidant atmosphere (Air, 80 mL/min) with a heating program consisting on a heating ramp of 10 °C per minute from 393 K to 1273 K and an isothermal heating step at this temperature for 30 minutes. Elemental analysis (EA) was performed in a CE Instrument EA-1110 CHN Elemental Analyzer. Transmission electron microscope (TEM) images were performed in a Philips CM-10. N₂ adsorption-desorption isotherms were recorded on a Micromeritics ASAP2010 automated sorption analyser. The samples were degassed at 120° C in vacuum overnight. The specific surfaces areas were calculated from the adsorption data in the low pressures range using the BET model. Pore size

was determined following the BJH method. UV-visible spectra were recorded with a JASCO V-650 Spectrophotometer. Fluorescence measurements were carried out in a JASCO FP-8500 Spectrophotometer. A VersaMax Absorbance Microplate Reader by Molecular Devices was used to determine solubilized formazan concentration in viability assays and to quantify protein extracts in Bradford assay. Confocal microscopy imaging was performed using a Zeiss LSM 710 microscope.

Synthesis of Mesoporous MCM-41 Nanoparticles (MSNs)

Mesoporous MCM-41 nanoparticles were synthesized by the following procedure: *n*-cetyltrimethylammonium bromide (CTAB, 1.00 g, 2.74 mmol) was first dissolved in deionized water (480 mL). Then, NaOH (3.5 mL, 2.00 mol L⁻¹) in deionized water was added to the CTAB solution, followed by adjusting the solution temperature to 80° C. TEOS (5.00 mL, 2.57 x 10⁻² mol) was then added dropwise to the surfactant solution. The mixture was stirred for 2 h to give a white precipitate. Finally, the solid product was centrifuged, washed with deionized water and dried at 60° C (MCM-41 as-synthesized). To prepare the final porous nanoparticles (MCM-41), the as-synthesized solid was calcined at 550° C using an oxidant atmosphere for 5 h in order to remove the template phase.

Synthesis of S1

In a typical synthesis, 400 mg of template-free MCM-41 were suspended in a solution of sulforhodamine B dye (203.22 mg, 0.35 mmol) in 35 mL of acetonitrile in a round-bottomed flask and was stirred for 24 h at room temperature. Afterward, 3-aminopropyltriethoxysilane (480 µL, 2 mmol) was added to the suspension and the mixture was stirred for 24 h at room temperature. Finally, the obtained solid was isolated by centrifugation and dried under vacuum. Then, 709 mg of this functionalized solid was suspended in 126.6 mL of water containing sulforhodamine B in order to inhibit the delivery of the dye from the pores to the bulk solution, and EDC (2.42g, 12.6 mmol) and poly(I:C) (177.23 mg, 4 µmol) were added. This suspension was stirred for 6 h at room temperature. Finally, this solid was isolated by centrifugation, washed with abundant water and dried at 37° C for 24 h.

Synthesis of S2

The solid **S2** was prepared following the same procedure described for **S1** but, in this case, the MCM-41 material was loaded with doxorubicin. For the preparation of this solid, 100 mg of calcined MCM-41 were suspended in a solution of doxorubicin (20 mg, 0.034 mmol) in 1.6 mL of water. After 24 h stirring at room temperature, the loaded nanoparticles were isolated by centrifugation and dried under vacuum. Afterward, the solid was resuspended in 8.5 mL of acetonitrile and 3-aminopropyltriethoxysilane (120 μ L, 0.5 mmol) was added. The mixture was stirred for 24 h at room temperature and the obtained solid was isolated by centrifugation and dried under vacuum. Afterward, 89 mg of this functionalized solid was suspended in 16.82 mL of a water solution containing doxorubicin and EDC (0.303 mg, 1.6 mmol) and poly(I:C) (21.14 mg, 0.5 μ mol) were added. This suspension was stirred for 6 h at room temperature. Finally, this solid was isolated by centrifugation, washed with abundant water and dried under vacuum.

Materials Characterization

The prepared solids were characterized using standard techniques. Figure 1 in Manuscript shows powder X-ray diffraction (PXRD) patterns of the nanoparticulated MCM-41 matrix as-synthesized, the calcined MCM-41, and the final **S1** solid. The MCM-41 as-synthesized (see Figure 1a) shows the typical four low-angle reflections of a hexagonal-ordered matrix indexed at (100), (110), (200), and (210) Bragg peaks. From the PXRD data of synthesized MCM-41, a d_{100} spacing of 43.11 Å was calculated. A significant displacement of the (100) peak in the PXRD of the calcined nanoparticulated MCM-41 was found corresponding to an approximate cell contraction of 3 Å (Figure 1b). This displacement and broadening of the (110) and (200) peaks are related to further condensation of silanol groups during the calcination step. Finally, Figure 1c shows the PXRD patterns for solid **S1**. For this material, reflections (110) and (200) are less intense due to a reduction in contrast related to the functionalization process and to the filling of mesopores with sulforhodamine B. Nonetheless, the intensity of the (100) peak in this pattern strongly indicates that the loading process with the dye and the additional

functionalization with 3-(aminopropyl)trimethoxysilane and poly(I:C) did not modify the mesoporous MCM-41 scaffold.

The N₂ adsorption-desorption isotherms of the nanoparticulated MCM-41 calcined material is shown in Figure SI-1a. A typical curve for mesoporous solids consisting of an adsorption step at intermediate P/P₀ values (0.25-0.4) is observed. This curve corresponds to a type IV isotherm, in which the observed step indicates nitrogen condensation inside the mesopores. The absence of a hysteresis loop in this interval and the narrow Barrett-Joyner-Halenda (BJH) pore distribution suggest there are uniform cylindrical mesopores (pore diameter of 2.76 nm and pore volume of 0.90 cm³ g⁻¹, calculated using the BJH model on the adsorption branch of the isotherm). The application of the Brunauer, Emmett and Teller (BET) model resulted in a value of 1045.7 m² g⁻¹ for the total specific surface area. From the PXRD, porosimetry and TEM studies, the a₀ cell parameter of 4.62 nm, pore diameter (2.76 nm), and value for the wall thickness (1.86 nm) were calculated. In addition to this adsorption step associated to the micelle-generated mesopores, a second feature appears in the isotherm at a high relative pressure (P/P₀>0.8). This adsorption corresponds to the filling of the large voids among the particles (pore diameter of 49.63 nm and pore volume of 0.27 cm³ g⁻¹, calculated by using the BJH model) and therefore must be considered as a textural-like porosity.

The N₂ adsorption-desorption isotherm of **S1** is typical of mesoporous systems with partially filled mesopores (see Figure SI-1b). In this case, and as expected, a lower N₂ adsorbed volume (BJH mesopore volume of 0.04 cm³ g⁻¹) and surface area (116.5 m² g⁻¹) were found when compared with the starting MCM-41 material (Table SI-1). In the same way, the N₂ adsorption-desorption isotherm of **S2** shows a low N₂ adsorbed volume (BJH mesopore volume of 0.06 cm³ g⁻¹) and a surface area value of 180.46 m² g⁻¹ (Table SI-1).

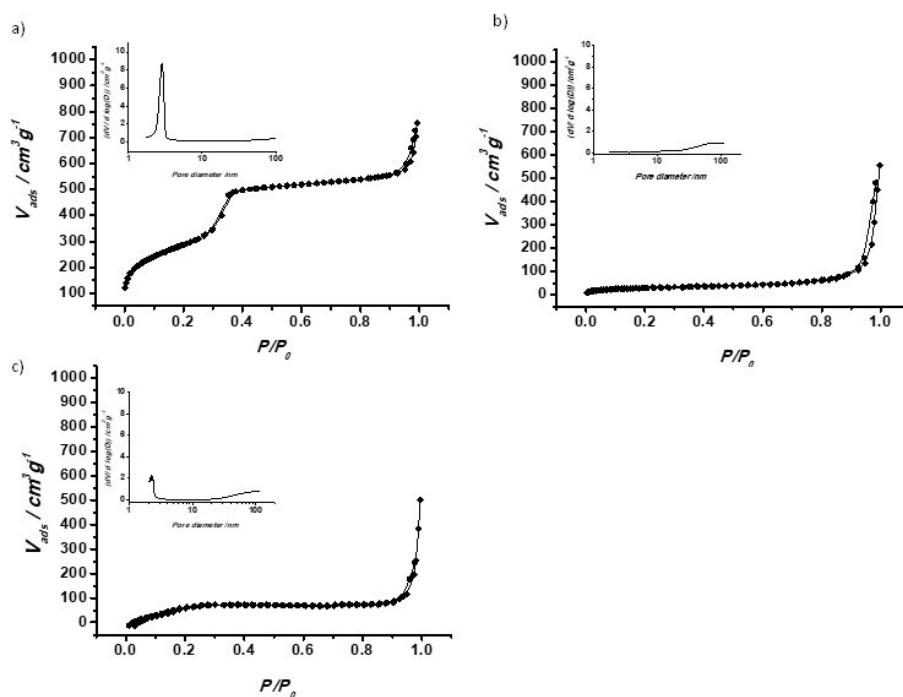


Figure SI-1. The N₂ adsorption-desorption isotherms for a) the MCM-41 calcined mesoporous material b) **S1** nanoparticles and c) **S2** nanoparticles. Inset: Pore size distribution

Table SI-1. BET-specific surface values, pore volumes and pore sizes calculated from the N₂ adsorption-desorption isotherms for selected materials.

Sample	S_{BET} [m ² g ⁻¹]	Pore Volume [a] [cm ³ g ⁻¹]	Pore size [a,b] [nm]
MCM-41	1045.7	0.90	2.76
S1	116.5	0.04	2.06
S2	180.46	0.06	2.18

The contents of grafted poly(I:C) and the loaded sulforhodamine B and doxorubicin in solids **S1** and **S2** respectively, were determined by elemental and thermogravimetric analyses (see Table SI-2).

Table SI-2. Content (α , mg/g of solid) of the different loading and functionalization moieties in **S1** and **S2**.

Sample	α_{dye}	$\alpha_{\text{doxorubicin}}$	$\alpha_{\text{Poly(I:C)}}$
S1	15.63	-----	191.82
S2	-----	204,5	79,9

Moreover, the content of sulforhodamine B and doxorubicin in solids **S1** and **S2** was also determined by UV-visible studies. The content of sulforhodamine B and doxorubicin present in the washing solutions was quantified and subtracted to the quantity used in the loading process of the solids. The contents calculated through this method compared well with those obtained from elemental and thermogravimetric analyses. The presence of phosphorus in **S1** and **S2** was also confirmed by microanalysis using SEM.

Delivery studies

Assays of *in vitro* cargo release of the **S1** and **S2** solids were performed using purified lysosomal extract as release medium. In a typical experiment, 1 mg of each **S1** or **S2** was suspended in 500 μL of deionized water; then, each suspension was divided into two aliquots of 250 μL and 1 mL of 10 mM PBS or 1 mL of purified lysosomal extract was added. To obtain the purified lysosomal extract the Lysosome Isolation Kit (LYSISO1) was used, following supplier's instructions for extractions from animal tissues and purification. Dye delivery from **S1** was monitored via the emission band of the dye centered at 575 nm ($\lambda_{\text{exc}} = 554\text{nm}$). The drug delivery from **S2** was monitored via the emission band of doxorubicin centered at 557 nm ($\lambda_{\text{exc}} = 480\text{nm}$). In the absence of purified lysosomal extract, negligible cargo release was observed, indicating that the nanoparticles were tightly capped. In contrast, in the presence of purified lysosomal extract the uncapping of the pores was clearly observed. This cargo delivery is triggered by the presence of lysosomal enzymes that break down poly(I:C) nanoparticles capping.

Cell culture and treatment

Materials **S1** and **S2**, and free poly(I:C) were independently tested *in vivo*, using SK-BR-3 human breast carcinoma cells. Cells were cultured at 37° C in DMEM medium containing 1000 mg/L glucose, phenol red, 10% fetal calf serum and 2 mM glutamine. **S1**, **S2** and poly(I:C) was dissolved in full-serum media and used at the concentration indicated in the figures.

Viability Assays

Quantitation of cell viability rates was determined using Cell Proliferation Reagent WST-1 following supplier's instructions. Cells were seeded in 96-well plates (25.000 cells/well) in triplicate. Nanoparticles and free poly(I:C) were added 48 h later during additional 48 h. Then, DMEM medium was removed and replaced with PBS with 1000 mg/L glucose to avoid phenol red interference with the absorbance reading, WST-1 was added and the plates were incubated during 1 h at 37° C. Finally, the absorbance at 490 nm was measured.

TLR3/Poly(I:C) complex inhibition

TLR3/Poly(I:C) interaction was tested realizing a viability assay using a TLR3/dsRNA complex inhibitor. SK-BR-3 cells were seeded in 96-well plates (25.000 cells/well) in triplicate and incubated during 48 h at 37° C. Then, the complex inhibitor was added to the plates at a concentration of 10 µg/mL; the plates were incubated during 4 h at 37° C and then treated with 50 µg/mL of equivalent poly(I:C) in **S1** during 48 h. Finally, cells viability was determined in the same way that the previous assay.

Confocal Microscopy Imaging

Internalization of nanoparticles in SK-BR-3 cells was observed *in vivo* by confocal fluorescence microscopy. About 8×10^5 SK-BR-3 cells per well were cultured on 6-well plates, and after 48 h cells were incubated with 50 µg/mL of equivalent poly (I:C) in **S1** and **S2** nanoparticles for 48 h more.

Western blotting

Caspase-3 and α -tubulin antibodies were used to probe blots of protein extracts prepared using Triton Lysis buffer (10 mM Tris, pH 7.4, 137 mM NaCl, 2 mM EDTA, 1% Triton X-100, 25 mM β -glycerophosphate, 1 mM sodium orthovanadate, 2 mM sodium pyrophosphate, 10% glycerol, 1 mM PMSF, and protease inhibitors cocktail). Immune complexes were detected by chemiluminescence.

***Chapter 4: Nanoparticle-cell-nanoparticle
communication by stigmergy to enhance
poly(I:C) induced apoptosis in cancer cells***

Nanoparticle-cell-nanoparticle communication by stigmergy to enhance poly(I:C) induced apoptosis in cancer cells

Amelia Ultimo,^[a] Cristina Giménez,^[a] Elena Aznar,^[a,b] Carmen Coll,^[a,b] M. Dolores Marcos,^[a,b,c] José R. Murguía^[a,b] Ramón Martínez-Mañez,^{*[a,b,c]} and Félix Sancenón^[a,b,c]

[a] A. Ultimo, Dr. C. Giménez, Dr. E. Aznar, Dr. C. Coll, Prof. M.D. Marcos, Dr. J.R. Murguía, Prof. R. Martínez-Mañez, Dr. F. Sancenón
Instituto Interuniversitario de Investigación de Reconocimiento Molecular y Desarrollo Tecnológico (IDM). Universitat Politècnica de València-Universitat de València, Spain
E-mail: rmaez@qim.upv.es

[b] Dr. E. Aznar, Dr. C. Coll, Prof. M.D. Marcos, Dr. J.R. Murguía, Prof. R. Martínez-Mañez, Dr. F. Sancenón
CIBER de Bioingeniería, Biomateriales y Nanomedicina (CIBERBBN)

[c] Prof. M.D. Marcos, Prof. R. Martínez-Mañez, Dr. F. Sancenón
Departamento de Química, Universitat Politècnica de València, Camino de Vera s/n, 46022, Valencia, Spain

Submitted

4.1 Abstract

Nanoparticle-cell-nanoparticle communication by stigmergy was demonstrated using two capped nanodevices. The first kind of nanoparticles (i.e. $S(\text{RA})_{\text{IFN}}$) is loaded with 9-cis-retinoic acid and capped with interferon- γ , whereas the second community of nanoparticles (i.e. $S(\text{sulf})_{\text{PIC}}$) is loaded with sulforhodamine B and capped with poly(I:C). The uptake of $S(\text{RA})_{\text{IFN}}$ by SK-BR-3 breast cancer cells enhanced the expression of TLR3 receptor facilitating the subsequent uptake of $S(\text{sulf})_{\text{PIC}}$ and cell killing.

4.2 Introduction

Nanotechnology is a highly multidisciplinary field and there has been a steadily growing number of applications in different areas, such as biomedicine, electronics, chemistry and computing in recent years.¹ Despite the progress made, there are still many challenges to be solved and there is a long way ahead in nanotechnology research and development before we realize its full potential. In particular, communication or cooperative behaviours at the nanoscale between nanodevices remains an almost unexplored topic. While new nanodevices are reported every year, communication and cooperation between them may expand the capabilities of single nanoparticles by allowing them to share information and to cooperate.²

Chemical or molecular communication, based on transmitting and receiving information sharing molecules (chemical messengers), is essential at cellular level and represents one of the communication forms used by living organisms (e.g. bacteria, insects and many mammals). Moreover, it has been demonstrated that molecular communication can also be established in

communities of nanoparticles.³ However, in contrast to interaction mediated by direct interchange of chemical messengers, there are many examples in the nature where swarm systems communicate (and therefore cooperate) by modifying the environment. This concept is called stigmergy.⁴ Just to mention some examples, ants deposit and sense chemical signals to form trails to sources of food or termites are able to build complex structures by modifying and locally sensing their physical environment.

The concept of stigmergy, proposed by the French entomologist Pierre-Paul Grasse, has been used to analyze self-organizing activities in a wide range of fields, including microorganisms, social insects, web communities and human society. However, its full power remains underappreciated and examples using nanoparticles remains almost unexplored. In this cooperation/communication protocol the trace left by an action in a medium stimulates subsequent actions. Stigmergy facilitates complex, coordinated activity without any need for planning, simultaneous presence, or even mutual awareness. Taking into account these concepts, one can imagine different communities of nanoparticles one of which performs an action and the trace of this action on the medium stimulates the performance of a second community of nanoparticles.

In order to explore this stigmergy concept in cell-nanoparticle communities it can be envisioned a first nanodevice acting as an allosteric activator which is able to increase the cell ability to interact with a second wave of nanoparticles. In such mechanism, there is nanoparticle-cell-nanoparticle communication through stigmergy; despite there is not communication through chemical messengers (therefore there is not mutual “awareness”) between the two communities of nanoparticles, they are able to act cooperatively (therefore communicate), overall developing a self-organizing activity.

As a proof of concept, we describe here the use of gated nanoparticles as promising nanostructures to chemically design

cooperation/communication networks.^{5,6}

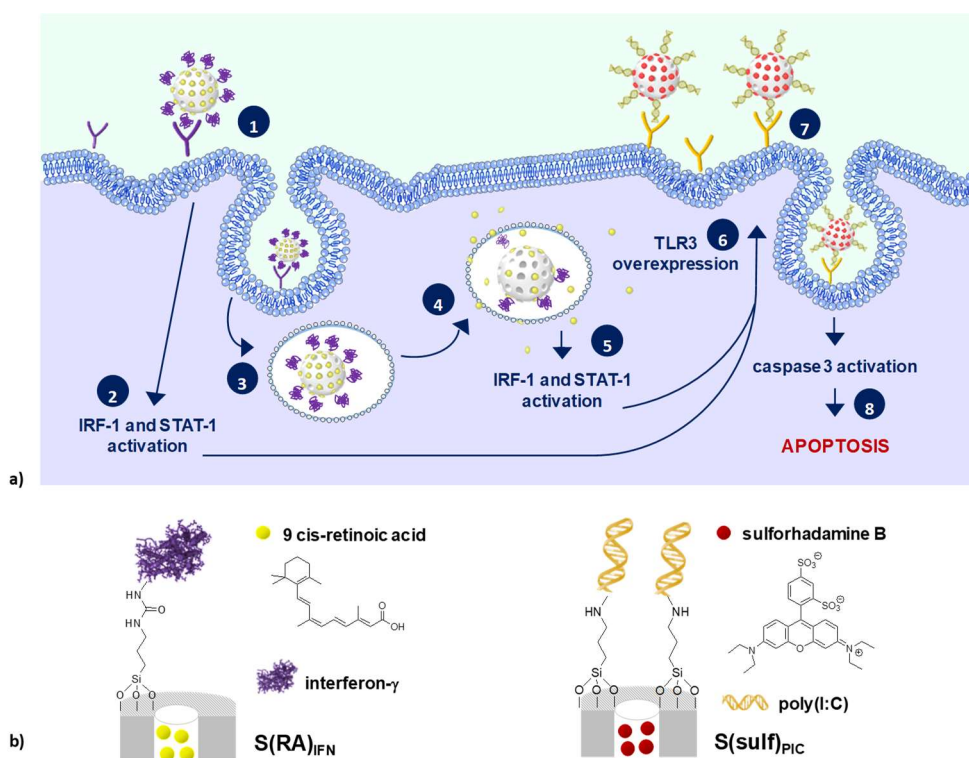
Gated materials are nanoscopic devices in which the release of molecules, biomolecules or nano-objects from a porous matrix can be triggered by a target external stimulus that can control the state of the molecular gate; i.e., closed or open.⁷ These systems show an ideal “zero release” until opened at-will with suitable stimuli. In the last few years, nanocontainers, most of them based in the use of mesoporous silica nanoparticles (MSNs), bearing gated scaffoldings have proved to be excellent candidates for the design of controlled-release nanomachines at different levels and for different applications.⁸⁻¹³

Part of our approach is based in the use of polyinosinic-polycytidylic acid (poly(I:C)), a synthetic dsRNA agonist of TLR3 that is known to induce direct inhibition of tumour growth in different cancer cell models. Currently, indeed, several ligands for TLR3 are being evaluated in different clinical trials. A general consequence of TLR3-ligands interactions is an intense inflammatory response and the recruitment of immune cells. Nevertheless, the induction of apoptotic mechanisms has also been observed in several cancers, through extrinsic pathways that lead to the final activation of effector caspases like caspase 3.^{14,15} Hence, targeting TLR3 receptor is an effective strategy to treat different malignancies expressing TLR3.

Another concept we have used is the employment of 9-cis-retinoic acid (RA) and interferon- γ (IFN) which are molecules known to induce the expression of TLR3 receptor in different studies.^{14,16-18} Both RA and IFN indirectly regulate TLR3 promoter, that contains IFN-stimulated response elements (ISRE)/IFN regulatory factor elements (IRF-E) and signal transducer and activator of transcription (STAT)-binding sites, as they determine the nuclear localization and the activity of transcription factors as IRF-1 or STAT-1.^{16,18-20}

The stigmergy cooperation protocol is based on the use of two sets of capped MSNs. The first community of MSNs (**S(RA)_{IFN}**) is loaded with 9-cis-retinoic acid and capped with an interferon- γ derivative, whereas in the second community

(**S(sulf)**_{PIC}) the payload is sulforhodamine B and the nanoparticles are capped with poly(I:C) (Scheme 1b). The cooperative behaviour of the two sets of nanoparticles is tested using SK-BR-3 cancer cells. The interaction of the capping interferon- γ on **S(RA)**_{IFN} solid with its receptor located in the membrane of SK-BR-3 cells, induces both an upregulation of TLR3 expression and the internalization of the nanoparticles. Consequently, the release of 9-cis-retinoic acid due to the degradation of the gating ensemble by the lysosomal enzymes takes place. The released molecules are also expected to induce a marked enhancement in TLR3 expression in SK-BR-3 cells. Poly(I:C) in the second set of nanoparticles is known to strongly interact with TLR3, and this is expected to have a cytotoxic effect as consequence of the activation of apoptotic signalling pathways. In this combination the first community of nanoparticles performs an action (induction of TLR3 expression) and the trace of this action (a larger number of TLR3 receptors) stimulates the performance of the second community of nanoparticles. A depiction of the designed cooperation system is presented in Scheme 1a.



Scheme 1. a) The mechanism of action of the cooperative nanosystems. 1. **S(RA)_{IFN}** nanoparticles interact with IFN receptor on the cell membrane; 2. IFN signalling activates IRF-1 and STAT-1 transcription factors; 3. **S(RA)_{IFN}** nanoparticles are endocytosed; 4. IFN capping moieties on **S(RA)_{IFN}** nanoparticles surface are degraded by lysosomal enzymes, allowing the release of RA from the mesopores; 5. RA signalling also activates IRF-1 and STAT-1; 6. TLR3 expression is induced; 7. enhanced interaction of **S(sulf)_{PIC}** nanoparticles with TLR3; 8. TLR3 activates extrinsic apoptotic pathways that lead to cell death. b) A schematic representation of **S(RA)_{IFN}** and **S(sulf)_{PIC}** nanoparticles.

4.3 Results and discussion

MSNs were prepared using well-known procedures using *n*-cetyltrimethylammonium bromide as structure directing agent and tetraethyl orthosilicate as silica source. The pores of the calcined MSNs were loaded with 9-cis-retinoic acid and the external surface functionalized with propylisocyanate moieties (solid **S(RA)_{NCO}**). Then, interferon-γ was attached

onto the external surface of $S(\text{RA})_{\text{NCO}}$, by means of the formation of urea bonds, yielding the final nanoparticles $S(\text{RA})_{\text{IFN}}$. In order to test the gating mechanism, similar nanoparticles but loaded with sulforhodamine B were also prepared ($S(\text{sulf})_{\text{IFN}}$). For the preparation of the second community of nanoparticles, the pores of the MSNs were loaded with sulforhodamine B and the external surface decorated with aminopropyl moieties ($S(\text{sulf})_{\text{NH}_2}$). Finally, the pores were capped upon reaction of the activated phosphate groups of poly(I:C) with the aminopropyl moieties grafted onto the external surface yielding solid $S(\text{sulf})_{\text{PIC}}$.

The prepared nanoparticles were characterized using standard procedures as powder X-ray diffraction, TEM, N_2 adsorption-desorption isotherms, thermogravimetry and elemental analysis (see Supporting Information for details). Moreover, sulforhodamine B release from $S(\text{sulf})_{\text{IFN}}$ and $S(\text{sulf})_{\text{PIC}}$ in the presence of a lysosomal extract was tested. In a typical experiment, a suspension of $S(\text{sulf})_{\text{IFN}}$ or $S(\text{sulf})_{\text{PIC}}$ in water was separated into two aliquots. Then, 1 mL of PBS (10 mM) or 1 mL of purified lysosomal extract was added and the resultant suspensions were stirred at room temperature for 24 h. At given times, aliquots were taken, centrifuged to eliminate the nanoparticles and the emission of the sulforhodamine B released was measured at 575 nm ($\lambda_{\text{ex}} = 554 \text{ nm}$). The release profiles are shown in Figure 1.

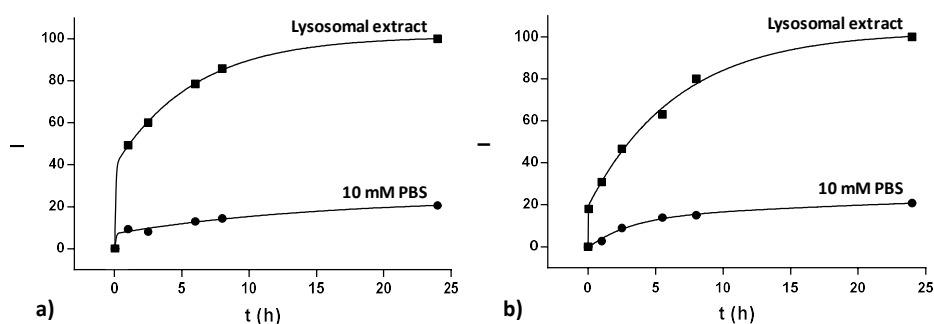


Figure 1. Cargo delivery profiles from solids (a) $S(\text{sulf})_{\text{IFN}}$ and (b) $S(\text{sulf})_{\text{PIC}}$, in the absence and in the presence of lysosomal extract.

As can be seen, sulforhodamine B release from solid **S(sulf)_{IFN}** and **S(sulf)_{PIC}** was low in the absence of lysosomal extract (release < 15 % of maximum release after 25 h), which indicates the correct capping of the material by the bulky interferon- γ (in **S(sulf)_{IFN}**) and poly(I:C) (in **S(sulf)_{PIC}**). In contrast, a remarkable cargo release occurred for both solids in the presence of lysosomal extract. This is attributed to enzymatic degradation of the interferon- γ and poly(I:C) caps, which induced sulforhodamine B release.

Cell viability assays with both **S(RA)_{IFN}** and **S(sulf)_{PIC}** solids were carried out. The underlying idea was to compare the cytotoxic effect exerted by poly(I:C) in SK-BR-3 cells using **S(sulf)_{PIC}** nanoparticles alone or in combination with a pre-treatment with **S(RA)_{IFN}**. Besides, in order to highlight the cooperation between nanoparticles, viability assays with free poly(I:C) and poly(I:C) combined with free 9-cis-retinoic acid and interferon- γ , at the same concentrations as when in the nanoparticles, were also carried out. The obtained results are presented in Figure 2a that shows dose-response curves after 48 h experiments carried out with **S(sulf)_{PIC}** alone (using the required amounts of nanoparticles to reach a poly(I:C) concentration in the 0.001-500 $\mu\text{g mL}^{-1}$ range) or treatment with **S(sulf)_{PIC}** after 4 h pre-treatment with **S(RA)_{IFN}** solid. For **S(RA)_{IFN}** it was used the appropriate quantity of nanoparticles to obtain a 9-cis-retinoic acid concentration of 0.3 $\mu\text{g mL}^{-1}$. Moreover, Figure 2a also shows the curves obtained when cells are treated with poly(I:C) alone (concentrations in the 0.001-500 $\mu\text{g mL}^{-1}$ range) or treated with poly(I:C) after 4 h pre-treatment of the cells with 9-cis-retinoic acid (0.3 $\mu\text{g mL}^{-1}$) and interferon- γ (15 ng mL^{-1}).

As can be seen in Figure 2a, free poly(I:C) cytotoxicity on SK-BR-3 cells is negligible at the tested concentrations, while it is only slightly enhanced after pre-treatment with free 9-cis-retinoic acid and interferon- γ , pointing out the importance of the nanoformulation when data is compared with the treatment using **S(sulf)_{PIC}** or **S(RA)_{IFN} + S(sulf)_{PIC}** combination (*vide infra*).

In order to confirm the TLR3-mediated **S(sulf)_{PIC}** nanoparticles internalization confocal microscopy measurements were carried out. For this purpose, SK-BR-3 cell cultures were treated during 48 h with **S(sulf)_{PIC}** nanoparticles ($50 \mu\text{g mL}^{-1}$ of equivalent poly(I:C)) and the release of the entrapped sulforhodamine B measured. The obtained results are shown in Figure SI-3. A clear sulforhodamine B fluorescence was observed in the cytosol of SK-BR-3 cells treated with **S(sulf)_{PIC}**, indicating the internalization of nanoparticles and the subsequent uncapping and dye release in the lysosomes. At the same time, cell morphology changes after nanoparticle endocytosis were analysed. As shown in Figure SI-3 (see white arrows), **S(sulf)_{PIC}** treated cells presented both nuclear fragmentation and cytoplasmic degradation, visible signs of apoptotic processes. These results confirmed the endocytosis of the **S(sulf)_{PIC}** nanoparticles and the cytotoxic effect exerted by the poly(I:C) coating by interaction with the TLR3 receptor that resulted in caspase-3 activation via receptor-mediated endocytosis of nanoparticles.

Most interestingly, when SK-BR-3 cells were pre-treated with **S(RA)_{IFN}** and then incubated with **S(sulf)_{PIC}**, a remarkable decrease in cells viability, when compared to that obtained when using **S(sulf)_{PIC}** alone, was observed. For example, at $25 \mu\text{g mL}^{-1}$ poly(I:C) concentration, cell viability was reduced from 90% to 65% when treated with **S(sulf)_{PIC}** alone or with both **S(RA)_{IFN}+S(sulf)_{PIC}** nanoparticles, respectively. Overall **S(RA)_{IFN}** and **S(sulf)_{PIC}** nanoparticles act cooperatively by stigmergy. The first community of nanoparticles (i.e. **S(RA)_{IFN}**) perform an action (delivery of interferon- γ and 9-cis-retinoic that act as chemical cues that enhance the overexpression of membrane TLR3 receptors) and the trace of this action (enhanced expression of TLR3 receptors) stimulates the performance of the second community of nanoparticles (i.e. **S(sulf)_{PIC}**) that are more effectively internalized and enhanced cell killing. This was confirmed by Western blot assays (Figure 2b) that demonstrated the induction of TLR3 expression in SK-BR-3 cells by **S(RA)_{IFN}** nanoparticles.

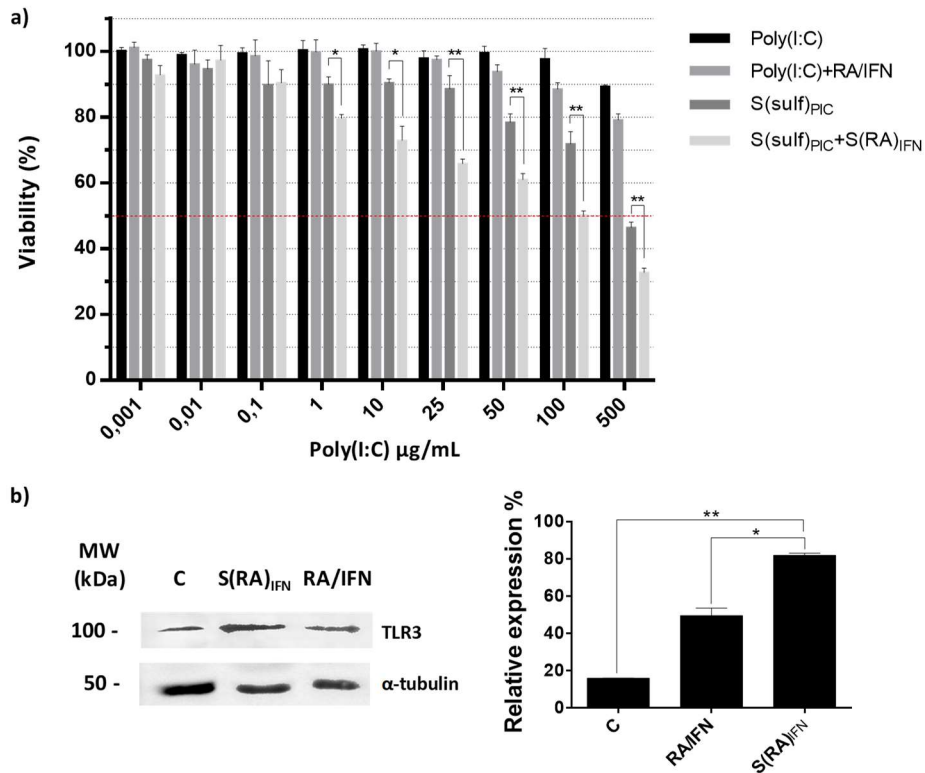


Figure 2. (a) Dose-response curves after 48h for cells treated with free poly(I:C), with 9-cis-retinoic acid and interferon- γ for 4h and then with poly(I:C), with **S(sulf)_{PIC}** and, finally, with **S(RA)_{IFN}** for 4h and then with **S(sulf)_{PIC}**. Cell viability was determined by using the cell proliferation reagent WST-1. Concentrations between 0.001 and 500 $\mu\text{g mL}^{-1}$ of free poly(I:C) and equivalent poly(I:C) in **S(sulf)_{PIC}** were tested. 15 ng mL^{-1} of interferon- γ and 0.3 $\mu\text{g mL}^{-1}$ of 9-cis-retinoic acid and equivalent 9-cis-retinoic acid in **S(RA)_{IFN}** were tested. All values are shown as the mean \pm SD (n=3). Asterisks indicate significant differences (*= $p < 0.01$, **= $p < 0.001$) when t test was applied. (b) Representative immunoblots showing induction of TLR3 in SK-BR-3 cells after a 24 h treatment with free 9-cis-retinoic acid (0.3 $\mu\text{g mL}^{-1}$) and interferon- γ (15 ng mL^{-1}) or with **S(RA)_{IFN}**. Relative expression of TLR3 was calculated by densitometry, normalizing by the loading control (α -Tubulin). Expression values are shown as the mean \pm SD (n=3). Asterisks indicate significant differences (*= $p < 0.001$, **= $p < 0.0001$) when t test was applied.

4.4 Conclusions

In summary, we present here a proof of concept of a nanoparticle-cell-nanoparticle communication model involving two different capped nanodevices. The first set of nanoparticles are loaded with 9-cis-retinoic acid and capped with interferon- γ (**S(RA)**_{IFN}), whereas in the second nanodevice sulforhodamine B was used as cargo and poly(I:C) chains as caps (**S(sulf)**_{PIC}). The uptake of **S(RA)**_{IFN} by SK-BR-3 breast cancer cells enhanced the overexpression of TLR3 receptor that facilitated the subsequent internalization of **S(sulf)**_{PIC}. As a consequence, a marked reduction in cells viability was observed when both communities of nanoparticles were used in a combined treatment, compared to that obtained with **S(sulf)**_{PIC} alone or by a combination of free 9-cis-retinoic, interferon- γ and poly(I:C). The results presented in this work demonstrate the possibility of developing stigmergy communication/cooperation strategies involving different communities of nanodevices and cells. Such stigmergy protocols may enhance nanocarrier outcomes and potentiate their applications in targeted transport and drug delivery, opening wide new scenarios of cooperation/communication between nanoparticles and leading to the design of a number of plausible networks with the aim to increase drug efficacy and to reduce dosages, side effects, and resistance.

Acknowledgements

We thank the Spanish Government (projects RTI2018-100910-B-C41 and RTI2018-101599-B-C22 (MCUI/FEDER, EU)) and the Generalitat Valenciana (project PROMETEO2018/024) for support. A.U. is grateful to the Ministry of Education, Culture and Sport for her doctoral FPU grant.

4.5 References

- 1 D. Schaming and H. Remita, *Found. Chem.*, 2015, **17**, 187.
- 2 S. Hauert and S. N. Bhatia, *Trends Biotechnol.*, 2014, **32(9)**, 448.

- 3 T. Nakano, M. J. Moore, F. Wei, A. V. Vasilakos and J. Shuai, *IEEE Trans. Nanobiosci.*, 2012, **11**, 135.
- 4 G. Theraulaz and E. Bonabeau, *Artif., Life* 1999, **5**, 97-116.
- 5 C. Giménez, E. Climent, E. Aznar, R. Martínez-Máñez, F. Sancenón, M. D. Marcos, P. Amorós and K. Rurack, *Angew. Chem. Int. Ed. Engl.*, 2014, **53**, 12629.
- 6 A. Llopis-Lorente, P. Díez, A. Sánchez, M. D. Marcos, F. Sancenón, P. Martínez-Ruíz, R. Villalonga and R. Martínez-Máñez, *Nat. Commun.*, 2017, **30**, 15511.
- 7 E. Aznar, M. Oroval, L. Pascual, J. R. Murguía, R. Martínez-Máñez and F. Sancenón, *Chem. Rev.*, 2016, **116**, 561
- 8 C. de la Torre, L. Domínguez-Berrocal, J. R. Murguía, M. D. Marcos, R. Martínez-Máñez, J. Bravo and F. Sancenón, *Chem. Eur. J.*, 2018, **24**, 1890.
- 9 A. García-Fernández, G. García-Laínez, M. L. Ferrándiz, E. Aznar, F. Sancenón, M. J. Alcaraz, J. R. Murguía, M. D. Marcos, R. Martínez-Máñez, A. M. Costero and Mar Orzáez, *J. Control. Release*, 2017, **248**, 60.
- 10 C. Yu, L. Qian, M. Uttamchandani, L. Li and S. Q. Yao, *Angew. Chem. Int. Ed.*, 2015, **54**, 10574.
- 11 C. Murugan, K. Rayappa, R. Thangam, R. Bhanumathi, K. Shanthi, R. Vivek, R. Thirumurugan, A. Bhattacharyya, S. Sivasubramanian, P. Gunasekaran and S. Kannan, *Sci. Rep.*, 2016, **6**, 34053.
- 12 S. H. van Rijt, D. A. Bölükbas, C. Argyo, S. Datz, M. Lindner, O. Eickelberg, M. Königshoff, T. Bein and S. Meiners, *ACS Nano*, 2015 **9(3)**, 2377.
- 13 A. Llopis-Lorente, B. Lozano-Torres, A. Bernardos, R. Martínez-Máñez and F. Sancenón, *J. Mater. Chem. B*, 2017, **5**, 3069.
- 14 F. Bianchi, S. Pretto, E. Tagliabue, A. Balsaria and L. Sfondrini, *Cancer Biol. Ther.*, 2017, **18(10)**, 747.
- 15 A. Ultimo, C. Giménez, P. Bartovsky, E. Aznar, F. Sancenón, M. D. Marcos, P. Amorós, A. R. Bernardo, R. Martínez-Máñez, A. M. Jiménez-Lara and J. R. Murguía, *Chem. Eur J.*, 2016, **22**, 1582.
- 16 A. R. Bernardo, J. M. Cosgaya, A. Aranda and A. M. Jiménez-Lara, *Cell Death Dis.*, 2013, **4**, e479.
- 17 N. Clarke, A. M. Jiménez-Lara, E. Voltz and H. Gronemeyer, *EMBO J.*, 2004, **23**, 3051.
- 18 A. Kajita, S. Morizane, T. Takiguchi, T. Yamamoto, M. Yamada and K. Iwatsuki, *J. Invest. Dermatol.*, 2015, **135**, 2005.
- 19 C. M. Horvat, *Sci. STKE*, 2004, **2004(260)**, tr8.
- 20 X. Weihua, V. Kolla and D. V. Kalvakolanu, *J. Biol. Chem.*, 1997, **272(15)**, 9742.

4.6 Supporting information

Chemicals

The chemicals tetraethylorthosilicate (TEOS), *n*-cetyltrimethylammonium bromide (CTAB), sodium hydroxide, sulforhodamine B, (3-aminopropyl)triethoxysilane (APTES), 1-Ethyl-3-(3-dimethylaminopropyl)carbodiimide (EDC), (3-isocyanatopropyl)triethoxysilane, 9-cis-retinoic acid, interferon- γ , D6046 DMEM medium, monoclonal anti- α -tubulin antibody, polyclonal anti-TLR3 antibody, anti-mouse IgG (whole molecule)-peroxidase antibody and the lysosome Isolation Kit (LYSISO1) were provided by Aldrich. Triethylamine was provided by Avantor Materials, Cell Proliferation Reagent (WST-1) by Roche, while polyinosinic:polycytidylic acid (poly(I:C)) was provided by American Custom Chemical Corporation. Western blotting detection reagents and analysis system kit and anti-rabbit IgG horseradish peroxidase linked antibody were purchased from GE Healthcare Life Sciences, while SK-BR-3 human breast carcinoma cells from American Type Culture Collection. All products were used as received.

General Techniques

The synthesised materials were characterized by powder XRD, TG analysis, elemental analysis, TEM, and N₂ adsorption-desorption techniques. Powder X-ray diffraction measurements were performed on a Seifert 3000TT diffractometer using CuK α radiation. Thermogravimetric analysis were carried out on a TGA/SDTA 851e Mettler Toledo equipment, using an oxidant atmosphere (Air, 80 mL/min) with a heating program consisting on a heating ramp of 10°C per minute from 393 K to 1273 K and an isothermal heating step at this temperature for 30 minutes. Elemental analysis was performed in a CE Instrument EA-1110 CHN Elemental Analyzer. Transmission electron microscopy (TEM) images were performed in a Philips CM-10. N₂ adsorption-desorption isotherms were recorded on a Micromeritics ASAP2010 automated sorption analyser. The samples were degassed at 120°C in vacuum overnight. The specific surfaces areas were calculated from the adsorption data in the low pressures range using the BET model. Pore size was

determined following the BJH method. UV-visible spectra were recorded with a JASCO V-650 spectrophotometer. Fluorescence measurements were carried out in a JASCO FP-8500 spectrophotometer. A VersaMax absorbance microplate reader by Molecular Devices was used to determine solubilized formazan concentration in viability assays and to quantify protein extracts in Bradford assay. Confocal microscopy imaging was performed using a Zeiss LSM 710 microscope.

Synthesis of Mesoporous Nanoparticles

Mesoporous silica nanoparticles (MSNs) were synthesised by the following procedure: *n*-cetyltrimethylammonium bromide (CTAB, 1.00 g, 2.74 mmol) was first dissolved in deionised water (480 mL). Then, NaOH (3.5 mL, 2.00 mol L⁻¹) in deionised water was added to the CTAB solution, followed by adjusting the solution temperature to 80°C. TEOS (5.00 mL, 2.57 x 10⁻² mol) was then added dropwise to the surfactant solution. The mixture was stirred for 2 h to give a white precipitate. Finally, the solid product was centrifuged, washed with deionised water and dried at 60°C (MSNs as-synthesised). To prepare the final porous nanoparticles (MSNs), the as-synthesised solid was calcined at 550°C using an oxidant atmosphere for 5 h in order to remove the template phase.

Synthesis of $S(RA)_{IFN}$

To obtain $S(RA)_{IFN}$ material, 50 mg of calcined MSNs were suspended in a solution of 9-cis-retinoic acid (1 mg, 3.3 x 10⁻³ mmol) in 250 µL of acetonitrile and were stirred for 24 h at room temperature and safe from light. Then, (3-isocyanatopropyl)triethoxysilane (61.9 µL, 0.25 mmol) was added and the suspension was stirred for 5.5 h at room temperature and safe from light ($S(RA)_{NCO}$). Afterwards, the solid was centrifuged and dried under vacuum. Solid $S(RA)_{NCO}$ (1 mg) was then suspended in a mixture of 700 µL of acetonitrile containing an excess of 9-cis-retinoic acid and 100 µL of a solution of interferon-γ (0.1 mg) in deionised water. Triethylamine (2 µL) were added to the mixture that was stirred during 2 h at room temperature and safe from light. Finally, this solid was isolated by centrifugation, washed with deionized water and dried under vacuum.

Synthesis of S(sulf)_{PIC}

In a typical synthesis, 400 mg of template-free MSNs were suspended in a solution of sulforhodamine B (200 mg, 0.34 mmol) in 35 mL of acetonitrile in a round-bottomed flask and were stirred for 24 h at room temperature. Afterwards, (3-aminopropyl)triethoxysilane (480 μ L, 2 mmol) was added to the suspension and the mixture was stirred for 24 h at room temperature (**S(sulf)_{NH2}**). Finally, the obtained solid was isolated by centrifugation and dried under vacuum. Then, 685 mg of this functionalised solid were dispersed in 122.3 mL of water containing sulforhodamine B (in order to inhibit the delivery of the dye from the pores to the bulk solution), EDC (2.34 g, 12.2 mmol) and poly(I:C) (171.25 mg, 3.8 μ mol) and the resulting suspension was stirred for 6 h at room temperature. Finally, this solid was isolated by centrifugation, washed with abundant water and dried at 37°C for 24 h.

Synthesis of S(sulf)_{IFN}

100 mg of template-free MSNs were suspended in a solution of sulforhodamine B (50 mg, 0.085 mmol) in 9 mL of acetonitrile in a round-bottomed flask and were stirred for 24 h at room temperature. Then, (3-isocyanatopropyl)triethoxysilane (123.8 μ L, 0.5 mmol) was added and the suspension was stirred for 5.5 h at room temperature, and successively centrifuged and dried under vacuum (**S(sulf)_{NCO}**). 4 mg of the dried solid were suspended in a mixture of 2.8 mL of acetonitrile containing an excess of sulforhodamine B, 400 μ L of a solution of interferon- γ (0.1 mg) in deionised water and 2 μ L of trimethylamine. The mixture was stirred during 2 h at room temperature and then centrifuged. The isolated solid was washed with deionized water and dried under vacuum.

Materials Characterization

The prepared solids were characterized using standard techniques. Figure SI-1a shows powder X-ray diffraction (PXRD) patterns of as-synthesized MSNs, calcined MSNs, **S(sulf)_{NCO}** and **S(sulf)_{PIC}**. The as-synthesized MSNs show the typical four low-angle reflections of a hexagonal-ordered matrix indexed at (100), (110), (200), and (210) Bragg peaks. The displacement of the (100) peak in the PXRD of the calcined MSNs and the broadening of the (110) and (200) peaks are related to

the further condensation of silanol groups during the calcination step. Finally, for solids **S(sulf)_{NCO}** and **S(sulf)_{PIC}**, reflections (110) and (200) are less intense due to a reduction in contrast related to the functionalization process and to the filling of mesopores with sulforhodamine B. Nonetheless, the intensity of the (100) peak in these patterns strongly indicates that the loading process with the dye and the additional functionalization with (3-isocyanatopropyl)triethoxysilane or with 3-(aminopropyl)trimethoxysilane and poly(I:C), respectively, did not modify the mesoporous MSNs scaffold.

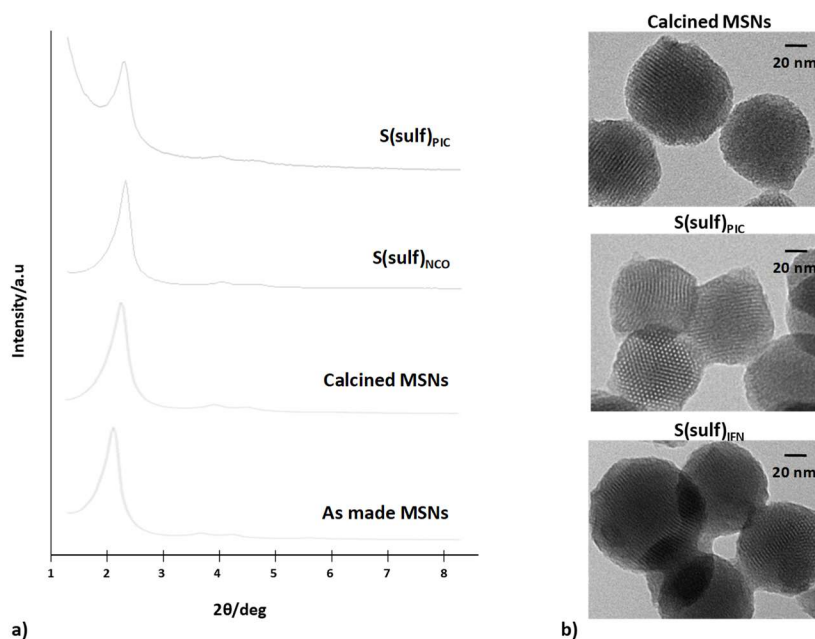


Figure SI-1. (a) Powder X-ray diffraction pattern of as made MSNs, calcined MSNs, solid **S(sulf)_{NCO}** and solid **S(sulf)_{PIC}** showing the typical reflections of the MSNs hexagonal array. (b) TEM representative images of calcined MSNs, solid **S(sulf)_{PIC}** and solid **S(sulf)_{IFN}** showing the typical porosity of the MSNs mesoporous matrix. Scale bars: 20 nm.

The N_2 adsorption-desorption isotherms of the calcined MSNs is shown in Figure SI-2a. A typical curve for mesoporous solids consisting of an adsorption step at intermediate P/P_0 values (0.25-0.4) is observed. This curve corresponds to a type IV isotherm, in which the observed step is due to nitrogen condensation inside the

mesopores. The absence of a hysteresis loop in this interval and the narrow Barrett-Joyner-Halenda (BJH) pore distribution suggest there are uniform cylindrical mesopores (pore diameter of 2.68 nm and pore volume of $0.81 \text{ cm}^3 \text{ g}^{-1}$, calculated using the BJH model on the adsorption branch of the isotherm). The application of the Brunauer-Emmett-Teller (BET) model resulted in a value of $1034.8 \text{ m}^2 \text{ g}^{-1}$ for the total specific surface area. From the PXRD, porosimetry and TEM studies, the a_0 cell parameter (4.41 nm), pore diameter (2.68 nm), and value for the wall thickness (1.8 nm) were calculated. In addition to this adsorption step associated to the micelle-generated mesopores, a second feature appears in the isotherm at a high relative pressure ($P/P_0 > 0.8$). This adsorption corresponds to the filling of the large voids among the particles (pore diameter of 46.61 nm and pore volume of $0.25 \text{ cm}^3 \text{ g}^{-1}$, calculated by using the BJH model) and therefore must be considered as a textural-like porosity. On the other hand, the N_2 adsorption-desorption isotherm of **S(sulf)_{pic}** is typical of mesoporous systems with partially filled mesopores (Figure SI-2b). In this case, and as expected, a lower N_2 adsorbed volume (BJH mesopore volume of $0.04 \text{ cm}^3 \text{ g}^{-1}$) and surface area ($127.3 \text{ m}^2 \text{ g}^{-1}$) were found when compared with the starting MSNs material.

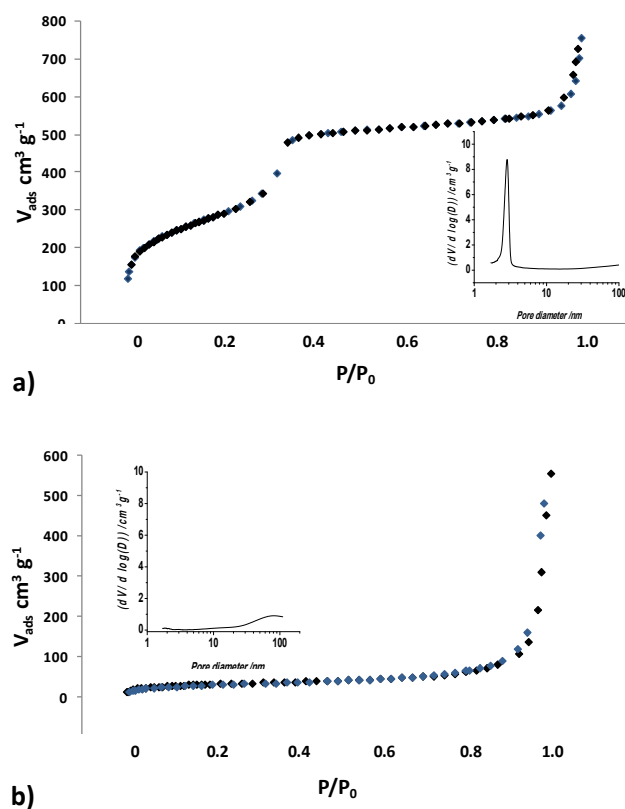


Figure SI-2. Adsorption-desorption isotherms for (a) calcined MSNs and (b) dye-loaded and functionalized $S(\text{sulf})_{PIC}$. Inset: pore-size distribution of both solids.

Table SI-1. BET-specific surface values, pore volumes and pore sizes calculated from the N_2 adsorption-desorption isotherms for calcined MSNs and $S(\text{sulf})_{PIC}$ material.

Sample	S_{BET} [m^2g^{-1}]	Pore Volume [cm^3g^{-1}]	Pore size [nm]
Calcined MSNs	1034.8	0.81	2.68
$S(\text{sulf})_{IC}$	127.3	0.04	2.02

The contents of loaded sulforhodamine B and grafted (3-isocyanatopropyl)triethoxysilane in **S(sulf)_{NCO}**, loaded 9-cis-retinoic acid in **S(RA)_{IFN}** and grafted poly(I:C) and loaded sulforhodamine B in **S(sulf)_{PIC}** were determined by elemental and thermogravimetric analyses (Table SI-2). Moreover, the content of 9-cis-retinoic acid in solid **S(RA)_{IFN}** was also determined by UV-visible studies. For this purpose, the content of 9-cis-retinoic acid present in the washing solutions was quantified and subtracted to the quantity used in the loading process of the solid. The contents calculated through this method compared well with those obtained from elemental and thermogravimetric analyses.

Table SI-2. Content (α , mg/g of solid) of the different loading molecules, of (3-isocyanatopropyl) triethoxysilane and of poly(I:C) in **S(sulf)_{NCO}**, **S(RA)_{IFN}** and **S(sulf)_{PIC}**.

Sample	$\alpha_{9\text{-cis-retinoic acid}}$	α_{dye}	$\alpha_{\text{isocyanate}}$	$\alpha_{\text{poly(I:C)}}$
S(sulf)_{NCO}	-	200	123.9	-
S(RA)_{IFN}	45.8	-	-	-
S(sulf)_{PIC}	-	16.2	-	179.6

Delivery studies

Assays of *in vitro* cargo release of **S(sulf)_{IFN}** and **S(sulf)_{PIC}** solids were performed using purified lysosomal extract as trigger. In a typical experiment, 1 mg of **S(sulf)_{IFN}** or **S(sulf)_{PIC}** was suspended in 500 μL of deionised water. Then, each suspension was divided into two aliquots of 250 μL and 1 mL of 10 mM PBS or 1 mL of purified lysosomal extract was added. To obtain the purified lysosomal extract the Lysosome Isolation Kit (LYSISO1) was used, following supplier's instructions for extractions from animal tissues and purification. Dye delivery from **S(sulf)_{IFN}** and **S(sulf)_{PIC}** was monitored via the emission band of the dye centred at 575 nm (λ_{ex} = 554 nm). In both cases, in absence of purified lysosomal extract, negligible cargo release was observed, indicating that the nanoparticles were tightly capped. In

contrast, in presence of purified lysosomal extract the uncapping of the pores was clearly observed (see Figure 2 in the manuscript). These facts demonstrated that cargo delivery is triggered by the presence of lysosomal enzymes that hydrolysed interferon- γ or poly(I:C) caps in **S(sulf)_{IFN}** and **S(sulf)_{PIC}** nanoparticles.

Cell culture and treatment

Poly(I:C), 9-cis-retinoic acid, interferon- γ and materials **S(RA)_{IFN}** and **S(sulf)_{PIC}** were tested *in vivo*, using SK-BR-3 human breast carcinoma cells. Cells were cultured at 37°C in DMEM medium containing 1000 mg L⁻¹ glucose, phenol red, 10% foetal calf serum and 2 mM glutamine. All the tested compounds and materials were dissolved in full-serum media just before treatments.

Viability Assays

Quantitation of cell viability rates was determined using cell proliferation reagent WST-1 following supplier's instructions. Cells were seeded in 96-well plates (25,000 cells/well) in triplicate. In the poly(I:C) or **S(sulf)_{PIC}** material alone assay, the compound at concentrations of 0.001, 0.01, 0.1, 1, 10, 25, 50, 100 and 500 $\mu\text{g mL}^{-1}$ or the nanoparticles at the same concentrations of equivalent poly(I:C) were added 48 h after seeding, during additional 48 h. Then, DMEM medium was removed and replaced with PBS with 1000 mg L⁻¹ glucose to avoid phenol red interference with the absorbance reading, WST-1 was added and the plates were incubated during 1 h at 37°C. Finally, the absorbance at 490 nm was measured. In the viability assay with poly(I:C) combined with 9-cis-retinoic acid and interferon- γ or with both **S(RA)_{IFN}** and **S(sulf)_{PIC}** nanoparticles, 48 h after seeding 0.3 $\mu\text{g mL}^{-1}$ of 9-cis-retinoic acid and 15 ng mL⁻¹ of interferon- γ or **S(RA)_{IFN}** solid at a concentration of 0.3 $\mu\text{g mL}^{-1}$ of equivalent 9-cis-retinoic acid was added to the plates during 4 h, and then the medium was removed and replaced with poly(I:C) or **S(sulf)_{PIC}** nanomaterial, respectively, in DMEM at the same concentrations of the previous assay. WST-1 adding and absorbance measuring were carried out as mentioned above. The obtained results are shown in Figure 3 in the manuscript.

Western blotting

TLR3 and α -tubulin antibodies were used to probe blots of protein extracts prepared using triton lysis buffer (10 mM Tris, pH 7.4, 137 mM NaCl, 2 mM EDTA, 1% Triton X-100, 25 mM β -glycerophosphate, 1 mM sodium orthovanadate, 2 mM sodium pyrophosphate, 10% glycerol, 1 mM PMSF, and protease inhibitors cocktail). Immune complexes were detected by chemiluminescence. Densitometric analysis was carried out with the ImageJ program.

Confocal Microscopy Imaging

Internalization of **S(sulf)_{PIC}** nanoparticles and dye release in SK-BR-3 cells was observed *in vitro* by confocal fluorescence microscopy (Figure SI-3). About 8×10^5 SK-BR-3 cells per well were cultured on 6-well plates, and 48 h later **S(sulf)_{PIC}** nanoparticles at $50 \mu\text{g mL}^{-1}$ of equivalent poly(I:C) were added for additional 48 h.

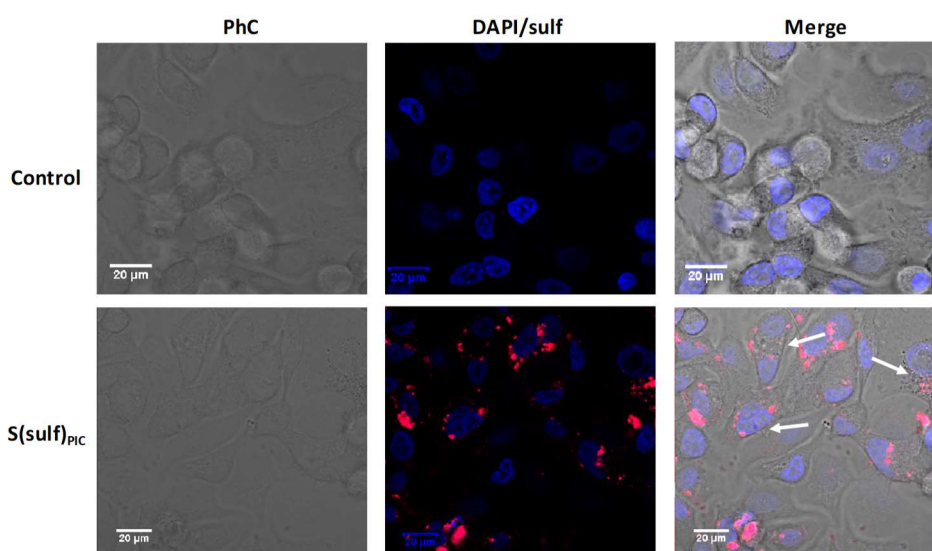


Figure SI-3. Internalization and release of sulforhodamine B (red) in SK-BR-3 cells. Cultures were incubated with **S(sulf)_{PIC}** during 48 h and examined by confocal microscopy. Cells nuclei were stained with DAPI (blue) before microscope observation. Representative images for phase contrast (PhC), DAPI, sulforhodamine B (sulf) and combined (merge) are shown. White arrows indicate cells apoptotic degradation (nuclei fragmentation, cytoplasm degeneration).

***Chapter 5: High Capacity Mesoporous Silica
Nanocarriers for Retinal Delivery of siRNA***

High Capacity Mesoporous Silica Nanocarriers for Retinal Delivery of siRNA

Amelia Ultimo,^{*[a]} Mar Orzaez,^[b,c] María Jose Santos-Martínez,^[d,e,f] Ramón Martínez-Mañez^[a,c,g,h] María D. Marcos,^[a,c,g,h] Félix Sancenón^[a,c,g,h] and Eduardo Ruiz Hernández^{*[e,f]}

[a] A. Ultimo, Prof. R. Martínez-Mañez, Prof. M.D. Marcos, Dr. F. Sancenón
Instituto Interuniversitario de Investigación de Reconocimiento Molecular y Desarrollo Tecnológico (IDM). Universitat Politècnica de València-Universitat de València, Spain
E-mail: amul1@doctor.upv.es

[b] Dr. M. Orzaez
Centro de Investigación Príncipe Felipe. Eduardo Primo Yúfera, 3. Valencia 46012, Spain

[c] Dr. M. Orzaez, Prof. R. Martínez-Mañez, Prof. M.D. Marcos, Dr. F. Sancenón
Unidad Mixta UPV-CIPF de Investigación en Mecanismos de Enfermedades y Nanomedicina, Universitat Politècnica de València, Centro de Investigación Príncipe Felipe, Valencia, Spain

[d] Dr. M.J. Santos-Martínez
School of Medicine, Trinity College Dublin (TCD), Dublin 2, Ireland

[e] Dr. M.J. Santos-Martínez, Dr. E. Ruiz Hernández
School of Pharmacy and Pharmaceutical Sciences, Trinity College Dublin (TCD), Dublin 2, Ireland

[f] Dr. M.J. Santos-Martínez, Dr. E. Ruiz Hernández
Trinity Biomedical Sciences Institute, TCD, Dublin 2, Ireland
E-mail: ruizhere@tcd.ie

[g] Prof. R. Martínez-Mañez, Prof. M.D. Marcos, Dr. F. Sancenón
Departamento de Química, Universitat Politècnica de València, Camino de Vera s/n, 46022, Valencia, Spain

[h] Prof. R. Martínez-Mañez, Prof. M.D. Marcos, Dr. F. Sancenón
CIBER de Bioingeniería, Biomateriales y Nanomedicina (CIBERBBN)

Submitted

5.1 Abstract

The main cause of subretinal neovascularization in wet age-related macular degeneration (AMD) is an abnormal expression in the retinal pigment epithelium (RPE) of the vascular endothelial growth factor (VEGF). Current approaches for the treatment of AMD present considerable issues that could be overcome by encapsulating anti-VEGF drugs in suitable nanocarriers, thus providing better penetration, higher retention times and sustained release. In this work, the ability of large pore-mesoporous silica nanoparticles (LP-MSNs) to transport and protect nucleic acid molecules is exploited to develop an innovative LP-MSNs-based nanosystem for the topical administration of anti-VEGF siRNA molecules to RPE cells. siRNA is loaded into LP-MSNs mesopores, while the external surface of the nanodevices is functionalized with polyethylenimine (PEI) chains that allow the controlled release of siRNA and promote endosomal escape to facilitate cytosolic delivery of the cargo. The successful results obtained in VEGF silencing in ARPE-19 RPE cells demonstrate that although further modifications are needed for improving their blood compatibility, the designed nanodevice is suitable as siRNA transporter.

5.2 Introduction

Nowadays, retinal vein occlusion, ocular tumours and several retinal diseases are known as the most common causes of progressive and irreversible angiogenesis-related blindness: i.e. age-related macular degeneration (AMD) in aged people, diabetic retinopathy in adults and retinopathy of prematurity in children.^[1-5] In particular, AMD is a multifactorial and progressive disease where genetic factors, the environment and age play an important role. The complex pathophysiology behind this condition leads to a progressive loss of central vision

due to damaged retinal pigment epithelium (RPE) and photoreceptors in the macula, the central area of the retina.^[6] AMD is responsible for more than half of the cases of legal blindness in elderly people in developed countries. The increased prevalence of the disease has been foreseen as a result of population ageing and underlines the urgency for implementing eye care therapies.^[7-10] In its late stages, the disease can evolve as dry or wet AMD, being the latter the one that affects the majority of patients with more severe vision loss and, as a consequence, worse quality of life.^[6,9]

Wet AMD occurs in patients who develop subretinal choroidal neovascularization (CNV), an abnormal growth of the choriocapillaris through the Bruch membrane that separates RPE from the choroid, the external highly vascularized layer which supplies retina's metabolic needs.^[11-13] It has been demonstrated that the persistent unregulated angiogenesis is mostly driven by an abnormal expression in the RPE of the vascular endothelial growth factor (VEGF), a primary mediator of angiogenesis and vascular permeability, which affects nearby tissues.^[7,14,15] VEGF production, that is constitutive in RPE in physiological conditions, can be altered due to many of the events related to AMD such as hypoxia, inflammatory responses or reduced nourishment of RPE cells because of defects in Bruch's membrane.^[5,7,14-16] Therefore, and due to its main role in retinal vascularization, VEGF represents the principal target of the developed therapeutic strategies.

During the last decade, in addition to surgery, intravitreal injections of anti-VEGF monoclonal antibodies or gene therapy products have become the standard of care for CNV and have contributed to importantly reduce the AMD-related blindness.^[4,5,7,17,18] Due to the complexity of the eye anatomy, intravitreal injections have been selected as standard route of administration to reach the posterior eye segment, the area behind the lens affected by retinal diseases. In fact, the physiological barriers that protect the eye from exogenous substances including the corneal epithelium, conjunctiva, tight junctions barriers, the anterior eye physiological clearance systems and the RPE expression of the P-glycoprotein efflux pump, prevent an efficient delivery and sufficient bioavailability to the retina of

those molecules when administered topically or systemically (<5% of instilled drug by drops and 1-2% of systemically administered doses reach the retina).^[1,2,4,5,19-21]

In 2004, Macugen[®] (pegaptanib, by Bauch & Lomb/Pfizer), a pegylated aptamer, was the first anti-VEGF factor approved by FDA for the treatment of wet AMD.^[17,22] Later, Lucentis[®] (ranibizumab, by Genentech/Novartis), a humanized antibody fragment that blocks the receptor binding domain of all isoforms of VEGF-A, and Eylea[®] (aflibercept, by Regeneron/Bayer), a recombinant fusion protein with higher affinity for VEGF-A became an established treatment for wet AMD.^[17,23,24] Nevertheless, despite the desirable therapeutic outcomes obtained, these approaches still present important issues, mainly due to their route of administration (i.e. intravitreal injections) and the need of frequent applications, given their short duration of action. Since these injections constitute a life-long medication for a chronic disease,^[1,4,20] the variety of side effects related to reiterated administration (pain, infection, vitreous haemorrhage, intraocular inflammation, glaucoma, retinal damage or detachment and cataract formation) also become a major hurdle for patient adherence. In addition, current treatments are costly and necessitate of specialized medical staff for administration so they are not globally accessible.

The ocular immune privilege is determined by physical barriers, the inhibitory microenvironment of immune-competent cells and ocular active regulation of systemic immune responses, that reduce the risk of inflammation.^[25,26] Considering this factor and the low amount of therapeutics for eye treatment, the possibility of modulating protein expression by nanocarrier-assisted gene therapy represents an interesting alternative for the treatment of AMD. A first attempt of anti-VEGF sense oligonucleotide ocular delivery was carried out in 2004 by means of lipid-lysine dendrimers, with successful *in vivo* results for up to two months after treatment.^[27] Nowadays, several clinical trials are being conducted for siRNA or aptamer based therapies against wet AMD.^[28]

For overcoming the major limitations associated to current therapeutic approaches for AMD, it should be noted that drugs encapsulation into nanodevices

can improve drug stability and solubility and can also provide a better penetration and accumulation in tissues with higher vascular permeability. By protecting the drug from rapid degradation or excretion, the use of nanocarriers leads to higher retention times and facilitates a tunable release.^[29-31] Among the large assortment of available nanocarriers, mesoporous silica nanoparticles (MSNs) provide several advantages for the loading, protection and delivery of biomolecules.^[32-34] MSNs present tunable pores with high loading capacity, large surface area, a scalable synthesis and the possibility of surface functionalization for developing targeted or controlled release systems, as well as for increasing their bioavailability and cellular uptake.^[35-41] In the case of LP-MSNs, the loading of nucleotides inside the pores can increase their protection.^[37] Several MSN-based systems have been studied *in vitro* for ocular and retinal delivery.^[42-46] In particular, pegylated and bevacizumab loaded MSNs, administered by subconjunctival injection, have recently demonstrated the ability to almost totally inhibit retinal neovascularization *in vivo* without toxic effects.^[46]

Based on the above, the main objective of the present work was to develop a LP-MSNs based nanosystem for the administration and controlled delivery of anti-VEGF siRNA molecules to retinal pigmented epithelial cells. LP-MSNs were synthesized, loaded with siRNA and finally functionalized with polyethylenimine (PEI) that acts as molecular gate for the controlled release of nucleic acid molecules while facilitating, as other cationic polyelectrolytes,^[47] the endosomal escape for cytosolic delivery. The obtained results in VEGF silencing in a human retinal pigment epithelial cell line (ARPE-19) highlight the noteworthy potential of the designed materials as siRNA carriers.

5.3 Results and discussion

Design and synthesis of functionalized LP-MSNs

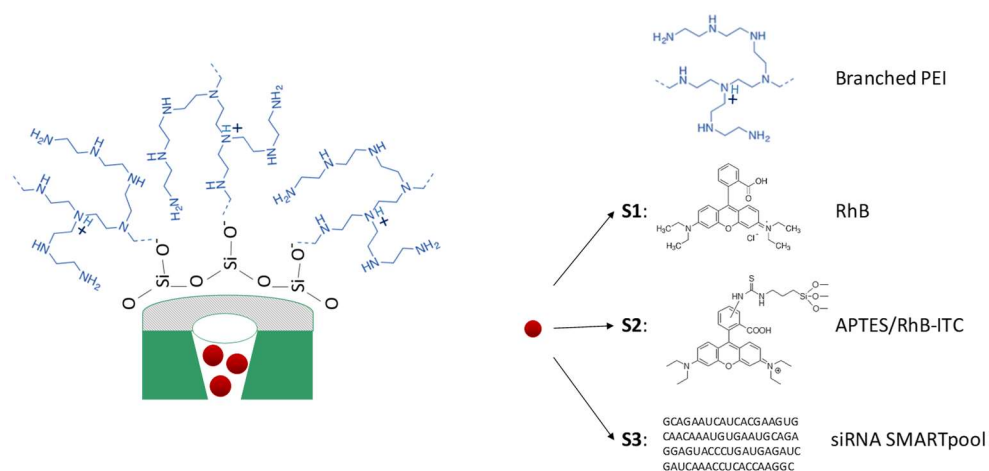
An AMD global burden projection for 2020 and 2040, with a high increase of prevalence in people over 75 years in Europe and Oceania and a large spread of

the disease in Asia have been foreseen due to population ageing.^[10] Therefore the development of innovative, more efficient and safer therapeutic approaches for the treatment of the disease is an urgent medical challenge. Current treatments, although providing favourable results in CNV control, present several serious drawbacks. In fact, the estimated half-life of ranibizumab or aflibercept in the aqueous humour, is less than five days,^[48] and monthly injections are required.

In this context, drug nanocarriers could represent an ideal means for enhancing drug bioavailability. Some nanosystems, such as the systemically administered liposomal Visudyne® for photodynamic therapy, have been suggested for the treatment of AMD.^[49,50] Other vehicles have been also proposed for anti-VEGF molecules. Tethadur (by pSivida), is a suspension of biodegradable mesoporous silica microparticles carrying aflibercept or ranibizumab into the pores that provides a gradual release. TheraKine has also developed biodegradable polymeric micro and nanoparticles for the sustained delivery of ranibizumab or bevacizumab during 6-9 months, that are in the process to be studied for use in humans. Also, biodegradable polymeric micro and nanoparticles for bevacizumab multi-month delivery were tested *in vivo* by Envisia Therapeutics.^[49,51]

The main objective of this work was to develop gated materials with the ability to efficiently deliver siRNA molecules to RPE cells. LP-MSNs were synthesized in order to allow highly accessible internal spaces for siRNA molecules transport. Branched PEI 10 K was selected as capping polymer for cargo controlled release, which was anchored to MSNs surface through electrostatic interactions. This PEI 10 K length was chosen as it has been demonstrated to have low cytotoxicity while keeping the ability to deliver nucleic acids in the cytoplasm.^[52] Three different types of functionalized nanoparticles were developed (**Scheme 1**): **S1**, loaded with rhodamine B (RhB) dye and capped with PEI chains, which allowed performing cargo release assay and verifying PEI capping ability; **S2**, covalently functionalised with rhodamine B isothiocyanate (RhB-ITC) through 3-aminopropyltriethoxysilane chains, and externally capped with PEI, employed to study nanoparticles cytotoxicity, cellular uptake and hemocompatibility of the nanoparticles; and **S3**,

the final solid loaded with anti-VEGFA siRNA and capped with PEI, developed for VEGF silencing in ARPE-19 cells.



Scheme 1. Schematic representation of the synthesized nanodevice. Anti-VEGF siRNA is loaded into the large mesopores, while the positively charged PEI chains are attached through electrostatic interaction to the negatively charged silica surface.

Nanoparticles characterization

TEM micrographs were taken to confirm nanoparticle size and morphology, as well as pore structure of synthesized LP-MSNs. The representative images reported in **Figure 1a**, show spherical monodispersed dendrimer-like nanoparticles with center-radial large pores. An average size of 105 ± 12 nm was calculated from 300 measurements taken from TEM images (**Figure 1b**). Hydrodynamic size distribution of both LP-MSNs and **S2** was also evaluated by DLS studies (**Figure 1c**). For LP-MSNs the resulting hydrodynamic diameter was 198 ± 9 nm, and 195 ± 2 nm for **S2** nanoparticles, with a polydispersity index of 0.23 and 0.17, respectively. It has been already shown that nanoparticles of 100-200 nm are preferable for ocular drug delivery since they avoid clearance and increase circulation within the ocular fluidic barrier, while at the same time reduce the risk of irritation produced by larger particles.^[1,49]

The zeta potential of the starting LP-MSNs nanoparticles was -40.4 mV, while after dye loading and functionalization with PEI in **S2** it increased to 27.2 mV due to the positive charge of the polymer.

Figure 1d shows the obtained adsorption-desorption isotherm for LP-MSNs. The curve shows a type-IV isotherm typical of dendrimer-like mesoporous structures.^[53] The Barrett-Joyner-Halenda (BJH) pore distribution graph indicates a broad distribution of pore size, with an average size of the main peak of 17 nm. The application of the Brunauer, Emmett and Teller (BET) model resulted in a value of 398 m² g⁻¹ for the total specific surface area. Finally, an amount of 45.6 µg/mg of siRNA loaded into **S3** mesopores was calculated as the difference between the amount measured using a NanoDrop Spectrophotometer in the reaction mix and in the supernatant after nanoparticles separation by centrifugation.

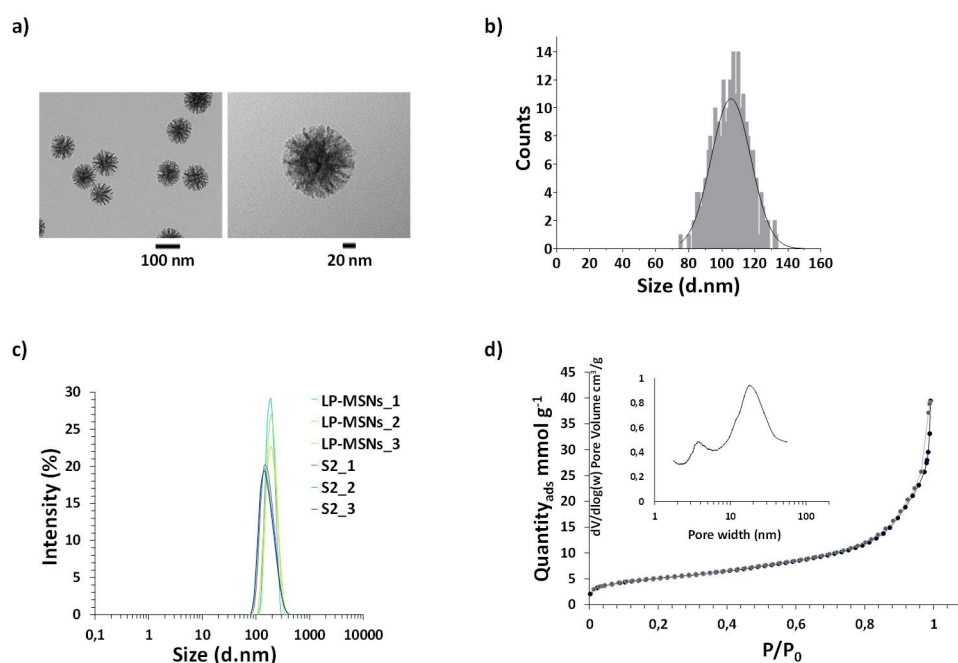


Figure 1. a) Representative TEM images of LP-MSNs. b) LP-MSNs size distribution obtained by measurements taken from TEM images. c) DLS intensity distribution of LP-MSNs and **S2** nanoparticles size. Three independent measurements for each type of nanomaterials are represented. d) N₂ adsorption-desorption isotherms for LP-MSNs. Inset: BJH pore size distribution.

Cargo release

The release of an entrapped guest in response to given changes in the biological environment is an essential capacity of the gatekeeping mechanisms used during the development of stimuli-responsive mesoporous nanomaterials. Hence, dye release assays were carried out to check the gating ability of the synthesized materials. **S1** nanoparticles loaded with RhB and externally functionalized with PEI were used to perform these studies. Purified lysosomal extract was used as release medium, as we speculate that cargo release would take place in the acidic environment of late endosomes and lysosomes, when proton sequestration by the polymer layer and the high ionic strength of the medium would allow PEI chains separation from the surface of the nanoparticles allowing dye delivery.^[54,55] As observed in **Figure 2**, when pH 7.2 buffered solution was used as blank medium, **S1** nanoparticles only released a small amount of RhB in 24 h, indicating that most of the cargo was still protected inside the pores. In contrast, the presence of the lysosomal extract produced a significant increase of dye fluorescence as a function of time. These results strongly confirmed the release triggering hypothesis.

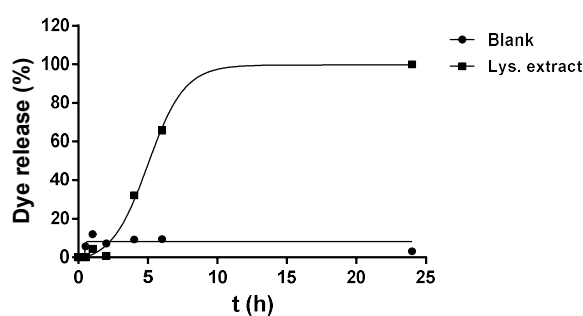


Figure 2. Normalized release profiles of RhB from **S1** nanoparticles in absence or in presence of purified lysosomal extract, obtained by measuring RhB fluorescence at 580 nm at different times.

Nanoparticles interaction and activity in ARPE-19 cells

Before proceeding to investigate the efficacy of the final nanoparticles in the cells of interest, the potential cytotoxic effect of **S2** in ARPE-19 cells was tested.

WST-1 viability tests at different times and concentrations of both, bare (i.e. LP-MSNs) and functionalised (i.e. **S2**) nanoparticles were performed. As observed in **Figure 3a**, LP-MSNs showed no cytotoxicity even at the highest concentrations up to 48h of incubation. In contrast, **S2** nanoparticles, externally functionalised with PEI, slightly decreased cells viability at 48 h at concentrations equal to or higher than 50 µg/mL. Besides, **S2** nanoparticles ability to enter ARPE-19 cells was confirmed by uptake studies monitored by both confocal microscopy and flow cytometry tracking RhB-ITC associated fluorescence. Confocal microscopy images demonstrate that nanoparticles uptake by ARPE-19 cells is a rapid process, since most nanoparticles co-localize with the cellular membrane after 1 h and almost all of them are inside the cytosol after 4 h (**Figure 3d**). Furthermore, the cell-associated fluorescence (CAF, resulting from percentage of positive cells × mean fluorescence/100) measured by flow cytometry indicated that cellular uptake is an energy-dependent mechanism, as it is quicker at 37 °C than at 4 °C during first hours of incubation, thus showing that nanoparticles are internalized by an endocytic pathway (**Figure 3b**).

Finally, the capacity of siRNA loaded nanoparticles to silence VEGF in retinal pigmented epithelial cells was tested incubating ARPE-19 cells with **S3** nanoparticles at different concentrations, corresponding to 1x, 2x or 4x the amount of free siRNA also tested, for 6 h and analysing in the supernatant the expression of VEGF levels by ELISA, 48 or 72 h after treatment. Untreated cells (negative control) and cells transfected with 100 nM free siRNA and lipofectamine were also analysed with the same ELISA Human VEGF test. The obtained results (**Figure 3c**) showed that **S3** represents a valid means for siRNA transport and delivery at cells of interest. In particular, the highest amount of **S3** used in the activity assays, that corresponds to 4x the amount of free siRNA added to the plates, significantly reduced VEGF expression at both 48 and 72 h. In fact, a knockdown of up to 70% and 75% at, respectively, 48 h and 72 h after treatment of ARPE-19 with **S3** nanoparticles was observed. Thus, the developed nanocarrier demonstrated to provide siRNA protection, cellular penetration, endosomal escape and consequent

cytoplasmic release, confirming its potential as an effective method for nucleic acid delivery.

As stated previously, several systems of nucleic acid nanocarriers for posterior eye delivery have been published. In particular, different studies have been carried out using poly(lactic-co-glycolic acid) (PLGA) nanoparticles for the delivery of anti-VEGF plasmids both intravitreally or systemically.^[28] A successful attempt to target RPE cells by topical instillation, instead, was made in 2014 with transferrin targeted small liposomes loaded with plasmid DNA.^[56] Nanoparticle surface functionalisation with polymers like chitosan, PEG or hyaluronic acid, or with ligands like transferrin, albumin, folate or RGD peptide, has been shown to increase the delivery to the posterior chamber of the eye, representing promising design strategies for the development of new drug nanovehicles.^[49] Such functionalization strategies are of special interest for the next stages of our investigation with the nanomaterials designed for this study.

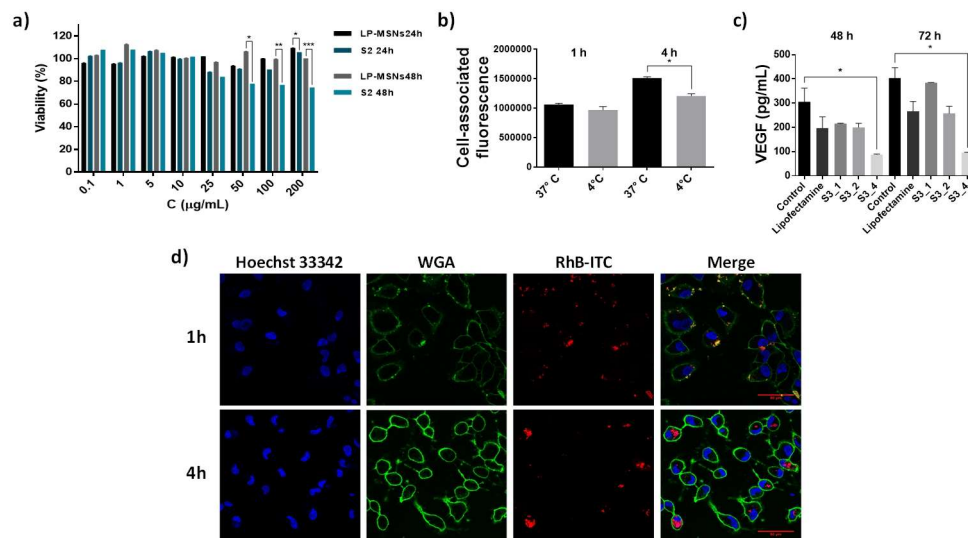


Figure 3. Biological validation of the developed nanomaterials. a) ARPE-19 cells viability after 24 or 48 h of incubation with different concentrations of LP-MSNs or S2 nanoparticles. Plates were analysed by measuring absorbance at 490 nm after 1 h of further incubation with Cell Proliferation Reagent WST-1. Data are expressed as mean \pm s.d. Asterisk indicates significant differences (*= $p < 0.05$, **= $p < 0.01$, ***= $p < 0.001$) when t test was applied. b) Cell-associated fluorescence over time of ARPE-19

cells treated with 50 µg/mL of **S2** and incubated at 37° C or 4° C is represented. Data are expressed as mean ± s.d. Asterisk indicates significant differences ($p < 0.01$) when t test was applied. c) VEGF levels (pg/mL) in ARPE-19 cells supernatant after transfection with 100 nM free siRNA or treatment with 1x (S3_1), 2x (S3_2) or 4x (S3_4) the amount of free siRNA added. Data are expressed as mean ± s.d. Asterisk indicates significant differences ($p < 0.05$) when t test was applied. d) Representative confocal microscopy images of ARPE-19 cells after 1 or 4 h of incubation at 37° C with 50 µg/mL of **S2**. Cell nuclei are stained with Hoechst 33342 (blue) and cellular membrane with WGA (green). **S2** nanoparticles are labelled with RhB-ITC (red).

Nanoparticles interaction with red blood cells and platelets

With regards to the potential toxicity of the synthesized nanomaterials, a recent study in rats demonstrated that ocular administration of high concentrations (10 mg/ml) of 100 nm silica nanoparticles over a 12-week time span had no significant toxicity on hematologic, biochemical or histopathologic parameters.^[57] Likewise, MSNs demonstrated no toxic consequences in retinal endothelial and neural cells *in vitro* and in mouse retina *in vivo*.^[12,46]

Nevertheless, two different assays were performed to investigate the potential toxicity of PEI functionalized nanoparticles **S2** on red blood cells (haemolysis) and blood platelets. **S2** nanoparticles at a concentration of 50 µg/mL induced 44% of haemolysis after 1 h of incubation with red blood cells when compared to 23% on red blood cells in the absence of **S2** (Triton X-100 was used as positive control and 100% of haemolysis) (**Figure 4a**). **S2** effect on platelet aggregation was also studied using a Quartz Crystal Microbalance with Dissipation technology (QCM-D). This is an extremely sensitive method capable of detecting microaggregation under flow conditions.^[58-61] that has been previously used for investigating the interaction of various nanoparticles with blood platelets.^[62-65] The principle of analysis of the QCM-D is based on the resonance frequency of a quartz crystal induced by applying an alternating electric field across the crystal. The device measures two parameters, frequency of vibration (f) and energy dissipation (D) simultaneously and in real time. An increase in mass bound to the sensor surface causes the crystal oscillation frequency to decrease (negative f shift). If the layer deposited on the sensor surface is rigid and thin, the decrease in f is proportional to the mass.^[66] However, if the layer attached to the sensor is thick and soft,

measurements based on changes in f may result in underestimation of the deposited mass. In those situations, the analysis of the dissipation factor, related to the viscoelastic properties of the adsorbed layer, becomes crucial.^[67] In fact, the perfusion of blood platelets through the QCM-D and their interaction with the surface of the sensors leads to the formation of a 'viscoelastic layer' as platelet aggregates deposit on the crystal. Therefore, when platelet function is investigated using QCM-D, more accurate measurements are obtained when both parameters (f and D) are investigated and analysed simultaneously.^[62-65] As observed in **Figure 4b**, a higher decrease in crystal oscillation frequency was recorded during the perfusion of platelet-rich plasma (PRP) in presence of 100 $\mu\text{g/mL}$ of **S2** nanoparticles, indicating an increase in mass bound to the quartz surface, namely, an increase in platelets aggregates. Consequently, an augmented energy dissipation was also observed under the same conditions (**Figure 4c**). In fact, the crystals' micrographs taken by optical microscopy after the perfusion of PRP in the absence or presence of **S2** clearly show the effect of the nanoparticles on the formation of larger platelets aggregates on the surface of the sensor (**Figure 4d**). Thus, although bare LP-MSNs showed negligible toxicity in several cell lines and in erythrocytes in previous assays run in our laboratories, PEI coated nanoparticles affected ARPE-19 cells viability and induced haemolysis and platelet aggregation, probably due to the external PEI layer.

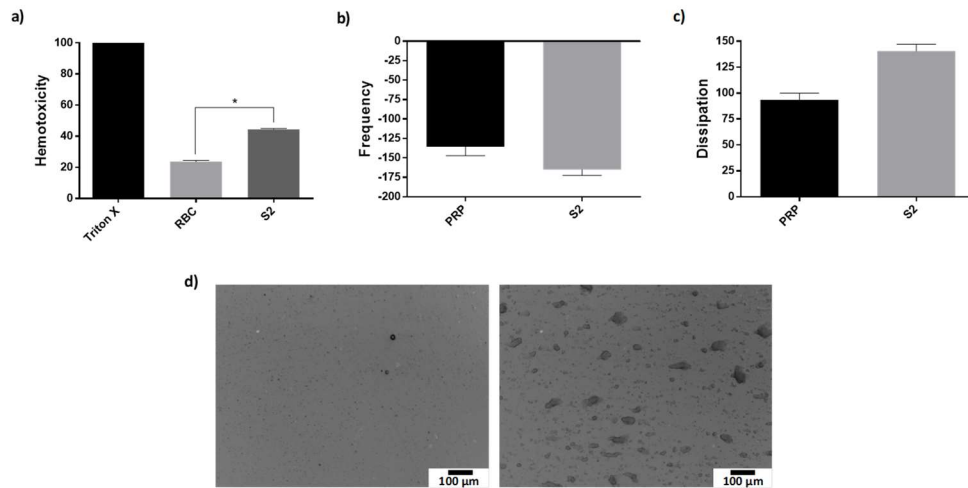


Figure 4. a) Haemolysis induced by **S2** nanoparticles compared to red blood cells (RBC) in the absence of nanoparticles. Triton X-100 was used as positive control. Data are expressed as mean \pm s.d. Asterisk indicates significant differences ($p < 0.001$) when t test was applied. b) Quantitative analysis of the effect of PRP in the absence or presence of **S2** nanoparticles on the frequency of the quartz crystal as measured by the QCM-D ($n=2$). c) Quantitative analysis of the effect of PRP in the absence or presence of **S2** nanoparticles on the energy dissipation as measured by the QCM-D ($n=2$). d) Representative micrographs of the surface of fibrinogen-coated polystyrene-coated quartz crystals as viewed by optical microscopy, showing platelet aggregates following the perfusion of PRP in the absence (image on the left) or presence (image on the right) of **S2** nanoparticles.

5.4 Conclusions

In summary, the results obtained in this work indicate the potential of the synthesized materials as the starting point for the development of topically administered nanovehicles based on LP-MSNs for the sustained attenuation of VEGF in the RPE by siRNA delivery. The developed system takes advantage of the high capacity and ease of access of the large pores of the mesoporous support to load and transport siRNA molecules, and of the capacity of PEI chains to promote endosomal escape to reach cytoplasmic delivery. The ability of the siRNA loaded material **S3** to enter retinal cells, effectively deliver its cargo and largely reduce the expression of VEGF in ARPE-19 cells has been demonstrated, holding great promise

for the next stages of the project. Nevertheless, further *in vivo* studies of the impact on visual function will be necessary to obtain a clinically acceptable product that could have high medical, social and economic relevance in the treatment of non-curable retinal disease.

5.5 Experimental section

Reagents

The chemicals cetyltrimethylammonium p-toluenesulfonate (CTATos), triethanolamine (TEA), tetraethylorthosilicate (TEOS), 3-aminopropyltriethoxysilane (APTES), rhodamine B (RhB), rhodamine B isothiocyanate (RhB-ITC), Lysosome Isolation Kit (LYSISO1), Fetal Bovine Serum (FBS), Hoechst 33342 and the Tyrode's solution were provided by Sigma-Aldrich. Branched polyethylenimine with MW 10,000 (bPEI 10,000) was purchased from Polysciences, Inc., and Cell Proliferation Reagent (WST-1) from Roche. 11320074 DMEM/F-12 medium, Lipofectamine 2000 and Wheat Germ Agglutinin Alexa Fluor 488 Conjugate were provided by Thermo Fisher Scientific, VEGFA ON-TARGETplus SMARTpool of siRNAs (a mixture of 4 siRNA sequences provided as a single reagent, giving advantages in both potency and specificity) by Dharmacon and the Quantikine ELISA Human VEGF kit by R&D Systems. ARPE-19 retinal pigmented epithelial cells were kindly provided by NanoBioCel: Micro and nanotechnologies, biomaterials and cells research group (University of the Basque Country and CIBER-BBN, Spain).

All reagents were used as received.

Synthesis of large pore-MSNs (LP-MSNs)

LP-MSNs were obtained following a reported method.^[53] Briefly, 0.96 g of CTATos and 0.1735 g of TEA were added to 50 mL of ultrapure water, and stirred at 80 °C and 400 rpm. After 1 h, 7.8 mL of TEOS were quickly added to the solution and stirred at 80 °C at 1000 rpm. 2 h later, the obtained LP-MSNs were centrifuged,

washed three times with ultrapure water and dried at 60 °C overnight. To remove the template from the pores, LP-MSNs were calcined at 550°C using an oxidant atmosphere for 5 h.

Functionalization of LP-MSNs

Three different functionalized nanomaterials were obtained from the bare LP-MSNs synthesized previously. In the case of solid **S1**, synthesized to carry out *in vitro* release studies, 150 mg of bare LP-MSNs were suspended with 150 mg of RhB dye in 10 mL of distilled water and stirred overnight. Then, the suspension was centrifuged, the pellet washed with ethanol and subsequently resuspended in 10 mL of ethanol. 75 mg of PEI and 15 mg of RhB were added and the solution was stirred during 3 h, washed and dried under vacuum. **S2** nanoparticles, instead, were designed to perform cellular assays, so the dye is not loaded but covalently linked into the pores. To do that, 60 mg of RhB-ITC were firstly suspended in 40 mL of acetonitrile with 400 µL of APTES and stirred during 5 h to form a stable linkage, and then 400 mg of bare LP-MSNs were added and the solution was stirred overnight. Once centrifuged, washed and dried under vacuum, 50 mg of the obtained material were resuspended in 4 mL of ethanol and 25 mg of PEI were added. The particles were stirred for 3 h and then centrifuged, washed and dried under vacuum. Solid **S3** is the final material loaded with siRNA, designed to achieve VEGF silencing in ARPE-19 cells. siRNA loading in LP-MSNs was carried out following a reported method.^[68] Briefly, 56 µL of siRNA were added to 0.7 mg of LP-MSNs, then 70 µL of 4 M guanidine hydrochloride solution and 40 µL ethanol were also added. Once mixed by vortex, the mixture was shaken at 270 rpm at 25 °C during 1 h, and finally centrifuged to collect loaded nanoparticles. Successively, the pellet was resuspended in 350 µL of ethanol with 350 µg of PEI, stirred for 3 h and then centrifuged, washed and dried under vacuum. The amount of siRNA from the starting mix and the amount remained in the supernatant were measured by Nucleic Acid quantification with NanoDrop Spectrophotometer.

Characterization

The obtained materials were characterized by several techniques. Transmission electron microscopy (TEM) images were obtained with a JEOL JEM-1010 microscope working at 100 kV. Samples were suspended in chloroform and then dropped on copper grids covered with carbon film and analysed once completely dried. Dynamic light scattering (DLS) and zeta potential studies were performed using a ZetaSizer Nano ZS (Malvern Instruments). N₂ adsorption-desorption isotherms were recorded in a Micromeritics TriStar II Plus automated analyser. Samples were previously degassed at 90 °C in vacuum overnight and measurements were performed at 77 K. Fluorescence measurements for *in vitro* release assays were run in a JASCO FP-8500 Spectrophotometer at room temperature. siRNA quantification was performed with a NanoDrop 2000 Spectrophotometer by Thermo Fisher Scientific. Cell viability, enzyme-linked immunosorbent assay (ELISA) and haemolysis results were analysed using a Perkin Elmer Wallac 1420 Victor2 microplate reader. Confocal microscopy imaging was performed with a Leica TCS SP8 HyVolution II (Leica Microsystems Heidelberg GmbH) inverted laser scanning confocal microscope. Flow cytometry measurements were taken with a CytoFLEX s flow cytometer by Beckman Coulter. Platelets concentration in donated blood was measured with a Beckman Coulter Z1 Particle Counter by Beckman Coulter Life Sciences. The platelets-nanoparticles interaction was studied using both a Quartz Crystal Microbalance (QCM-D) (Q-Sense AB) with Q-Sense software (QSoft₄₀₁) and an Olympus BX51M microscope (Mason Technology).

Cargo release from S1 nanoparticles

Dye release from solid **S1** was studied. Purified lysosomal extract obtained from animal tissue using the Lysosome Isolation kit LYSIS01 was employed as release medium, while pH 7.2 citrate-phosphate buffer was the blank. 6 mg of solid **S1** were suspended in 400 µL of buffer and divided into two aliquots of 200 µL. Then, 1.5 mL of release medium or blank was added to each aliquot, which was stirred 24 h. During this time several aliquots were extracted and observed by a

fluorescence spectrophotometer (RhB λ_{ex} : 550 nm, λ_{em} : 580 nm). Two independent assays were run giving similar results.

Cell culture conditions

ARPE-19 retinal pigmented epithelial cells were used for the *in vitro* evaluation of the synthesized nanoparticles. Cells were cultured at 37 °C in an atmosphere of 5% carbon dioxide and 95% air, in DMEM/F-12 containing 2.5 mM L-glutamine, phenol red and 10% fetal bovine serum. Cells underwent passage twice a week.

Viability assay

ARPE-19 cells viability rates were studied after incubation in the presence of LP-MSNs and **S2** nanoparticles. For this purpose, 3,500 cells/well were seeded in 96-well plates in triplicate and treated with different concentrations (from 0,1 to 200 $\mu\text{g}/\text{mL}$) of LP-MSNs or **S2** after 24 h, and incubated during 24 or 48 h. Viability was determined using Cell Proliferation Reagent WST-1 following supplier's instructions. WST-1 was added during 1 h and then the absorbance was measured at 490 nm. Three independent assays were carried out.

Cellular uptake

Internalization of **S2** nanoparticles was studied by flow cytometry and confocal fluorescence microscopy. To carry out flow cytometry experiments, 250,000 cells/well were seeded in 6-well plates, incubated during 24 h and then treated with **S2** nanoparticles at 50 $\mu\text{g}/\text{mL}$ and incubated at 37 °C or 4 °C for 1 and 4 h. Once washed and resuspended in cold PBS, cell-associated fluorescence (CAF) was measured by flow cytometry. Data collection involved 10,000 counts per sample. To obtain confocal microscopy images, ARPE-19 cells were seeded over glass coverslips (250,000 cells/well) in 6-well plates and allowed to settle during 24 h. Then, **S2** nanoparticles at 50 $\mu\text{g}/\text{mL}$ were added, and plates were incubated for 1 or 4 h at 37 °C. Wheat germ agglutinin (WGA) membrane stain at 5 $\mu\text{g}/\text{mL}$ and

Hoechst 33342 at 2 µg/mL were added, and after several washes with PBS the coverslips were observed with a Leica TCS SP8 HyVolution II. Both experiments were carried out in duplicates.

S3 Activity assay

To evaluate the efficacy of VEGFA siRNA loaded nanomaterial, ARPE cells were seeded (250,000 cells/well) in 6-well plates and allowed to adhere for 24 h. Then, cells were treated in 1% serum with 100 nM of free siRNA or with different amounts of **S3** corresponding to 1x, 2x or 4x the amount of free siRNA added. Cells were incubated during 6 h at 37 °C, afterwards the media were replaced with fresh DMEM/F-12 and the supernatant collected after 48 or 72 h and VEGF expression analyzed by ELISA. The Quantikine ELISA Human VEGF test was run following the instructions of the provider. Two independent experiments were done.

Hemotoxicity

Following informed consent, blood was collected from two healthy volunteers who had not taken drugs known to affect platelet function for at least 14 days prior to the study. Whole blood was carefully mixed with 3.15% sodium citrate (9:1). To test the potential toxicity of the developed materials in red blood cells, *ex vivo* erythrocytes lysis after 1 h of exposure to 50 µg/mL of **S2** or to Triton X-100, a surfactant used as positive control, were monitored following a reported method.^[69] After a centrifugation step for the elimination of intact erythrocytes, haemoglobin absorbance at 405 nm was measured. Two independent assays were run in triplicates. The potential interaction between platelets and **S2** nanoparticles was also studied. For those experiments, platelet-rich plasma (PRP) was obtained by centrifugation at 250 g for 20 minutes at room temperature, and the concentration of platelets measured with a Beckman Coulter Z1 Particle Counter and adjusted to 250,000 platelets/µL using Tyrode's solution. The effect of nanoparticles on platelet aggregation was investigated using a Quartz Crystal Microbalance (QCM-D). QCM-D consists of an electronic unit connected to an enclosed chamber platform housing four temperature and flow controlled modules

arranged in parallel configuration and attached to a peristaltic pump. Polystyrene-coated gold quartz crystals with a fundamental frequency of 5 MHz were used as sensors. The crystals were incubated with a solution of 100 g/mL of fibrinogen in phosphate buffered saline (PBS) for 20 minutes prior to experiments, and then mounted in the flow chamber and perfused with PBS for 10 minutes to remove unbound fibrinogen. PRP was perfused through the device at a flow rate of 100 μ L/min during 30 minutes in the presence and absence of 100 μ g/mL of **S2** nanoparticles at 37 °C as described previously.^[58] Changes in frequency of vibration (f) and energy dissipation (D) were measured during the perfusion at real time by the software provided with the device (Qsoft₄₀₁).

To analyze the morphology of platelet aggregates deposited on the crystals, the sensors were taken from the flow module immediately after the perfusion of PRP in the absence or presence of 100 μ g/mL **S2** nanoparticles and micrographs captured using a Olympus BX51M microscope.

Acknowledgements

This research was funded by the Wellcome Trust Institutional Strategic Support Fund and the European Research Council under Grant agreement No. 758887. We also thank Spanish Government (projects RTI2018-100910-B-C41 and RTI2018-101599-B-C22 (MCUI/FEDER, EU)) and the Generalitat Valenciana (project PROMETEO2018/024) for support. A.U is grateful to the Ministry of Education, Culture and Sport for her doctoral fellowship.

5.6 References

- [1] R. Bisht, A. Mandal, J. K. Jaiswal, I. D. Rupenthal, *Wiley Interdiscip. Rev. Nanomedicine Nanobiotechnology*, **2018**, *10*, 1.
- [2] I. P. Kaur, S. Kakkar, *J. Control. Release*, **2014**, *193*, 100.
- [3] D. H. Jo, J. H. Kim, J. H. Kim, *Arch. Pharm. Res.*, **2010**, *33*, 1557.
- [4] M. A. Kamaledin, *Nanomedicine Nanotechnology, Biol. Med.*, **2017**, *13*, 1459.
- [5] H. H. Shen, E. C. Chan, J. H. Lee, Y. S. Bee, T. W. Lin, G. J. Disting, G. S. Liu, *Nanomedicine*, **2015**, *10*, 2093.

- [6] K. Michalska-Małecka, A. Kabiesz, M. Nowak, D. Spiewak, *Eur. Geriatr. Med.*, **2015**, *6*, 69.
- [7] A. C. Bird, *J. Clin. Invest.*, **2010**, *120*, 3033.
- [8] D. G. Birch, F. Qi Liang, *Int. J. Nanomedicine*, **2007**, *2*, 65.
- [9] C. Volz, D. Pauly, *Eur. J. Pharm. Biopharm.*, **2015**, *95*, 158.
- [10] W. L. Wong, X. Su, C. M. Cheung, R. Klein, C. Y. Cheng, T. Y. Wong, *Lancet Glob. Heal.*, **2014**, *2*, e106.
- [11] J. Ryu, H. Seong, N. A. Yoon, S. W. Seo, J. W. Park, S. S. Kang, J. M. Park, Y. S. Han, *Mol. Med. Rep.*, **2016**, *14*, 5395.
- [12] D. H. Jo, J. H. Kim, Y. S. Yu, T. G. Lee, J. H. Kim, *Nanomedicine Nanotechnology, Biol. Med.*, **2012**, *8*, 784.
- [13] J. P. Marques, R. Silva, *Encyclopedia of Ophthalmology*, (Eds: U. Schmidt-Erfurth, T. Kohnen), Springer, Berlin, Heidelberg **2014**, 50.
- [14] J. Tong, Y. Yao, *Clin. Biochem.*, **2006**, *39*, 267.
- [15] A. F. Moleiro, G. Conceição, A. F. Leite-Moreira, A. Rocha-Sousa, *J. Ophthalmol.*, **2017**, *2017*, 1.
- [16] S. Y. Kim, C. Mocanu, D. S. Mcleod, I. A. Bhutto, C. Merges, M. Eid, P. Tong, G. A. Luttly, *Exp. Eye Res.*, **2003**, *77*, 433.
- [17] G. C. M. Cheung, T. Y. Y. Lai, F. Gomi, P. Ruamviboonsuk, A. Koh, W. K. Lee, *Asia-Pacific J. Ophthalmol.*, **2017**, *6*, 527.
- [18] F. A. Sloan, B. W. Hanrahan, *JAMA Ophthalmol.*, **2014**, *132*, 456.
- [19] A. Patel, K. Cholkar, V. Agrahari, A. K. Mitra, *World J. Pharmacol.*, **2013**, *2*, 47.
- [20] X. Wang, S. Wang, Y. Zhang, *Drug Deliv.*, **2016**, *23*, 2897.
- [21] B. G. Kennedy, N. J. Mangini, *Mol. Vis.*, **2002**, *8*, 422.
- [22] E. S. Gragoudas, A. P. Adamis, E. T. Cunningham, M. Feinsod, D. R. Guyer, *N. Engl. J. Med.*, **2004**, *351*, 2805.
- [23] E. Unsal, M. O. Cubuk, *J. Curr. Ophthalmol.*, **2019**, *31*, 66.
- [24] A. Sariyeva Ismayilov, E. Esen, S. Sızmaz, A. N. Demircan, *Clin. Exp. Optom.*, **2019**, doi: 10.1111/cxo.12877.
- [25] C. Campa, C. E. Gallenga, E. Bolletta, P. Perri, *Curr. Gene Ther.*, **2017**, *17*, 194.
- [26] R. Zhou, R. R. Caspi, *F1000 Biol. Rep.*, **2010**, *2*, 3.
- [27] R. J. Marano, N. Wimmer, P. S. Kearns, B. G. Thomas, I. Toth, M. Brankov, P. E. Rakoczy, *Exp. Eye Res.*, **2004**, *79*, 525.
- [28] S. M. Saraiva, V. Castro-López, C. Pañeda, M. J. Alonso, *Eur. J. Pharm. Sci.*, **2017**, *103*, 5.
- [29] E. Ruiz-Hernández, M. Hess, G. J. Melen, B. Theek, M. Talelli, Y. Shi, B. Ozbakir, E. A. Teunissen, M. Ramírez, D. Moeckel, F. Kiessling, G. Storm, J. W. Scheeren, W. E. Hennink, A. A. Szalay, J. Stritzker, T. Lammers, *Polym. Chem.* **2014**, *7*, 1674.
- [30] H. O'Neill, C. H. Herron, C. L. Hastings, R. Deckers, A. Lopez-Noriega, H. M. Kelly, W. E. Hennink, C. O. McDonnell, F. J. O'Brien, E. Ruiz-Hernandez, G. P. Duffy, *Acta Biomater.* **2017**, *48*, 110.
- [31] D. Muñoz-Espín, M. Rovira, I. Galiana, C. Giménez, B. Lozano-Torres, M. Paez-Ribes, S. Llanos, S. Chaib, M. Muñoz-Martín, A. C. Ucero, G. Garaulet, F. Mulero, S. G. Dann, T. VanArsdale, D. J. Shields, A. Bernardos, J. R. Murguía, R. Martínez-Máñez, M. Serrano, *EMBO Mol. Med.* **2018**, *10*, e9355.
- [32] C. de la Torre, I. Casanova, G. Acosta, C. Coll, M. J. Moreno, F. Albericio, E. Aznar, R. Mangués, M. Royo, F. Sancenón, R. Martínez-Máñez, *Adv. Funct. Mater.* **2015**, *25*, 687.
- [33] A. Ultimo, C. Giménez, P. Bartovsky, E. Aznar, F. Sancenón, M. D. Marcos, P. Amorós, A. R. Bernardo, R. Martínez-Máñez, A. M. Jiménez-Lara, J. R. Murguía, *Chem. Eur. J.* **2016**, *22*, 1582.
- [34] N. Z. Knezevic, E. Ruiz-Hernández, W. E. Hennink, M. Vallet-Regí, *RSC Adv.* **2013**, *3*, 9584.

- [35] C. Argyo, V. Weiss, C. Bräuchle, T. Bein, C. Bräuchle, T. Bein, *Chem. Mater.*, **2014**, *26*, 435.
- [36] V. Mamaeva, C. Sahlgren, M. Lindén, *Adv. Drug Deliv. Rev.*, **2013**, *65*, 689.
- [37] J. G. Croissant, Y. Fatieiev, A. Almalik, N. M. Khashab, *Adv. Healthc. Mater.*, **2018**, *7*, 1700831.
- [38] E. Aznar, M. Oroval, L. Pascual, J. R. Murguía, R. Martínez-Máñez, F. Sancenón, *Chem. Rev.* **2016**, *116*, 561.
- [39] A. Llopis-Lorente, B. Lozano-Torres, A. Bernardos, R. Martínez-Máñez, F. Sancenón, *J. Mater. Chem. B* **2017**, *5*, 3069.
- [40] E. Ruiz-Hernández, A. Baeza, M. Vallet-Regí, *ACS Nano* **2011**, *5*, 1259.
- [41] A. Baeza, E. Guisasola, E. Ruiz-Hernández, M. Vallet-Regí, *Chem. Mater.* **2012**, *24*, 517.
- [42] W. Qu, B. Meng, Y. Yu, S. Wang, *Int. J. Nanomedicine*, **2018**, *13*, 4379.
- [43] M. Gary-Bobo, Y. Mir, C. Rouxel, D. Brevet, O. Hocine, M. Maynadier, A. Gallud, A. De Silva, O. Mongin, M. Blanchard-Desce, S. Richeter, B. Looock, P. Maillard, A. Morère, M. Garcia, L. Raehm, J. O. Durand, *Int. J. Pharm.*, **2012**, *432*, 99.
- [44] W. Qu, B. Meng, Y. Yu, S. Wang, *Mater. Sci. Eng. C*, **2017**, *76*, 646.
- [45] Y.-T. Liao, C.-H. Lee, S.-T. Chen, J.-Y. Lai, K. C.-W. Wu, *J. Mater. Chem. B*, **2017**, *5*, 7008.
- [46] J.-G. Sun, Q. Jiang, X. P. Zhang, K. Shan, B. H. Liu, C. Zhao, B. Yan, *Int. J. Nanomedicine*, **2019**, *14*, 1489.
- [47] B. González, E. Ruiz-Hernández, M. J. Feito, C. López de Laorden, D. Arcos, C. RamírezSantillán, M. C. Matesanz, M. T. Portolés, M. Vallet-Regí, *J. Mater. Chem.* **2011**, *21*, 4598.
- [48] H. Kaji, N. Nagai, M. Nishizawa, T. Abe, *Adv. Drug Deliv. Rev.*, **2018**, *128*, 148.
- [49] K. Nayak, M. Misra, *Biomed. Pharmacother.*, **2018**, *107*, 1564.
- [50] R. Hennig, A. Goepferich, *Eur. J. Pharm. Biopharm.*, **2015**, *95*, 294.
- [51] J. Shen, G. W. Lu, P. Hughes, *Pharm. Res.*, **2018**, *35*, 217.
- [52] T. Xia, M. Kovochich, M. Liong, H. Meng, S. Kabehie, S. George, J. I. Zink, A. E. Nel, *ACS Nano*, **2009**, *3*, 3273.
- [53] X. Du, L. Xiong, S. Dai, F. Kleitz, S. Zhang Qiao, *Adv. Funct. Mater.*, **2014**, *24*, 7627.
- [54] C. Hom, J. Lu, M. Liong, H. Luo, Z. Li, J. I. Zink, F. Tamanoi, *Small*, **2010**, *6*, 1185.
- [55] R. V. Benjaminsen, M. A. Matthebjerg, J. R. Henriksen, S. M. Moghimi, T. L. Andresen, *Mol. Ther.*, **2013**, *21*, 149.
- [56] T. Lajunen, K. Hisazumi, T. Kanazawa, H. Okada, Y. Seta, M. Yliperttula, A. Urtti, Y. Takashima, *Eur. J. Pharm. Sci.*, **2014**, *62*, 23.
- [57] M. Kim, J.-H. Park, H. Jeong, J. Hong, W. S. Choi, B.-H. Lee, C. Y. Park, *Sci. Rep.*, **2017**, *7*, 1.
- [58] M. J. Santos-Martinez, A novel method for the measurement of flow-induced platelet activation at nanoscale resolution level. *PhD thesis*, **2009**, Trinity College (Dublin, Ireland).
- [59] M. J. Santos-Martínez, C. Medina, A. Prina-Mello, J. Conroy, S. P. Samuels, Y. Volkov, M. W. Radomski, *Kardiochir. Torakochi.* **2010**, *7*, 365.
- [60] M. J. Santos-Martinez, A. Prina-Mello, C. Medina, M. W. Radomski, *Analyst.* **2011**, *136*, 5120.
- [61] C. Larkin, E. Breen, T. Krzysztof, E. Simon, M. Radomski, T. Ryan, M. J. Santos-Martinez, *Platelets* **2018**, *29*, 301.
- [62] M. J. Santos-Martinez, I. Inkielewicz-Stepniak, C. Medina, K. Rahme, D. M. D'Arcy, D. Fox J. D. Holmes, H. Zhang, M. W. Radomski, *Int. J. Nanomedicine* **2012**, *7*, 243.
- [63] M. J. Santos-Martinez, K. Rahme, J. J. Corbalan, C. Faulkner, J. D. Holmes JD, L. Tajber, C. Medina, M. Radomski, *J. Biomed. Nanotechnol.* **2014**, *10*, 1004.
- [64] M. J. Santos-Martinez, K. A. Tomaszewski, C. Medina, D. Bazou, J. F. Gilmer, M. W. Radomski, *Int. J. Nanomedicine* **2015**, *10*, 5107.

- [65] S. P. Samuel, M. J. Santos-Martinez, C. Medina, N. Jain, V. A. Gerard, M. W. Radomski, Y. Gun'ko, A. Prina-Mello, Y. Volkov, *Int. J. Nanomedicine* **2015**, *10*, 2723.
- [66] G. Sauerbrey, *Z. Phys.* **1959**, *155*, 206.
- [67] C. Fredriksson, S. Kihlman, M. Rodahl, B. Kasemo, *Langmuir* **1998**, *14*, 248.
- [68] X. Li, Q. R. Xie, J. Zhang, W. Xia, H. Gu, *Biomaterials*, **2011**, *32*, 9546.
- [69] B. C. Evans, C. E. Nelson, S. S. Yu, K. R. Beavers, A. J. Kim, H. Li, H. M. Nelson, T. D. Giorgio, C. L. Duvall, *J. Vis. Exp.*, **2013**, *73*, e50166.

Chapter 6: Conclusions and perspectives

The development of innovative nanopharmaceutical products for drug transport is an exciting area in the field of nanomedicine, although several challenges still need to be overcome. Among the large variety of nanocarriers available for drug delivery, mesoporous silica materials have demonstrated in recent years a high potential for the targeted administration and on-command delivery of active molecules at desired sites. In this context, the work presented in this PhD thesis is aimed to design and develop new bio-gated nanosystems based on different kinds of mesoporous silica nanomaterials to achieve an improved therapeutic efficacy of antitumor compounds or antiangiogenic molecules.

The third chapter of this work presents a polyinosinic-polycytidylic acid (poly(I:C)) gated nanodevice able to target TLR3 receptor in breast cancer. The poly(I:C)-TLR3 interaction activates caspase 3-dependent apoptotic pathways in the studied cell line and allows the dsRNA-conjugated nanoparticles cellular uptake, enabling the degradation of the poly(I:C) moieties in the lysosomes and the release of the cargo loaded into the mesopores. Two gated nanoparticles loaded with a dye and with doxorubicin were synthesized, and both demonstrated a marked cytotoxicity in breast cancer cells. Nevertheless, loading the mesopores with doxorubicin enhanced the cytotoxic effect of the poly(I:C)-gated nanoparticles, suggesting a synergetic labour in killing cancer cells. Thus, the results obtained in this study demonstrate the potential of dsRNA-conjugated nanocarriers as effective strategies to improve the therapeutic efficacy of current antineoplastic drugs in TLR3-expressing cancers.

In the fourth chapter the design of a nanoparticles cooperation/communication strategy based on two different kinds of gated nanomaterials is reported. The main objective of this project was to demonstrate the possibility to apply the concept of stigmergy, understood as the ability of two or more individuals to indirectly communicate through environmental modifications, to functionalized nanosystems with medical purposes. In particular, a first kind of nanoparticles loaded with 9-cis-retinoic acid and capped with interferon- γ , and a second one

loaded with sulforhodamine B and capped with poly(I:C) were used. The uptake of the first kind by breast cancer cells enhanced the expression of TLR3 receptor, which augmented the subsequent internalization of poly(I:C)-gated nanoparticles increasing their cytotoxicity. These results highlight the enormous possibilities in the design of cooperation approaches involving different kinds of nanopharmaceuticals and intended to improve their therapeutic outcomes.

Finally, in the fifth chapter an approach for the topical administration of anti-vascular endothelial growth factor (VEGF) siRNA to retinal pigmented epithelial cells is described. Dendrimer-like mesoporous silica nanoparticles were selected as carriers due to their more voluminous and easy accessible inner spaces, that make them suitable for the transport of siRNA molecules. Thus, anti-VEGF siRNA was loaded into the mesopores, and then the external surface was coated with polyethylenimine chains to avoid the early delivery of the cargo and facilitate the endosomal escape once the nanoparticles are endocytosed. Although a further optimization of the presented siRNA delivery system is needed, promising outcomes in VEGF silencing in retinal pigmented epithelial cells were achieved.

As a general conclusion, the results presented in this PhD thesis show how mesoporous silica nanomaterials provide great adaptability and appropriateness for the development of gated nanodevices for several biomedical applications. Furthermore, the possibility to establish an indirect communication strategy at the nanoscale has been explored, and encouraging conclusions can be drawn from this assay. The reported materials can be considered as a starting point for the development of optimized and deeply characterized systems with proper pharmaceutical features, being clearly manifest the plethora of opportunities that they can offer for future research projects.

*Gracias al Ministerio de Educación, Cultura y Deporte por la beca
concedida para realizar esta tesis doctoral.*